Analytical modeling of reach-scale and network-scale dynamics of flow regimes

presented to the Faculty of Science of the University of Neuchâtel to satisfy the requirements of the degree of Doctor of Philosophy in Science

by

Behnam Doulatyari

Supervisory Committee:
Prof. Dr. Mario Schirmer, Université de Neuchâtel (Director of the thesis)
Prof. Dr. Daniel Hunkeler, Université de Neuchâtel (Co-director of the thesis)
Prof. Dr. Gianluca Botter, Università degli Studi di Padova (Technical supervisor)
Prof. Dr. Alberto Bellin, Università degli Studi di Trento (External reviewer)

Defended : 03.11.2015

Université de Neuchâtel
2015

UNIVERSITÉ DE NEUCHÂTEL

Faculté des sciences
Secrétariat-décanat de Faculté
Rue Emile-Argand 11
2000 Neuchâtel - Suisse
Tél: + 41 (0)32 718 2100
E-mail: secretariat.sciences@unine.ch

IMPRIMATUR POUR THESE DE DOCTORAT

La Faculté des sciences de l'Université de Neuchâtel autorise l'impression de la présente thèse soutenue par

Monsieur Behnam DOULATYARI

Titre:

"Analytical modeling of reach-scale and network-scale dynamics of flow regimes"

sur le rapport des membres du jury composé comme suit:

- Prof. ass. Mario Schirmer, Université de Neuchâtel, directeur de thèse
- Prof. Daniel Hunkeler, Université de Neuchâtel, co-directeur de thèse
- Prof. Gianluca Botter, Università degli Studi di Padova, Italie
- Prof. Alberto Bellin, Università degli Studi di Trento, Italie

Neuchâtel, le 1er décembre 2015

Le Doyen, Prof. B. Colbois

ACKNOWLEDGMENT

First and foremost I would like to thank my parents and brother for always believing in me and supporting me through all my crazy plans. I love you, and I dedicate this thesis to you as a small token of appreciation for all that you have done for me.

My special thanks go to my supervisors Mario Schirmer and Gianluca Botter. Mario, thank you for giving me this great opportunity. I feel very fortunate to have had such a wonderful, supportive and generous supervisor. Your encouragement through out my time at eawag has been a great source of motivation. Gianluca, thank you for all the long skype conversation, phone calls and discussions in Padova. I am continuously amazed by your new ideas and enthusiasm for your work. None of this would have happened without you. Thank you for providing me the opportunity to visit Padova. It allowed for a wonderful personal and professional experience. Thank you for your patience, encouragement, and everything that you have taught me. I am forever grateful to both of you for all that you have done for me.

I would like to express my great appreciation to Daniel Hunkler and Alberto Bellin for their time and input on this thesis work. Dirk Radny, thank you for all your help, your friendship and for making work enjoyable. Gabriele Chiogna, Karina Cano Paoli, Basudev Biswal and Andrea Betterle, thank you for your collaboration and all the discussions. My special thanks are extended to the staff of i4, in particular Elisa Alessicelegon and Pietro Fanton. This work would not have come together without your dedication and hard work. I am grateful for all your support and friendship. I would like to also thank the people in my group, W+T department, particularly Annette Johnson and Rolf Kipfer, and all the staff at eawag for their assistance and providing a great working environment. Exceptional thanks to all the friends and colleagues in the Advocate project. This was a great experience and it certainly made my PhD memorable. Steve Thornton, thank you for the great talks. Thank you also to my former colleagues at Worley Parsons for encouraging me to take on this challenge.

I am very grateful for the support and good times given by my friends here in Switzerland, in no specific order: Peter, Nina, Tim, Goska, Sarah, David, Christian, Simon, Natallia, Sergio, Ana, Anja, Kirsten, Numa, Anna-Caterina, Elham, Bahare, Navid, Lina; and elsewhere in the world: Maggie, Judy, Eva, Davood, Ryan, Ruth, Oksana, Natalia, Uwe, Niloofar, Chisenga, Wadzi, Nacho, Farhana. Thank you for making these past four years memorable. Particular thanks goes to Bas; your ill advised ideas after midnight and the subsequent colorful discussions at Odeon were a source of inspiration! To my comrades in VF, Ricky, Davide, Stefano; it has been an absolute joy. Thank you for all the wonderful and inappropriate conversations!

Aljona, thank you for being the source of joy in my life, and for putting up with my grumpy old man attitude while I was writing the thesis!

Roxana, Yasha, Nasim, Allan and Sandy, thank you for all the years of friendship and for always keeping me grounded.

This work was funded by the European Community's Seventh Framework Program (FP7/2007-2013 under grant agreement n265063) and by the Swiss National Science Foundation (SNF, Projects No. 200021-149126).

SUMMARY

Sustainable management of river networks is an important topic in hydrology today. Rivers and streams are a significant source of drinking water, as well as energy production and other human valued services. Spatial and temporal patterns of flow regimes have a significant impact on ecological and anthropogenic uses of fresh water within entire river basins. Developing tools for management of streamflows hinges on a deep understanding of the hydrologic form and function at the basin scale, and the interplay between the key driving processes. This study is centered on providing a process-based description of flow regimes and their spatial variability, with the purpose of developing tools for catchment-scale management of streamflows and studying ecologically relevant processes. Simple methods that allow a spatially explicit characterization of flow regimes with limited data and calibration requirements are extremely valuable for efficient management of water resources in data scars regions.

In order to meet these research goals, a modeling method was developed in this thesis for the prediction of streamflow regimes, based solely on catchment-scale climatic and morphological features. The method was tested in eleven test catchment distributed evenly in the United States, east of the rocky mountains. Considering the minimal data requirements (rainfall, potential evapotranspiration and digital elevation maps), the method was capable of capturing the patterns of observed streamflows reasonably well in all cases. This method was then expanded and applied point-wise along the river network of a test basin in north eastern Switzerland. A custom geo-database and a Web GIS platform were created for the management of data and model application. Predicted values of relevant flow statistics were validated at six subcatchment outlets, where discharge data was available, with satisfactory results. Strong seasonal signature of rainfall was identified as the dominant driving force of flow regimes. The seasonal variability of the streamflows showed a complex pattern, influenced by climatic gradients and by the increasing variability of hydrologic response observed at larger scales. The modeling method and data management framework presented here offer a novel and robust approach for assessing the spatial patterns of streamflows based on limited information.

The spatial and temporal variability of river flows bear important influence on ecological processes at the reach and basin scales. In this thesis, the effect of streamflow dynamics on riparian vegetation growth was studied using a lumped stochastic framework which explicitly incorporates the randomness of exposure and submersion periods implied by the streamflow variability, and links such a randomness to climatic and landscape properties. The framework was applied to the terminal reach of two catchments characterized by contrasting flow regimes. The results illustrated the role of vegetation specific traits and water availability as limiting factors, and flow regime variability as the driver for patterns of riparian vegetation biomass along the river reach.

ZUSAMMENFASSUNG

Der nachhaltigen Bewirtschaftung von Flusssystemen kommt eine wichtige Rolle zu, da Flüsse und Bäche einen signifikanten Anteil der Trinkwasserversorgung und der Energieproduktion ausmachen. Hierbei kommt dem räumlichen und zeitlichen Muster von Abflussregimen eine besondere Bedeutung zu, da hiervon sowohl ökologische als auch anthropogene Nutzungen innerhalb eines Einzugsgebietes direkt abhängen. Die Entwicklung von Werkzeugen, die ein nachhaltiges Bewirtschaften von Flüssen und Bächen unterstützen, hängt dabei stark von einem umfassenden Verständnis der hydrologischen Zusammenhänge auf Einzugsgebietsskala ab. Die vorliegende Arbeit liefert eine prozessbasierte Beschreibung von Abflussregimen und deren räumliche Variabilität, mit dem Ziel, Werkzeuge bereitzustellen, die eine Bewirtschaftung von Flusssystemen auf Einzugsgebietsskala ermöglichen. Für Bereiche, in denen nur bedingt Daten vorhanden sind, sind einfach anwendbare Methoden bei gleichzeitig geringen Anforderungen an die Modellkalibration von grösster Bedeutung für ein effizientes Wasserressourcenmanagement.

Um die oben genannten Forschungsziele zu erreichen, wurde innerhalb der vorliegenden Arbeit eine Modelliermethode entwickelt, um Abflussregime zu charakterisieren, wobei als Eingangsdaten für die Modellierung lediglich klimatische und morphologische Eigenschaften des Einzugsgebietes einfliessen. Die entwickelte Methode wurde in 11 Einzugsgebieten in den USA getestet. Trotz der geringen Anzahl an Eingangsdaten (d.h. Niederschlagshöhe, potentielle Evapotranspiration und digitale Geländemodelle) gelang es in allen Fällen, die verschiedenen Abflussmuster zu beschreiben. Die Methode wurde im nächsten Schritt dahingehend erweitert, dass Aussagen zum Abflussverhalten für diskrete definierte Punkte eines Flusssystems ermöglicht werden. Die Anwendung der erweiterten Methode erfolgte für ein Einzugsgebiet im Nordosten der Schweiz. Hierfür wurde eine benutzerdefinierte Geodatenbank und eine WebGIS-Plattform aufgebaut und sowohl Eingangsdaten als auch die Modellierungsmethode implementiert. Die dann prognostizierten Werte der Abflusscharakteristik wurden für 6 Teileinzugsgebietsauslässe, an denen gemessene Abflussdaten vorliegen, erfolgreich validiert. Der saisonal stark variierende Niederschlag konnte als dominante Einflussgrösse für das Abflussverhalten identifiziert werden. Weiterhin zeigte sich ein saisonal variables, komplexes Abflussmuster, welches vornehmlich vom klimatischen Gradienten beeinflusst ist aber auch von der unterschiedlich starken hydrologischen Reaktion, welche grossskalig beobachtet werden kann. Insgesamt stellt das innerhalb vorliegender Arbeit entwickelte Datenmanagement in Verbindung mit der implementierten Modellierungsmethode einen neuen und robusten Ansatz dar, um auf Grundlage von nur wenigen Eingangsdaten räumliche Abflussmuster für diskrete Punkte eines Flusssystems zu erhalten.

Die räumliche und zeitliche Variabilität von Abflüssen haben einen bedeutenden Einfluss auf ökologische Prozesse, sowohl innerhalb einzelner Flussabschnitte als auch im gesamten Einzugsgebiet. In der vorliegenden Arbeit wurde deshalb auch der Effekt von Abflussdynamiken auf

die ufernahe Vegetation und deren Wachstum mittels eines lumped stochastischen Ansatzes untersucht. Hierbei wurde explizit darauf geachtet, dass die Zufälligkeit der (Licht-) Exposition und der Überschwemmungsphasen, beides eine Funktion des Abflussregimes, Berücksichtigung finden. Der gewählte Ansatz wurde für zwei Einzugsgebietsbereiche angewendet, welche sich durch ihr unterschiedliches Abflussverhalten unterscheiden. Als Ergebnis der Arbeit zeigte sich, dass sowohl die Vegetation als auch die Wasserverfügbarkeit als limitierende Faktoren und die Variabilität des Abflusses als treibende Faktoren für die Gesamtbiomasse in Ufernähe genannt werden können.

RÉSUMÉ

La gestion raisonné des réseaux de riviére est un sujet important en hydrologie de nos jours. Les riviéres et les fleuves sont une source significative d'eau potable, au temps bien qu'une source de production énergétique et service écosystémique. Le motif spatial et temporel du régime hydrique a un impact majeur sur l'utilisation par la nature et l'humain de l'eau douce à l'intérieur d'un bassin hydrique entier. Le développement d'outils adressé à la gestion du flux hydrique dépend du cadre d'une compréhension approfondi de la forme et de la fonction hydrologique à l'échelle d'un bassin, et l'interaction entre les processus fonctionnel clés. Cette étude est orienté afin de fournir une description basé sur les processus du régime hydrique et sa variabilité spatial, avec pour but de développé un outils pour la gestion à l'échelle d'un bassin versant des flux hydrique et l'étude des processus relevant écologique. Les méthodes simple qui permettent une caractérisations spatial explicite du régime hydrique requérant un nombre limité de données et de calibration sont extrémement précieuse pour une gestion de la ressource en eau dans les régions pauvre en données.

Afin de satisfaire ces buts de recherche, une technique de modélisation a été développé dans cette thse pour la prédiction du régime hydrique, basé uniquement sur les caractéristiques climatiques et morphologiques de la zone de captage. La méthode a été testé sur onze captages test distribué uniformément au Etat Unis, à l'est des Montagne Rocheuses. Compte tenu des exigences minimales de données (pluie, potentiel d'évapotranspiration et du modle numérique de terrain), la méthode a été capable de reproduire le motif observé du flux hydrique de maniére raisonnable dans tous les cas. Cette méthode a été ensuite transposé et appliqué point par point le long d'un réseau hydrique d'un bassin test dans le nord-est de la Suisse. Une base de donnée géoréférencée et une plateforme internet SIG a été créer pour la gestion des données et l'application des modéles. Les valeurs prédites par les flux statistique approprié ont été validé dans six exutoires d'un sous-bassin versant, où les données d'écoulement étaient disponible, avec satisfaction. Une forte signature saisonnale des pluies a été identifié comme la principal force motrice du régime hydrique. La variabilité saisonnale de flux hydrique présente un motif complexe, influencé par le gradient climatique and par l'augmentation de la variabilité sur la réponse hydrique observé à large échelle. La méthode de modélisation et la structure de la gestion des données présenté ici offre une nouvelle et robuste approche pour l'évaluation des motifs spatial d'un flux hydrique basé sur une nombre limité d'information.

La variabilité spatiale et temporelle d'un flux de rivire supporte d'importante influence des processus écologique au niveau des biefs et du bassin. Dans cette thése, l'effet de la dynamique de riviére sur la végétation du long des riviéres a été étudié par une approche stochastique qui incorpore explicitement le hasard des propriétés climatiques et paysagéres. La structure a été appliqué au bras final de deux captages caractérisé par des régimes hydriques différents. Les résultats illustrent le rôle des traits spécifiques de la végétation et la disponibilité en eau comme facteur limitant, et de la variabilité du régime hydrique comme conducteur du motif de la végétation le long des biefs de riviére.

Keywords: Streamflow Regime, Stochastic-analytic model, Physically-based model, Flow Duration Curve, Spatial pattern, Catchment-scale, River Networks, Geo-database, Riparian vegetation

CONTENTS

LIST OF FIGURES

LIST OF TABLES

1. INTRODUCTION

Large-scale management of water resources often involves various tasks such as flood protection, providing sufficient river base flow, guaranteeing access to quality drinking water under all environmental conditions, providing adequate irrigation water, among others. These needs have to be met while protecting river corridors, which play an important role in biodiversity, soil conservation, and water quality. At the same time, river systems are among environments most disturbed by humans activity. Effective management of water resources in complex river networks is vital, particularly in the context of changing climatic conditions and increasing anthropogenic demand.

Modeling methods for integrated water resources management, often rely on substantial data about the quality and quantity of water. However, availability of reliable data differs strongly among regions, and data scars regions often coincide with most vulnerable environments and populations. Therefore, developing modeling methods with limited data requirement would be very beneficial for achieving better practices in areas where data acquisition and availability is a limiting factor.

The variability of streamflows is commonly portrayed by means of the flow duration curve (FDC) and the probability density function (PDF) of streamflows. These statistic descriptors can either be directly obtained at gauged sections of the river, or estimated using empirical or physically based models in areas where discharge time series are not available. Empirical models use the concept of hydrologic similarity to infer the hydrological signature of an ungauged catchment based on the observation of neighboring gauged catchments featuring similar characteristics [*Wagener and Wheater,* 2006; *Castellarin et al.,* 2007; *Ganora et al.,* 2009]. Physically based approaches, instead, consider runoff formation by accounting for climatic forcing and catchments echo-morphological characteristics [*Beven and Kirkby,* 1979; *Botter et al.,* 2007a; *Yokoo and Sivapalan,* 2011; *Cheng et al.,* 2012; *Booker and Woods,* 2014]. Even though physically based approaches can be challenging, they allow for an improved understanding of the processes that control the water cycle by setting causal relationships among the drivers of the process.

In particular, *Botter et al.* [2007a, 2009] developed a stochastic analytic model, where the temporal variability of discharge reflects the randomness of the underlying rainfall and climatic forcing and the heterogeneity of the hydrological processes by which the water is transferred from hillslopes to the catchment outlet. In this model, the seasonal flow duration curve is expressed as a function of four physically-based parameters that embed climatic (rainfall and potential evapotranspiration) and geomorphological features (digital elevation models). Rainfall time series are among the most commonly available data forms, and with advances in weather radar estimates and satellite based measurements their coverage has become more ubiquitous. Furthermore, advances in remote sensing technologies have provided easily accessible global maps of potential evapotranspiration. These data in combination with water balance models (such

as, but not limited to, *Budyko,* [1974]; *Milly,* [1994]; *Porporato et al.* [2004]; *Sivapalan et al.* [2011]) can be used to estimate the catchment-scale water balance. The catchment response has traditionally been estimated through analyzing flow recessions in observed discharge time series. However, recent studies have proposed models for estimating the hydrologic response of the catchment based on the geomorphic relationship between the river network structure and recession properties of streamflows [*Harman et al.,* 2009a; *Biswal and Marani* 2014]. Given the wide availability of high resolution digital elevation models (DEMs), estimating the hydrologic response of the catchment through methods utilizing this relationship, can be very valuable in poorly gauged areas.

Predicting the statistics of flow regime at the catchment outlet provides information regarding the amount and variability of flows at-a-station. However, many hydrological and ecological processes and dynamics along river networks are affected by the spatial variability of flow regimes. The effects of flow regulation and hydrologic alterations (e.g. river restoration, creation of retention areas) vary with location within the catchment. Additionally, spatially explicit properties of flow regime are important for assessment of ecological processes, particularly when habitat suitability and the movement of species along the network is considered (e.g. *Ziv et al.,* [2012]; *Mcluney et al.,* [2014]; *Bertuzzo et al.,* [2012]; *Muneeperakul et al.,* [2007a]).

Despite recent advances in the characterization of flow regimes in spatially explicit settings [e.g. *Costa-Cabral et al.,* 2008; *Rigon et al.,*; *Formetta et al.,*; *Schaefli et al.,* 2014], the analysis and prediction of variability of flow duration curves along individual river networks still represents an area where research is needed. The ability to estimate the flow regime point-wise along the river network would allow for characterization of spatial variability of water resources within complex river systems as well as the ability to evaluate catchment-scale impact of water infrastructures.

The spatio-temporal variability of streamflows is widely recognized as a major driver for ecological processes occurring in riverine systems. Riparian zones are particularly important, because they possess an unusually diverse array of species and plant communities [*Naiman and Decamps,* 1997]. They also play an important role in many biogeochemical processes and contribute to controlling erosion, sediment transport and habitat diversity [*Naiman and Decamps,* 1997; *Nilsson and Svedmark,* 2002; *Muneepeerakul et al.,* 2007a,b]. Riparian zones can experience significant changes due to flow regulation [*Tealdi et al.,* 2011], since the natural dynamic disturbances caused by flooding, are an important driver for biological productivity. In order to maintain biodiversity and ecological integrity, riparian ecosystems are in need of protection and restoration [*Nilsson and Svedmark,* 2002].

Flow regimes drive river ecosystem dynamics both directly, by means of the natural variability of streamflows impact on life cycles of biological species (e.g. riparian vegetation) [*Ward et al.,* 2001; *Bunn and Arthington,* 2002], and indirectly, through modulating ecologically important physical variables dependent on the flow magnitude (e.g., stream velocity and sediment transport, connectivity between the river and floodplains) [*Constantz,* 1998; *Smith et al.,* 2003; *Stanley et al.,* 1997]. At the reach-scale, river stage fluctuations determine the pattern of exposure and inundation for a given point. These fluctuations are stochastic in nature since they mirror the stochastic fluctuation of the streamflows, driven by climatic and landscape features of the contributing catchment. Moreover, the morphological features of the river transect modulate the dynamics of these pulses at each transect. Therefore, developing simple process-based modeling

methods for exploring the dynamics of riparian systems explicitly as a function of the driving hydrologic regime, deserves attention. Such methods would help the understanding of how changes in climate and landscape attributes will propagate to streamflow regimes and in-stream ecological processes.

Aims and objectives

The general objective of this Ph.D. thesis was to improve the understanding of ecohydrological processes, by developing a catchment-scale modeling framework for comprehensibly describing flow regimes and their spatial variability, using simple physically-based analytical models that require minimal calibration and computational burden. A firm understanding of the processes involved, and rigorous analytical characterization of them, formed the basis of this research. Particular attention was devoted to applicability of the method in data scars regions. The specific research objectives of this research are as follows:

- Developing and verifying a modeling method for estimating statistics of streamflows based on limited data.
- Establishing a modeling method for predicting catchment-scale spatial variability of flow regimes.
- Creating a versatile and user friendly tool for data management and implementation of the above models.
- Quantitative evaluation of the control exerted by the flow regime on ecological dynamics in riverine system, in particular for the growth and decay of riparian vegetation.

Fulfillment of these objectives were the necessary step in creating an easy to use process-based method that can aid in large-scale management of water resources.

Thesis structure

The research goals stated above have been accomplished, and they are presented in this PhD thesis as follows:

In chapter 2, a modeling method is presented which is capable of estimating streamflow probability distributions solely based on catchment-scale information about climate and landscape. A physically-based analytic model of streamflow dynamics was combined with existing water balance models and a geomorphological recession model. The method was applied to 11 test catchments and results are discussed.

Chapter 3, describes the custom geo-database and Web GIS platform created for data management and model application to estimate spatial patterns of flow regime. The method was applied point-wise along the river network of a test basin, Thur river, in north eastern Switzerland.

Model prediction for relevant flow statistics were validated at six subcatchment outlets. Emerging catchment-scale patterns of the relevant flow statistics and model parameters are discussed. The scaling of recession parameters with respect to catchment area were also explored.

In chapter 4, the signature of catchment-scale hydro-climatic processes in the patterns of vegetation biomass along a river transect were studied and modeled. The model was applied to the terminal reach of two different catchments characterized by contrasting flow regimes. Patterns of riparian vegetation under different flow regimes are described. The change of climatic features and its impact on mean vegetation biomass along the transect were explored through analysis of long-term observed rainfall patterns.

In chapter 5, the key findings are summarized and overall conclusions are stated. Furthermore, an outlook on potential direction and challenges for continuing and expanding this research is presented.

2. PREDICTING STREAMFLOW DISTRIBUTIONS AND FLOW DURATION CURVES FROM LANDSCAPE AND CLIMATE

Doulatyari, B.[12], A. Betterle[123], S. Basso[12], B. Biswal[4], M. Schirmer[12], G. Botter[3] (2015), Predicting streamflow distributions and flow duration curves from landscape and climate, *Adv. Water. Res.*, 83, 285-298, doi:10.1016/j.advwatres.2015.06.013.

Abstract

Characterizing the probability distribution of streamflows in catchments lacking in discharge measurements represents an attractive prospect with consequences for practical and scientific applications, in particular water resources management. In this paper, a physically-based analytic model of streamflow dynamics is combined with a set of water balance models and a geomorphological recession flow model in order to estimate streamflow probability distributions based on catchment-scale climatic and morphologic features. The models used are described and the novel parameterization approach is elaborated on. Starting from rainfall data, potential evapotranspiration and digital terrain maps, the method proved capable of capturing the statistics of observed streamflows reasonably well in eleven test catchments distributed throughout the United States, east of the rocky mountains. The method developed offers a unique approach for estimating probability distribution of streamflows where only climatic and geomorphologic features are known.

2.1 Introduction

The probability distribution of streamflows and the associated flow duration curve provide information on the availability of water resources in a catchment. This is important both for anthropogenic exploitation of flows (e.g. industrial and civil uses or power generation) and the maintenance of functioning ecological processes within the riverine environment [*Postel and Richter,* 2003; *Ziv et al.,* 2012; *Hurford et al.,* 2014]. Streamflow probability distributions summarize main features of the flow regime, as well as flow dynamics related to different geomorphological and climatic settings. For this reason, they have long been a key tool for water resource management [*Vogel and Fennessey,* 1995].

[1] EAWAG Swiss Federal Institute of Aquatic Science and Technology, Department of Water Resources and Drinking Water, Duebendorf, Switzerland.
[2] University of Neuchâtel, The Centre of Hydrogeology and Geothermics (CHYN), Neuchâtel, Switzerland.
[3] University of Padova, Department ICEA and International Center for Hydrology "Dino Tonini", Padua, Italy.
[4] Indian Institute of Technology Hyderabad, Department of Civil Engineering, Hyderabad, India.

The absence of dense discharge measurement networks makes the assessment of river flow availability challenging. Extensive literature exists on estimation of flow duration curves in sparsely gauged and ungauged catchments [*Merz and Blöschl,* 2004; *Blöschl et al.,* 2006; *Castellarin et al.,* 2004; *Oudin et al,* 2008; *Castiglioni et al.,* 2010; *Hrachowitz et al.,* 2013]. Both empirically-based and physically-based approaches are suitable for this task. Among the former, statistical models employ discharge time series observed at instrumented outlets of neighboring catchments or within identified homogeneous regions to predict the flow regime of ungauged basins using the concept of hydrologic similarity [*Wagener and Wheater,* 2006; *Castellarin et al.,* 2007; *Ganora et al.,* 2009]. Physically-based approaches, instead, mimic the hydrologic response of the basin to rainfall inputs by describing the underlying processes of soil moisture dynamics and rainfall-runoff transformation [*Beven and Kirkby,* 1979; *Botter et al.,* 2007a; *Yokoo and Sivapalan,* 2011; *Cheng et al.,* 2012; *Booker and Woods,* 2014]. Such models have the advantage of setting causal relationships among climate input, morphological features, and geopedologic attributes allowing for an improved understanding of the physical processes that control the hydrologic cycle [*Wagener et al,* 2007; *Gupta et al.,* 2008; *Hrachowitz et al.,* 2013].

Many studies have highlighted the relationship between channel network structure and hydrologic response of the catchment [*Rinaldo,* 1991; *Rinaldo et al.,* 1995; *Rodriguez-Iturbe et al.,* 2009; *Biswal and Marani,* 2010; *Mutzner et al.,* 2013; *Gosey and Kirchner,* 2014]. In particular, geomorphological interpretations of recession dynamics have been proposed, which have been used to infer geomorphic signatures of the hydrologic response [*Harman et al.,* 2009a; *Biswal and Marani* 2014]. Given the wide availability of high resolution Digital Elevation Models (DEM), the link between geomorphological attributes of the landscape and flow properties is particularly interesting for improving our ability to describe flow regimes in poorly gauged areas.

Landscape properties and catchment morphology have also been recognized as major determinants of vegetation patterns, water use efficiency and hydrologic partitioning [*Troch et al.,* 2009; *Rodriguez-Iturbe et al.,* 2009; *Voepel et al.,* 2011; *Thompson et al.,* 2011a; *Jaramillo and Destouni,* 2014]. The understanding of the major drivers of the water balance has a long history, which is rooted in pioneering works by *Thornwaite* [1948], *Longbein* [1949] and *Budyko* [1974] who first demonstrated the dependence of hydrologic partitioning on climate features, as well as on the competition between available soil water and available energy for vaporization. More recent works have highlighted that the seasonality and stochasticity of rainfall, vegetation features, and landscape properties are also important for attaining reliable predictions of water balance [*Milly,* 1994; *Porporato et al.,* 2004; *Donohue et al.,* 2007; *Zhang et al.,* 2008]. Despite the inherent difficulty in incorporating the effects of soil, vegetation and climate heterogeneity into low dimensional catchment-scale formulations, our understanding of the spatio-temporal variability of hydrologic partitioning between streamflow and evapotranspiration has improved significantly in recent years [*Sivapalan et al.,* 2001; *Thompson et al.,* 2011b; *Zanardo et al.,* 2012; *Berghuijs et al.,* 2014]. These advances can provide important clues for the prediction of water resources in rivers and for forecasting of their response to climate change [*Destouni et al.,* 2013].

In this study, we present and exemplify a physically-based method capable of predicting the flow regime in the absence of discharge data. The method is grounded in the stochastic analytic model developed by *Botter et al.* [2007a]. This is a mechanistic approach where the dynamics of daily streamflows are linked to a spatially-integrated soil water balance forced by intermittent rainfall. This paper adopts the version of the model in which the hydrologic response of the

catchment is assumed to be non-linear [*Botter et al.,* 2009; *Ceola et al.,* 2010]. The four physically-based parameters that define the flow duration curve are estimated based on climatic (rainfall and potential evapotranspiration) and geomorphological data (DEMs), integrating established water balance models [*Budyko,* 1974; *Milly,* 1994; *Porporato et al.,* 2004; *Sivapalan et al.,* 2011] with a geomorphic recession flow model (GRFM) [*Biswal and Marani,* 2010]. In particular, for the application discussed in this paper, a set of gauged catchments is used for estimating the parameters of the water balance models based on climate data. Such parameters are then employed for the prediction of streamflow probability distributions in a different set of test catchments. Moreover, the prediction of flow regimes in these test catchments exploits the geomorphic relationship between the river network structure and recession properties of flows, evidenced by *Biswal and Marani* [2010]. The overall work-flow of method and main model parameters are introduced in Figure 2.1.

This paper is organized as follows: section 2 provides a summary of the hydro-climatic data, the selection criteria for the study catchments, and the essential information about these catchments. In section 3, we introduce the analytical model for the probability density function of streamflows and define the relevant model parameters. Section 4 outlines the method proposed for the parameter estimation in the absence of discharge data. In particular, the performance of different water balance models were tested for the estimation of the frequency of flow producing events. The ranking of the water balance models and the results of predicting the streamflow regimes are discussed in section 5. In section 6 the limitation of the proposed method are elaborated on. Section 7 provides the overall conclusions of this study.

2.2 Study Catchments and Hydro-climatic Data

49 catchments were considered in this study which were divided in two sets: (*i*) catchments used for calibration of the water balance model, hereafter referred to as calibration catchments (Table 2.1); (*ii*) catchments were streamflow distribution was predicted from climate and morphological data (hereafter referred to as test catchments), taking advantage of the calibrated water balance models (Table 2.2). The catchments are distributed relatively evenly throughout the United States, east of the Rocky Mountains. The size of the basins span between 40 and 2000 km^2 and include many different climatic regions. All the study catchments are not impacted by significant regulation or storage. Figure 2.2 shows the spatial distribution of the 49 catchments across the US. The northern catchments (marked with a dotted circle) experience relevant snow precipitations during winter. The presence of snow may significantly impact the water balance across seasons, in particular by storing water inside the catchment in winter (when precipitation occurs) and releasing the stored water in spring (when the snow melting increases the runoff coefficient). Thus, in the catchments affected by snow dynamics, results from winter and spring were disregarded in the application of water balance models at the seasonal scale.

Potential evapotranspiration (PET) data has been acquired through two different data bases: (*i*) The 'MODIS global evapotranspiration Project' (MOD16), available from the Montana University (`http://www.ntsg.umt.edu`), which includes a dataset providing PET at 1 km^2 resolution for 10^9 Million km^2 global vegetated land areas at 8-day, monthly and annual time resolution, based on the Penman-Monteith method; (*ii*) The 'CGIAR-CSI Global-Aridity and Global-PET Database' [*Zomer et al.,* 2007], a freely available global PET database (`http:`

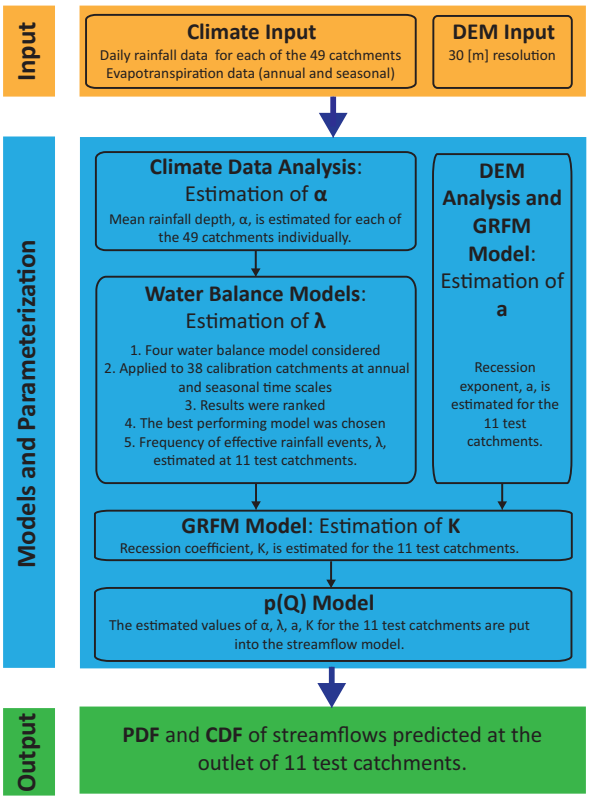

Fig. 2.1: The overall work-flow of the modeling method is presented here. The four physically-based parameters of the streamflow model, used for predicting the flow duration curve, are estimated based on climatic and geomorphological data.

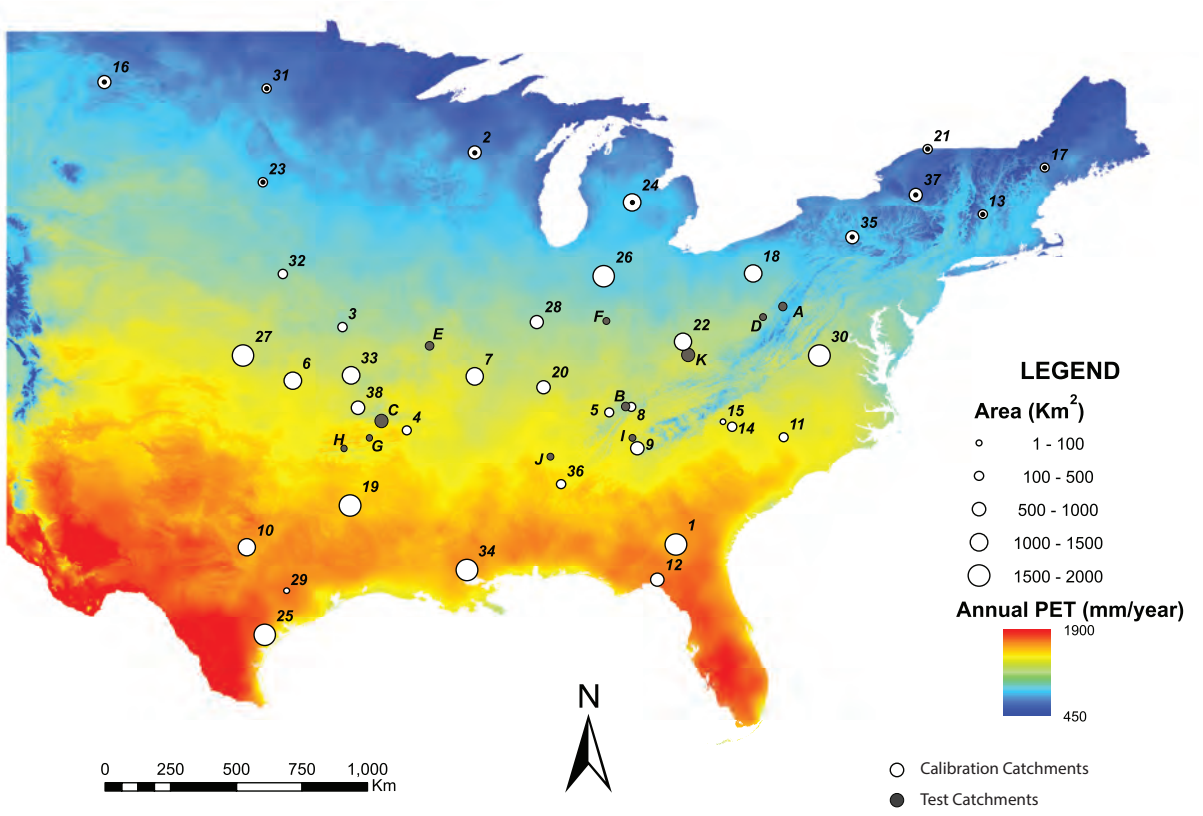

Fig. 2.2: Spatial distribution of the 38 catchments used for the calibration of the water balance models and 11 test catchments (A through K) where the flow regime is predicted. The *CGIAR* average annual potential evapotranspiration is shown on the background to represent the underlying heterogeneity of climate regimes. The approximate size of each catchment is also depicted. The catchments marked with a dotted circle experience relevant snow precipitations during winter.

`//www.cgiar-csi.org`) based on the Hargreaves method. This information was integrated into a geographical information system (ESRI ArcGis 10.0). Spatially averaged value of PET was calculated for every catchment and every PET dataset. The results of both models were compared and it was found that the MODIS model provides larger estimates of PET with respect to the CGIAR model, both at seasonal and annual time scales. However, the difference is relativity small and constant, thereby allowing for the comparison between the two models to be viable. For each catchment, daily rainfall records provided by the American National Oceanic and Atmospheric Administration (NOAA), and daily discharge records provided by the United States Geological Survey (USGS) were used. Available time series typically span several decades. The 49 catchments considered in this study were chosen such that synchronous rainfall and discharge data were available for at least 10 years (Table 2.1). The exact location of the discharge gauges were determined on a detailed map of the river network of the United States provided by the NOAA (info: `http://www.nws.noaa.gov/geodata/catalog/hydro/metadata/riversub.htm`; download: `https://www.ncl.ucar.edu/Applications/Data/`). The contributing catchments and drainage networks upstream of the discharge gauging stations were then estimated. For each streamflow gauging station selected in the study, a representative rainfall station (located as close as possible to the center of the catchment area) was selected. The reliability of using

just one rainfall gauge for each catchment was supported by previous studies [see *Botter et al.,* 2013], which proved that given the size of the basins (Table 2.1) selected in this study, the spatial variability of daily rainfall statistics is weak, and the use of a single rainfall station does not introduce any remarkable bias in the analysis.

2.3 Analytical Model of p(Q): Linking Flow Regime to Geomorphoclimatic Data

The river flow regime can be characterized by the seasonal probability density function (PDF) of daily streamflows described in this work through the analytical mechanistic model developed by *Botter et al.* [2009]. This model is based on a catchment-scale soil water balance forced by stochastic rainfall which is modeled (at daily timescale) as a marked Poisson process with frequency λ_P $[T^{-1}]$ and exponentially distributed depths with average α $[L]$ [*Rodriguez-Iturbe et al.,* 1999; *Porporato et al.,* 2004; *Botter et al.,* 2007a]. In this method the dynamics of the specific streamflow Q (per unit catchment area) is made up of two components: (i) instantaneous jumps (effective rainfall) corresponding to rainfall events filling the soil water deficit in the root zone. Effective rainfall events take place with frequency $\lambda < \lambda_P$ and are also represented by a marked Poisson process; (ii) power law decays in between events, as implied by a non-linear catchment-scale storage-discharge relationship [*Brutsaert and Nieber* 1997; *Porporato and Ridolfi,* 2003; *Kirchner,* 2009; *Botter et al.,* 2009]. Therefore, the temporal dynamics of Q during a given season is described by the following relation:

$$\frac{dQ\,(t)}{dt} = -KQ\,(t)^a + \xi_Q(t) \tag{2.1}$$

where $\xi_Q(t)$ represents the stochastic noise (the sequence of state dependent random jumps of Q, associated with those rainfall events which produce streamflow); $K[L^{1-a}T^{2-a}]$ and a are the coefficient and exponent of the power law relation that describes the rate of decrease of Q during the recession. The steady-state PDF of streamflows can be derived from the solution of the master equation associated to equation (2.1) [*Botter et al.,* 2009] as:

$$p(Q) = CQ^{-a} \exp\left(-\frac{Q^{2-a}}{\alpha K(2-a)} + \frac{\lambda Q^{1-a}}{K(1-a)}\right) \tag{2.2}$$

where C is a suitable normalizing constant. Equation (2.2) expresses the seasonal flow regime as a function of four physically-based parameters that embed the geomorphic and climate features of the contributing catchment. While mean discharge is only a function of α and λ (see section 4.2), all four model parameters contribute to defining the shape of $p(Q)$, leading to the emergence of a variety of regimes (see Figure 11 in *Botter et al.,* 2009). Note that Equation (2.2) holds only for cases where $a > 1$, which include the large majority of catchments in real world settings [*Biswal and Marani,* 2010; *Mutzner et al.,* 2013]. The cases where $a < 1$ can be handled using a similar approach [*Botter et al.,* 2009].

The flow duration curve is expressed by the cumulative distribution function (CDF) of Q and can therefore be calculated by integrating equation (2.2):

$$D(Q) = \int_Q^{+\infty} p(x)dx \tag{2.3}$$

	USGS Code	Catchment	Area [km^2]	Streamflow Gauging Station	Rainfall Gauging Station	State	Period
1	02316000	Alapaha River	1717	Alapaha	Alapaha Exp Stn	GA	1951-2013
2	05399500	Big Eau Pleine River	580	Stratford	Stratford 1NW	WI	1950-2013
3	06893100	Blue River	170	Kenneth	Stilwell	KS	2003-2013
4	07261000	Cadron Creek	438	Guy	Greenbrier	AR	1961-2013
5	03419800	Calfkiller River	453	Sparta	Sparta Waste Water Plan	TN	2003-2013
6	07172000	Caney River	1153	Elgin	Cedar Vale 5 SSE	KS	1961-2013
7	07021000	Castor River	1090	Zalma	Zalma 4E	MO	1951-2013
8	03539778	Clear Creek	440	Lancing	Lancing 6 NW	TN	1999-2013
9	02380500	Coosawattee River	611	Ellijay	Ellijay	GA	1951-2013
10	08101000	Cowhouse Creek	1167	Pidkoke	Pidcoke	TX	1976-2013
11	02133500	Drowning Creek	474	Hoffman	Jackson Springs 5 WNW	NC	1954-2013
12	02326000	Econfina River	513	Perry	Perry	FLA	1957-2013
13	01170100	Green River	107	Colrain	Whitingham	MA	1969-2013
14	02143500	Indian Creek	179	Laboratory	Lincoln 4 W	NC	1952-2013
15	02143040	Jakob Fork	67	Ramsey	Casar	ND	1961-2013
16	06339100	Knife River	531	Manning	Fairfield	ND	1971-2013
17	01057000	Little Androscoggin River	190	South Paris	West Paris	ME	1980-2013
18	03109500	Little Beaver Creek	1284	East Liverpool	Millport 3NE	OH	1951-2013
19	07346070	Little Cypress Bayou	1748	Jefferson	Harleton	TX	1951-2013
20	03438000	Little River	632	Cadiz	Hopkinsville	KY	1951-2013
21	04270200	Little Salmon River	239	Bombay	Malone	NY	1985-2013
22	03216500	Little Sandy River	1036	Grayson	Grayson 3 SW	KY	1951-2013
23	06478540	Little Vermillion River	204	Salem	Montrose	SD	1968-2013
24	04115000	Maple River	1124	Maple Rapids	Saint Johns	MI	1951-2013
25	08189500	Mission River	1787	Refugio	Beeville 5 NE	TX	1987-2013
26	03326500	Mississinewa River	1766	Marion	Marion 2 N	IN	1951-2013
27	07144780	Nf Ninnescah River	1847	Caheny	Hutchinson 10 SW	KS	1984-2013
28	03346000	North Fork Embarras River	824	Oblong	Casey	IL	1951-2013
29	08160800	Redgate Creek	45	Columbus	Columbus	TX	1964-2013
30	02034000	Rivanna River	1717	Palmyra	Charlottesville 2 W	VA	1951-2013
31	05060500	Rush River	300	Amenia	Casselton Agronomy	ND	1986-2013
32	06803000	Salt Creek	433	Roca	Roca	NE	1953-2013
33	07185765	Spring River	1101	Carthage	Mt Vernon	MO	1968-2013
34	07375500	Tangipahoa River	1673	Robert	Hammond 5 W	GA	1981-2013
35	01518000	Tioga River	730	Tioga	Covington 2 WSW	GA	1958-2013
36	02462000	Valley Creek	383	Oak Grove	Bankhead Dam	GA	1959-2013
37	01343060	West Canada Creek	668	Wilmurt	Piseco	NY	2003-2013
38	06444000	White River	811	Crawford	Ft Robinson	NE	1941-2013

Tab. 2.1: Summary information about the 38 catchments used for the calibration of water balance models.

	USGS Code	Catchment	Area [km^2]	Streamflow Gauging Station	Rainfall Gauging Station	State	Period
A	03075500	Youghiogheny River	347	Oakland	Oakland 1 SE	MD	1951-2013
B	03539600	Daddys Creek	360	Hebbertsburg	Crossville mep ap	TN	1958-2013
C	07257006	Big Piney Creek	793	Highway 164	Deer	AR	1995-2013
D	03052500	Sand Run	37	Buckhannon	Buckhannon	WV	1951-2013
E	07015720	Bourbeuse River	350	High Gate	vichy rolla	MO	1966-2014
F	03368000	Brush Creek	30	Nebraska	north vernon	IN	1956-2014
G	07260000	Dutch creek	211	Waltreak	gravelly	AR	1946-2014
H	07335700	Kiamichi River	103	Big Cedar	mena	OK	1966-2014
I	02384540	Mill creek	21	Crandall	chatsworth	GA	1986-2014
J	02450250	Sipsey Fork	239	Grayson	haleyville	AL	1967-2014
K	03211500	Johns Creek	534	Van Lear	fishtrap lake	KY	1970-2014

Tab. 2.2: Summary information about the 11 test catchments.

Closed-form analytical expressions of $D(Q)$ are available only for special cases (e.g. $a \in \mathbb{N}$).

The above model considers streamflows at the daily time scale and fast components of the hydrologic response are implicitly incorporated in the non-linear storage-discharge relationship that drives the soil drainage. The major assumptions underlying the analytical formulation shown in equation (2.2) are: (*i*) the Poisson distribution of flow-producing events; (*ii*) the exponential distribution of the daily rainfall (and effective rainfall) depths; (*iii*) the lack of inter-event variability of recession features; (*iv*) the spatial homogeneity of climate and landscape properties at the catchment scale. Moreover, the interference caused by snow accumulation and melting is not explicitly included in the formulation. The possible presence of carryover flows across different seasons (when significant) is accounted for by suitably adjusting the frequency of flow producing events λ. Extensive applications and generalizations of this approach have been published in previous studies [*Botter et al.,* 2010a, 2013; *Ceola et al.,* 2010; *Pumo et al.,* 2013; *Schaefli et al.,* 2013; *Mejia et al.,* 2013; *Müller et al.,* 2014].

2.4 Estimating the Parameters of p(Q)

The PDF of streamflows (equation (2.2)) relies on four parameters: α, λ, K, and a, which incorporate important climatic and geomorphologic features of the catchment. In the eleven test catchments the value of α is estimated from rainfall data, while a and K are estimated through a geomorphic recession model that is applied locally. The value of λ is estimated for each test catchment through water balance models that are independently calibrated based on rainfall and discharge data from 38 different catchments in the same study area. The estimation methods are explained in detail below.

2.4.1 Computation of α

Mean rainfall depth (α) is estimated by means of daily rainfall data recorded at climatic stations within the boundaries of each catchment. In particular, α is calculated as the mean precipitation during wet days (i.e. days with rainfall depth above zero) in the considered season.

2.4.2 Computation of λ

According to the analytical formulation described in section 3, the filtering performed by catchment scale soil moisture dynamics leads to a decrease in frequency of events (from λ_p to λ) without impacting the distribution of the depths [*Porporato et al.,* 2004; *Botter et al.,* 2007a]. The long-term mean of P and Q can then be expressed as $\langle P \rangle = \alpha \lambda_p$ and $\langle Q \rangle = \alpha \lambda$, respectively. Hence, the frequency of effective rainfall events λ can be estimated as $\lambda = \phi \, \lambda_p$, where λ_p is the frequency of rainfall events (estimated as the relative fraction of rainy days in the seasonal time series) and $\phi = \langle Q \rangle / \langle P \rangle$ is the average seasonal runoff coefficient (i.e. the ratio of mean discharge to mean precipitation). ϕ can be estimated by means of calibrated water balance models using precipitation and PET data.

Code	Number of parameters	Main Equation	Notes	Relevant References
WB1	0	$\phi = 1 - \left[D_I(1 - e^{-D_I})\, tanh\left(\frac{1}{D_I}\right)\right]^{0.5}$	$D_I = \langle PET \rangle / \langle P \rangle$	Budyko, 1974
WB2	1-4	$\phi = \frac{D_I \gamma^{\frac{\gamma}{D_I}} e^{-\gamma}}{\gamma\, \Gamma(\gamma/D_I, \gamma)}$	$\gamma = \frac{(s_1 - s_w) n Z}{\alpha}$; s_w = the wilting point; n = porosity; Z = rooting depth; s_1 = proxy of field capacity;	Porporato et al., 2004
WB3	2	$\phi = 1 - (1 - D_I) \sum_{j=0}^{\infty} \left[1 + j\gamma(D_I^{-1} - 1)k^{-1}\right]^{-k} {D_I}^j$ for $D_I < 1$ $\phi = 1 - (1 - D_I^{-1}) \sum_{j=0}^{\infty} \left[1 + (j+1)\gamma(1 - D_I^{-1})k^{-1}\right]^{-k} {D_I}^{-j} 1$ for $D_I > 1$	-	Milly, 1994
WB4	4	$\phi = \frac{1 + \widetilde{\langle P \rangle}\varphi}{1 + \varphi + \widetilde{\langle P \rangle}\varphi}$	$\varphi = \frac{PET - \lambda_u PET}{\langle P \rangle - \lambda_s W_p}$; $\widetilde{\langle P \rangle} = \frac{\langle P \rangle - \lambda_s W_p}{(1 - \lambda_s) W_p}$; PET =potential evapotranspiration; W_p =upper bound of mean catchment wetting; λ_s and λ_u = empirical parameters	Sivapalan et al., 2011

Tab. 2.3: Water balance models.

Four existing water balance models were tested and compared by analyzing their ability to predict observed runoff coefficients at 38 catchments within the study region (Table 2.3). The models are: the empirical *Budyko* [1974] approach (WB1), the stochastic physically-based approaches of *Porporato et al.* [2004] (WB2) and *Milly et al.* [1994] (WB3), and the semi-empirical method proposed by *Sivapalan et al.* [2011] (WB4). The models adopted, their governing equations for estimation of average seasonal runoff coefficients, as well as appropriate references are listed in Table 2.3. The main features of each model are explained in detail in the supplementary information. Each model has a different number of parameters, which were calibrated in order to maximize model performances. The number of catchments used for calibration of the water balance model was deliberately maximized to test each model under a broad range of hydro-climatic conditions and identify the best approach in general within the study area. In this paper, we assume the spatial variability of the water balance within the study region can be explained by the underlying heterogeneity of the precipitation and PET. Hence, model parameters were assumed to be spatially homogeneous, so that the calibrated parameters can be exported to other catchments within the study region, including the eleven test catchments where flow regimes are predicted. An alternative approach where the parameters of the water balance models were allowed to be spatially variable, across a predefined set of geographic-climatic sub regions, was also tested. This approach provided a very small improvement of model performance despite a significant increase in number of calibration parameters, and was therefore discarded.

Some of the models applied here are based on hypotheses that only hold at the annual timescale (WB3), or they have been previously applied mainly at the annual level (WB1). Because of this reason they are best applicable to estimate annual runoff coefficients. To get an estimate of the inter-seasonal variability of streamflow regimes during the year, the knowledge of seasonal average runoff coefficients would instead be desirable. To this aim, a novel approach has been developed in order to describe the inter-seasonal variability of the water balance based on annual estimates.

The average annual runoff coefficient ($\phi_a = \frac{\langle Q \rangle_a}{\langle P \rangle_a}$) can be expressed as a weighted mean of the seasonal average runoff coefficients. Accordingly, the seasonal runoff coefficient $\phi_i = \frac{\langle Q \rangle_i}{\langle P \rangle_i}$ can be calculated by multiplying the annual runoff coefficient ϕ_a by a Seasonal Multiplication Factor ψ_i which expresses the inherent seasonality of the water balance:

$$\phi_i = \phi_a \psi_i \tag{2.4}$$

where ϕ_a is estimated using one of the four water balance models described above, and $\psi_i = \phi_i / \phi_a$ is the ratio between seasonal and annual runoff coefficient during the season i. Note that the typical subdivision into four seasons, broadly following the calendar dates, has been adopted in this paper. Equation (2.4) expresses the idea that even though the annual runoff coefficient may vary significantly among catchments, the seasonal pattern may be relatively uniform across a wide range of conditions. Despite some scattering, the results obtained in the 38 study catchments corroborate the assumption that ψ_i are quite homogenous (see Figure 2.3). The values of ψ_i were thus assumed to be spatially uniform and were calibrated based on observed rainfall and streamflow data.

2.4.3 Computation of a and K

The estimation procedure for the recession parameters a and K is rooted in the idea that recession properties are strongly related to the morphology of the stream network [*Biswal and Marani,*

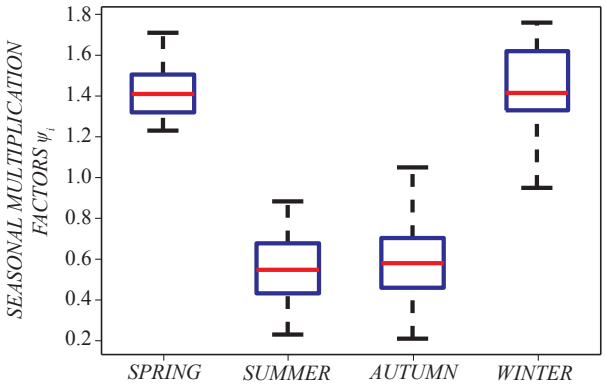

Fig. 2.3: Seasonal multiplication factors for the four seasons: spring (March, April, May), summer (June, July, August), autumn (September, October, November), winter (December, January, February). The box plot shows the 25%, 50% and 75% quantiles as well as the entire range of observed values across the 38 study catchments.

2010; *Mutzner et al.,* 2013; *Biswal and Nagesh Kumar,* 2014a; *Biswal and Marani,* 2014]. During recessions both the streamflow and the active drainage network – which represents the fraction of the network that actively contributes to the flow at the outlet – decrease over time [*Gregory and Walling,* 1968; *Weyman,* 1970; *Godsey and Kirchner,* 2014]. The active drainage network (ADN hereafter) is thus assumed to expand and contract following the related streamflow fluctuations. The theoretical apparatus on which the GRFM model is grounded, as well as the performance of the model under various settings are detailed in a series of recent papers (*Biswal and Nagesh Kumar* [2013]; *Biswal and Marani* [2014] and references therein), where the relevant details can be found. In summary, the specific streamflow Q is expressed as:

$$Q = \frac{q\,G}{A} \tag{2.5}$$

where G is the length of the active drainage network, q is the flow generation rate per unit channel length, and A the catchment area. Three simplifying assumptions are then introduced: (i) drainage density is spatially uniform; (ii) both the flow generation per unit channel length q and the speed at which the ADN contracts towards the outlet (c) are constant; (iii) the changes of G through time are expressed in terms of the changes of G induced by changes of the maximum path length within the ADN, l (which is the maximum distance between a point of ADN and the furthest source of the network): $dG/dt = dG/dl \cdot dl/dt = c\,dG(l)/dl$.

Under these assumptions, the recession equation $dQ/dt = KQ^a$ can be rewritten as [*Biswal and Marani,* 2014]:

$$\frac{N(l)}{A} = \rho' \left(\frac{G(l)}{A}\right)^a \tag{2.6}$$

where $N(l) = dG(l)/dl$ is the number of links in the network at a distance l from the outlet, and $\rho' = Kq^{a-1}/c$. Equation (2.6) states that the recession exponent a can be estimated from the morphology of the basin by analyzing the scaling exponent of the geomorphic relationship between $N(l)$ and $G(l)$. These functions can be derived from the analysis of digital terrain maps. The scaling exponent of the functions $G(l)$ vs. $N(l)$ can be easily calculated through least-squared regression, thereby allowing an objective estimate of the recession exponent from morphological data.

In order to estimate the recession coefficient K, we first calculate the temporal mean of Equation (2.5) such that $\langle Q \rangle = q\, D_d$, where $D_d = \langle G \rangle / A$. Noting the analytical expression of mean specific discharge from the streamflow model, mentioned in the previous section, q can then be expressed as: $q = \frac{\alpha\lambda}{D_d}$. Combining this equation with the definition of ρ', mentioned before, leads to:

$$K = \rho' c q^{1-a} = \theta(\alpha\lambda)^{1-a} \tag{2.7}$$

where $\theta = \rho' c / D_d^{1-a}$. Equation (2.7) expresses that K is inversely related to the mean discharge $\alpha\lambda$, as well as to the recession exponent a. Moreover, K has been associated with mean humidity conditions in the catchment [*Shaw and Riha,* 2012; *Shaw et al.,* 2013; *Biswal and Nagesh Kumar,* 2014b]. Empirical analysis based on observed recessions in multiple catchments suggests that the value of θ is fairly constant across different catchments and seasons. Therefore, here we assume θ to be constant and calculate its value based on summer season streamflows in a randomly selected pilot catchment (Williams Basin, US where $\theta = 0.23\, d^{-1}$). Equation (2.7) can then be used to predict K based on a, α and λ.

In the eleven test catchments where the prediction of flow regime was performed, the river network was estimated based on 30 m USGS DEMs (obtained from: `http://gdex.cr.usgs.gov/gdex/`). These catchments can be broadly classified as gently sloping (average slope $< 5\%$). Therein, the D8 flow direction algorithm [*Mark*, 1988] was used to obtain the flow direction maps, and subsequently the flow accumulation maps. A Flow accumulation threshold of $0.09\, km^2$ was then imposed to delineate channel networks for these eleven test catchments.

2.5 Results

2.5.1 Water Balance Model Ranking

For the presentation of the results of the water balance models, the following notation has been used to uniquely identify each model and the set of possible variants adopted. Each water balance model is labeled by a string which is composed of four parts:

$$\underbrace{\mathbf{WB1}}_{1}.\underbrace{\mathbf{ET1}}_{2}.\underbrace{\mathbf{A}}_{3}\underbrace{\mathbf{(1)}}_{4}$$

(1) refers to the specific water balance model (Table 2.3); (2) identifies the potential evapotranspiration dataset used in the model calibration: ET1 refers to $CGIAR$ while ET2 refers to $MODIS$; (3) denotes the model time scale: A implies the model has been applied at the annual time scale; S implies the model has been applied at the seasonal time scale; Sc implies that the model has been applied at the annual time scale and then the seasonal water balance has been evaluated by making use of the seasonal multiplication factors ψ; (4) specifies the numbers of model parameters used in the calibration (when necessary).

Many of the models considered include the average rooting depth Z as a key parameter. Z drives the maximum soil moisture storage capacity $nZ(s_1 - s_w)$. Hence, for convenience and without any loss of generality, s_w, s_1 and n are assumed to be constant throughout all simulations (and equal to 0.2, 0.5 and 0.35, respectively), while only Z was calibrated. Note that different

Rank	Model	Number of parameters	Δ AIC	MSE	Parameters
1	WB4.ET1.A	1	0.0	0.0079	$\lambda_u = 0.2$
2	WB4.ET2.A	1	8.0	0.0097	$\lambda_u = 0.2$
3	WB1.ET1.A	0	11.6	0.0112	-
4	WB2.ET1.A	1	16.6	0.0121	$Z = 420mm$
5	WB2.ET2.A	1	26.8	0.0157	$Z = 300mm$
6	WB3.ET1.A	2	29.8	0.0161	$Z = 900mm$, $k = 0.525$
7	WB1.ET2.A	0	36.9	0.0214	-
8	WB3.ET2.A	2	38.8	0.0203	$Z = 700mm$, $k = 0.525$

Tab. 2.4: Ranking of water balance models applied at the annual time scale.

versions of each model were implemented, where either a single value of Z or different values of Z for each season (or two seasons) were considered.

With regards to the four water balance models, the deviance of observed vs. modeled results was first quantified by the Mean Square Error (MSE), defined as $MSE = 1/N \sum_{i=1}^{N} \epsilon_i^2$ where ϵ is the difference between modeled and observed runoff coefficients, and N is the number of cases in which the models are tested ($N = 38$). Furthermore, performances of each model has been objectively quantified by means of the *Akaike Information Criterion* (AIC) [*Akaike,* 1973]. The method provides a rigorous way for model selection based on the maximization of the log-likelihood function between experimental data and model estimates. The goodness of fit of each model is discounted by accounting for the number of parameters that are fitted to observations. The formulation of AIC used to rank the different water balance models in this study is as follows [*Burnham and Anderson*, 2002]:

$$AIC = 2\,N\,MSE + 2(M + 1), \tag{2.8}$$

where N is the number of independent catchments used to evaluate the models and M is the number of calibrated parameters. Table 2.4 summarizes the performances of the water balance models applied at the annual time scale and values of calibrated parameters that optimize model performance.

WB1 and WB2 prove quite effective at the annual timescale, especially in association with ET1. Overall, WB4 seems to be the best model in order to estimate the average annual water balance in the study area. Though, its performance is only slightly better than those of WB1 which has no calibrated parameters. It is noteworthy to mention that the calibration of the annual models led to reasonable values of Z in all cases ($500 < Z < 1000$), in agreement with previous studies [*Allen et al.,* 1998]. In general all models perform better when coupled with the ET1 dataset.

Table 2.5 summarizes the results of the water balance models applied at the seasonal time scale. The performance of WB1 at seasonal scale is not as good as those at annual time scale. However, considering the absence of calibrated parameters in the Budyko approach, WB1 performance at the seasonal time scale is notable. Similarly, WB4 performances at the seasonal timescale are also quite poor, which is possibly a result of the coupling with the seasonal coefficients. Nonetheless, the overall performance of the method utilizing annual models and the seasonal multiplication factors are comparable to the performance of the same models applied across seasons. The observed inter-catchment variability of ψ_i across the study area (in the set of

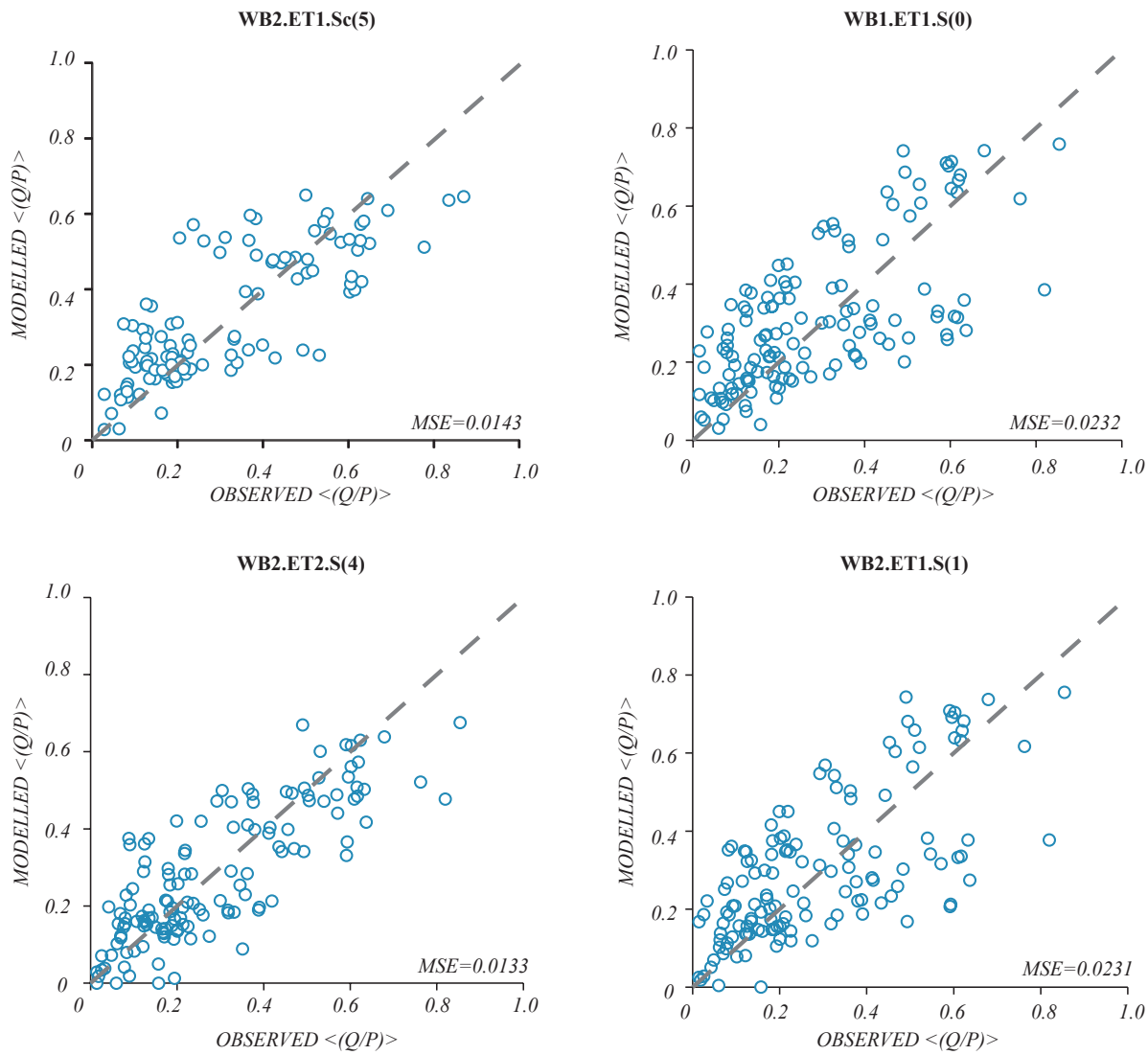

Fig. 2.4: Scatter-plots of observed vs. estimated runoff coefficients by a select number of calibrated models at the seasonal time scale. The value of MSE is also included.

38 calibration catchments) is relativity low (Figure 2.3) despite the broad range of hydro-climatic conditions explored. When the seasonal multiplication factors are used, the best performing models are WB2 and WB3. Overall, at seasonal time scale, WB2 was found to be the best performing model, especially when the rooting depths Z was separately calibrated for each season.

Figure 2.4 shows the scatter-plots of a select number of calibrated models – including the three best performing models– at the seasonal time scale for the 38 calibration catchments. On the y-axis the modeled value of the runoff coefficient is shown, while the observed value, calculated as the ratio between the average seasonal precipitation and runoff, is shown on the x-axis. Despite some scattering, WB1 and WB2 (presented here) exhibit satisfying performances in estimating the seasonal runoff coefficients.

The performances of all four models at the seasonal time scale, without differentiation between the two PET datasets and the different versions of each model implemented, are shown in

Rank	Model	Number of parameters	Δ AIC	MSE	Parameters
1	WB2.ET2.S	4	0	0.0133	$Z_{wi} = 570mm$, $Z_{sp} = 195mm$, $Z_{su} = 510mm$, $Z_{au} = 975mm$
2	WB2.ET1.S	4	1.0	0.0134	$Z_{win} = 1500mm$, $Z_{sp} = 240mm$, $Z_{su} = 570mm$, $Z_{au} = 1500mm$
3	WB2.ET1.Sc	5	11.7	0.0143	$Z = 420mm$, $\psi_{wi} = 1.44$, $\psi_{sp} = 1.42$, $\psi_{su} = 0.56$, $\psi_{au} = 0.59$
4	WB2.ET1.S	2	21.6	0.0161	$Z_{su,sp} = 450mm$, $Z_{au,wi} = 1500mm$
5	WB2.ET2.S	2	34.3	0.0177	$Z_{su,sp} = 330mm$, $Z_{au,wi} = 900mm$
6	WB2.ET2.Sc	5	41.1	0.0184	$Z = 300mm$, $\psi_{wi} = 1.44$, $\psi_{sp} = 1.42$, $\psi_{su} = 0.56$, $\psi_{au} = 0.59$
7	WB3.ET1.Sc	6	43.8	0.0186	$Z = 900mm$, $k = 0.0525$, $\psi_{wi} = 1.44$, $\psi_{sp} = 1.42$, $\psi_{su} = 0.56$, $\psi_{au} = 0.59$
8	WB2.ET2.S	1	60.8	0.0219	$Z = 435mm$
9	WB1.ET2.S	0	63.0	0.0226	-
10	WB3.ET2.Sc	6	66.5	0.0215	$Z = 700mm$, $k = 0.0525$, $\psi_{wi} = 1.44$, $\psi_{sp} = 1.42$, $\psi_{su} = 0.56$, $\psi_{au} = 0.59$
11	WB1.ET1.S	0	66.6	0.0232	-
12	WB2.ET1.S	1	68.0	0.0231	$Z = 615mm$
13	WB1.ET1.Sc	4	100.7	0.0281	$\psi_{wi} = 1.44$, $\psi_{sp} = 1.42$, $\psi_{su} = 0.56$, $\psi_{au} = 0.59$
14	WB4.ET1.Sc	5	103.7	0.0271	$\lambda_u = 0.2$, $\psi_{wi} = 1.44$, $\psi_{sp} = 1.42$, $\psi_{su} = 0.56$, $\psi_{au} = 0.59$
15	WB4.ET2.Sc	5	109.7	0.0300	$\lambda_u = 0.2$, $\psi_{wi} = 1.44$, $\psi_{sp} = 1.42$, $\psi_{su} = 0.56$, $\psi_{au} = 0.59$
16	WB1.ET2.Sc	4	134.9	0.0367	$\psi_{wi} = 1.44$, $\psi_{sp} = 1.42$, $\psi_{su} = 0.56$, $\psi_{au} = 0.59$

Tab. 2.5: Ranking of water balance models applied at the seasonal time scale. Subscripts of Z indicate the different seasons (sp = spring, su = summer, au = autumn, and wi = winter).

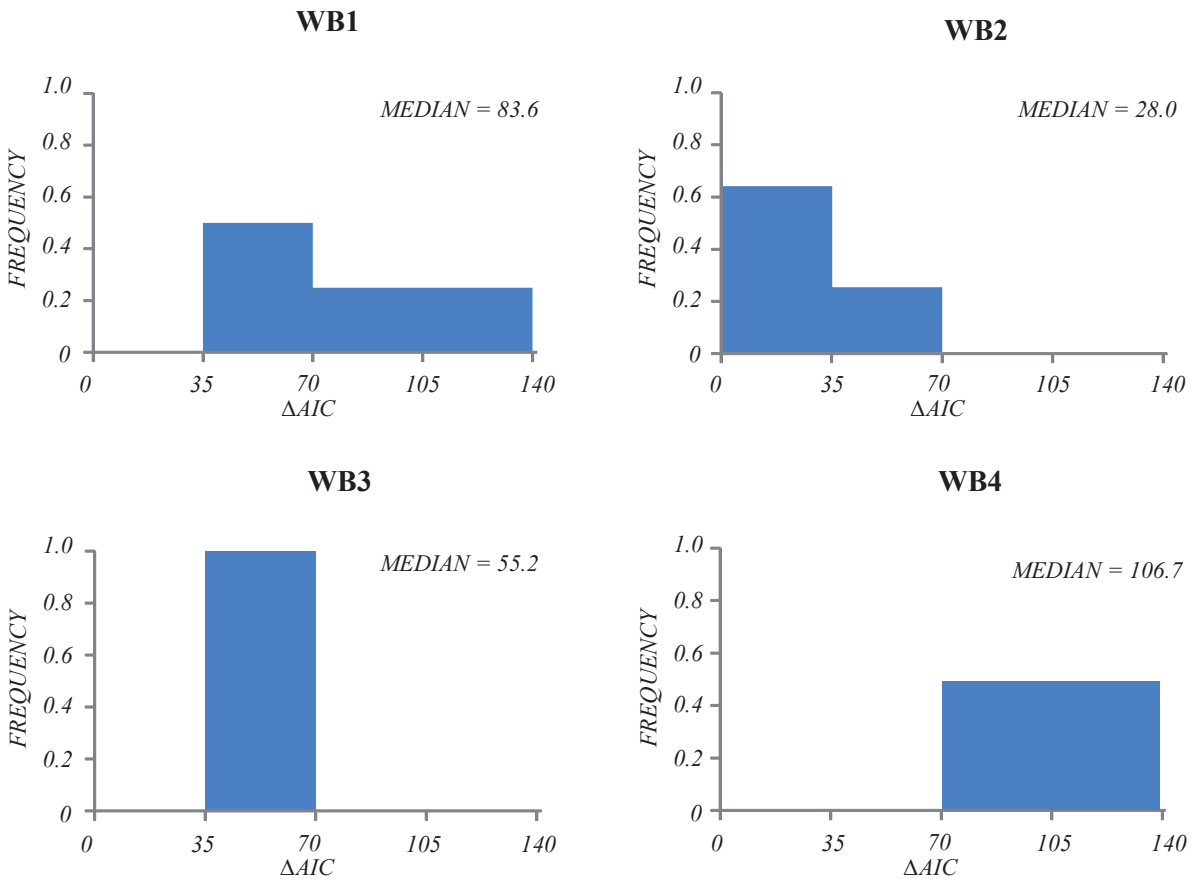

Fig. 2.5: Frequency distribution of ΔAIC for all water balance models. The median value of ΔAIC is also included.

Figure 2.5. The histograms represent the frequency distribution of ΔAIC among the variants of each model and are complemented with the median value of ΔAIC, thereby allowing an objective assessment of the overall performances of each approach. WB2.ET2.S(4) is characterized by the smallest mean value of ΔAIC, implying that (on average) it outperforms the other models.

Lastly, WB2.ET2.S(4) was utilized for predicting the runoff coefficient at 11 test catchments. The ability of WB2.ET2.S(4) to describe the seasonal water balance at the eleven test catchments is analyzed in Figure 2.6, which compares observed vs. estimated values of the runoff coefficient for all the available seasons. Performance is relatively good in most cases, especially in view of the fact that no specific information on observed discharge at the test catchments has been used. A slight underestimation of runoff coefficients is observed for energy limited catchments and seasons, which is a possible by-product of neglecting surface runoff in the water balance model. One outlier is noticeable in the right hand side of the plot. This point refers to the spring season of a mountainous catchment (Youghiogheny river) that is possibly affected by snow melt during this season.

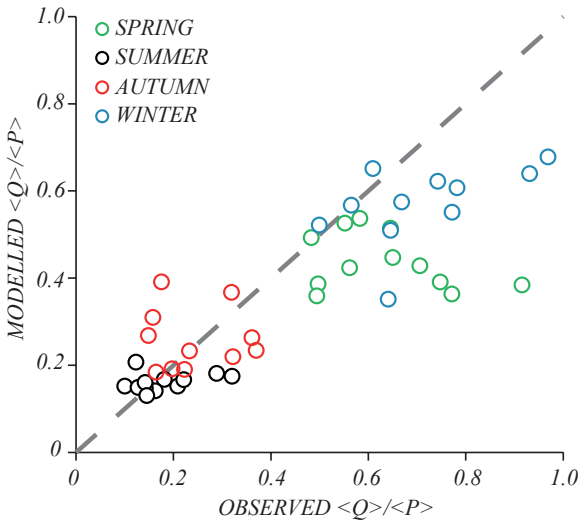

Fig. 2.6: Scatter-plot of the seasonal average runoff coefficient for the eleven test catchments based on the WB2.ET2.S(4) water balance model.

2.5.2 *Prediction of $p(Q)$*

Streamflow distributions for every season were predicted at 11 catchments, corresponding to 44 seasonal regimes (Table 2.2). The test catchments are basins with natural streamflows, not affected by regulation or significant snow dynamics, and are distributed across the study region. It is important to note, this study is aimed at presenting and exemplifying the general methodology and therefore, an extensive regional study is beyond the scope of the paper.

The parameters of the analytical streamflow PDF were estimated for the eleven test catchments using only climate and landscape data as discussed in Section 4. Table 2.6 shows the resulting values of α, λ, a and K for each season in the eleven test catchments. For comparison, the observed values of λ, a and K were also calculated based on discharge data [*Biswal and Marani,* 2010; *Ceola et al.,* 2010]. In agreement with results depicted in Figure 2.6, the estimates of λ based on precipitation and PET data show a broad agreement with the corresponding estimates based on discharge data. The geomorphological estimates of a (which are assumed to be independent of the season) show variable performances across the different catchments. In most cases there is a general agreement with the median value of the recession exponent calculated based on discharge data, while in a few cases a visible deviation is observed. The geomorphological estimates of K instead, are in agreement only in half the cases when compared to the estimated value of the recession coefficient based on discharge observation. The lower performance is most noticeable in catchments located in water limited regions. This can be attributed to the discrepancy between the flow generation processes in such environments and the underlying assumptions of the geomorphological model discussed in section 4 [see *Biswal and Nagesh Kumar,* 2013]. It is important to note that the value of θ (calculated based on observed discharge time series via Equation 2.7) is weakly variable across different catchments and seasons ($CV \approx 0.4$), thereby corroborating the reliability of the assumption that θ is constant in Equation (2.7).

Catchment Name	Season	Estimated from Climate and Geomorphologic Data				Estimated from Discharge Data		
		$\alpha[cm]$	$\lambda[\frac{1}{d}]$	$K[\frac{cm^{(1-a)}}{d^{(2-a)}}]$	$a[-]$	$\lambda[\frac{1}{d}]$	$K[\frac{cm^{(1-a)}}{d^{(2-a)}}]$	$a[-]$
Youghiogheny River (A)	*Spring*	0.73	0.19	0.84	1.65	0.45	0.45	1.68
	Summer	0.89	0.07	1.48	1.65	0.13	1.09	1.75
	Autumn	0.74	0.09	1.30	1.65	0.15	1.27	1.90
	Winter	0.63	0.35	0.62	1.65	0.50	0.57	1.84
Daddy Creek (B)	*Spring*	1.08	0.18	0.87	1.81	0.26	0.61	1.73
	Summer	1.02	0.06	2.31	1.81	0.05	1.05	1.44
	Autumn	1.04	0.07	1.91	1.81	0.07	1.42	1.67
	Winter	0.95	0.26	0.71	1.81	0.31	0.71	1.89
Big Piney Creek (C)	*Spring*	1.61	0.16	1.16	2.19	0.17	0.45	1.57
	Summer	1.17	0.03	9.75	2.19	0.04	0.92	1.54
	Autumn	1.79	0.10	1.99	2.19	0.04	1.25	1.71
	Winter	1.31	0.14	1.68	2.19	0.14	0.57	1.71
Sand Run River (D)	*Spring*	0.72	0.18	1.85	2.02	0.38	0.76	1.73
	Summer	0.95	0.07	3.79	2.02	0.09	1.43	1.52
	Autumn	0.76	0.08	3.84	2.02	0.12	1.86	1.76
	Winter	0.56	0.35	1.19	2.02	0.51	0.93	1.86
Bourbeuse River (E)	*Spring*	0.99	0.14	1.40	1.90	0.17	2.01	1.76
	Summer	1.17	0.04	1.20	1.90	0.05	1.98	1.47
	Autumn	1.11	0.05	3.81	1.90	0.05	2.78	1.76
	Winter	0.72	0.09	2.77	1.90	0.16	2.16	1.86
Brush Creek (F)	*Spring*	1.03	0.15	1.74	2.10	0.2	2.91	1.96
	Summer	1.17	0.05	5.20	2.10	0.05	3.95	1.63
	Autumn	1.00	0.05	5.89	2.10	0.05	8.41	1.92
	Winter	0.84	0.18	1.86	2.10	0.20	2.63	1.87
Dutch Creek (G)	*Spring*	1.51	0.14	1.36	2.15	0.14	1.07	1.78
	Summer	1.33	0.04	7.47	2.15	0.02	1.11	1.47
	Autumn	1.57	0.06	3.41	2.15	0.03	1.46	1.67
	Winter	1.26	0.13	1.80	2.15	0.12	0.96	1.76
Kiamichi River (H)	*Spring*	1.45	0.17	0.74	1.85	0.22	0.49	1.58
	Summer	1.21	0.04	2.86	1.85	0.06	0.56	1.26
	Autumn	1.56	0.11	1.05	1.85	0.09	0.76	1.51
	Winter	1.14	0.17	0.93	1.85	0.23	0.47	1.67
Mill Creek (I)	*Spring*	1.18	0.14	3.28	2.50	0.23	0.85	2.22
	Summer	1.10	0.06	12.06	2.50	0.10	1.19	2.00
	Autumn	1.30	0.07	8.00	2.50	0.10	2.92	2.23
	Winter	1.10	0.22	1.84	2.50	0.29	0.82	2.14
Sipsey Fork (J)	*Spring*	1.58	0.16	0.77	1.90	0.17	0.75	1.84
	Summer	1.28	0.06	2.21	1.90	0.04	3.10	1.85
	Autumn	1.47	0.08	1.49	1.90	0.04	5.46	2.03
	Winter	1.47	0.22	0.63	1.90	0.20	0.77	1.89
Johns Creek (K)	*Spring*	0.82	0.16	2.96	2.25	0.21	0.59	1.58
	Summer	0.96	0.06	8.53	2.25	0.05	1.34	1.53
	Autumn	0.87	0.07	7.90	2.25	0.08	0.42	1.54
	Winter	0.60	0.24	2.55	2.25	0.30	0.31	1.20

Tab. 2.6: Estimated value of model parameters for all seasons at the eleven test catchments.

Equation (2.2) is used to model the "period-of-record" PDFs in the eleven test catchments. The agreement between modeled and observed PDFs (and the associated CDFs) was first evaluated through visual inspection. Model performances were then objectively quantified by comparing modeled and observed moments of the PDF, and by computing half the integral difference between the analytical and observed flow PDFs [*Botter et al.,* 2013]. The accuracy of the model was further analyzed by the Mean Squared Relative Error (MSRE) of selected flow statistics (see Table 1 in [*Biondi et al.,* 2012]).

As an example, Figure 2.7 presents the observed (bars) and modeled (solid line) seasonal streamflow PDFs at Daddy creek, US. The analytical model captures the shape of the observed

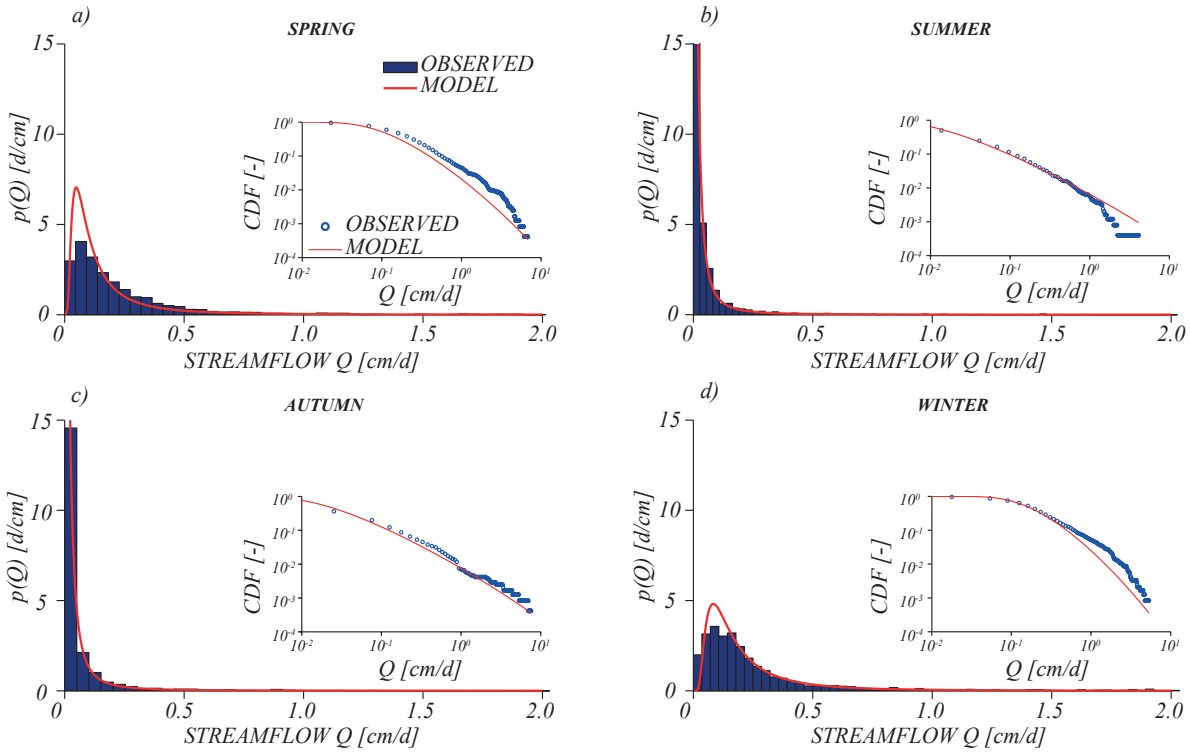

Fig. 2.7: Observed (circles and bars) and modeled (solid lines) PDFs and CDFs for (a) spring, (b) summer, (c) autumn and (d) winter at Daddy Creek, TN. The integral difference between modeled and observed PDFs is equal to (a) 0.220, (b) 0.212, (c) 0.203, and (d) 0.163.

probability distribution of flows relatively well in all seasons. Though, the model seems to slightly underestimate the high flows, providing lower probability for large events as compared to the observations. The ability of the model to catch the change in shape of the streamflow distribution across different seasons is particularly valuable. On a seasonal time scale, a catchment can produce both erratic and persistent regimes [*Botter et al.,* 2013]. In persistent regimes, the humped shape of the PDF indicates larger frequency of events contributing to streamflow with reduced flow variability. In contrast, in erratic regimes the monotonically decreasing shape of the PDF signifies smaller frequency of flow-producing events and enhanced flow variability. In Daddy Creek, there is a shift in streamflow PDF from hump-shaped in spring and winter seasons to monotonically decreasing in summer and autumn seasons (Figure 2.7). This is consistent with rainfall and PET patterns across the seasons (see *Botter* [2014]).

The insets of Figure 2.7 present the observed (circles) and modeled (solid line) CDFs of all seasons at Daddy Creek. A logarithmic scale has been used in order to better represent the behavior of the curves for large streamflows. The modeled CDFs are slightly shifted downward as compared to the observed CDFs. This is as a result of the reduced amount of water available for streamflow generation estimated by the water balance model. Nevertheless, the shape of the CDF seems to be reasonably captured in most seasons.

Figure 2.8 shows the observed (bars) and modeled (solid line) PDFs for the summer season at four other test catchments. During the summer season an erratic regime is observed as a result of low rainfall and enhanced transpiration rates, which imply increased frequency of the

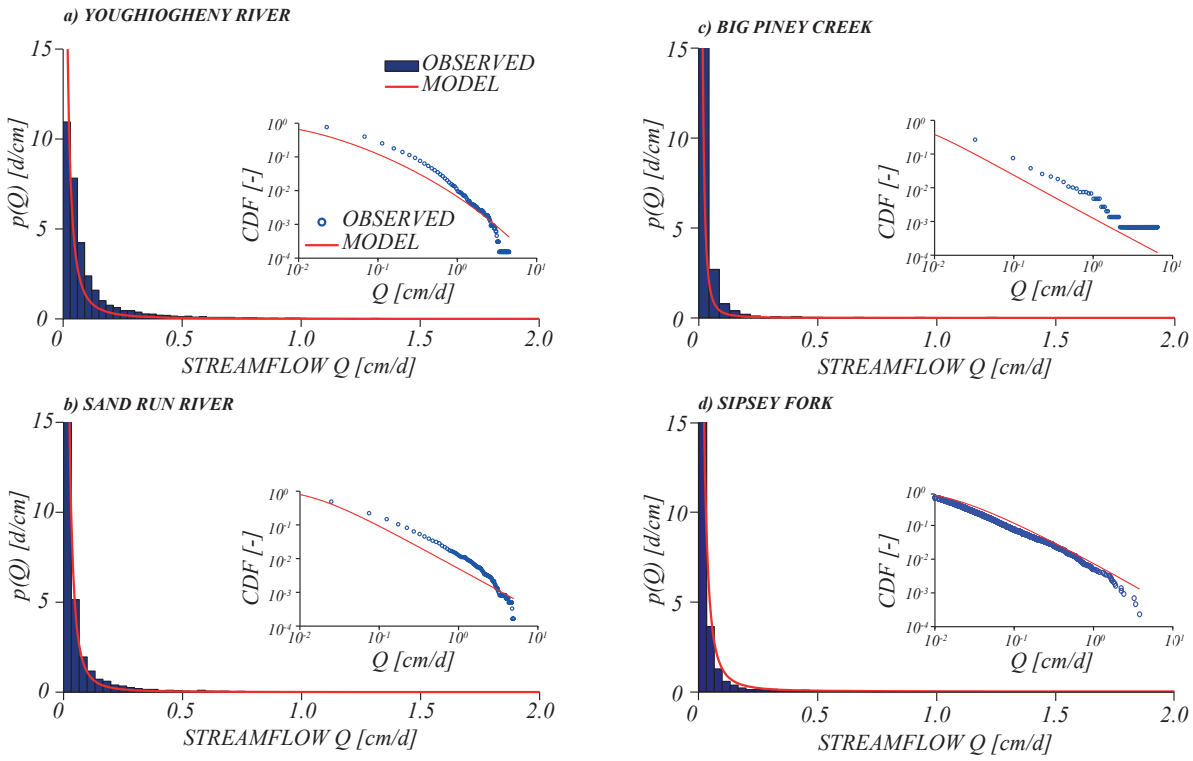

Fig. 2.8: Observed (bars) and modeled (solid lines) PDFs for summer season at (a) Youghiogheny River, MD, (b) Sand Run River, WV, (c) and Big Piney Creek, AR, (d) Sipsey Fork, AL. The integral difference between modeled and observed PDFs is equal to (a) 0.190, (b) 0.232, (c) 0.048, and (d) 0.225. The insets show the associated observed (circles) and modeled (solid line) CDFs for each plot.

smallest discharge events (see Figure 1*c* in [*Botter et al.,* 2013]). The analytical model reasonably captures the shape of the streamflow PDFs in all cases. The associated modeled CDFs (insets of Figure 2.8) show a similar behavior as discussed above.

The ability of the model to capture observed flow statistics have been further investigated by analyzing the model performance in reproducing the mean ($\langle Q \rangle$) and coefficient of variation of daily discharge (CV_Q). Figure 2.9 shows the seasonal $\langle Q \rangle$ (a) and CV_Q (b) observed at all catchments plotted against the corresponding modeled values. The model estimates of both $\langle Q \rangle$ and CV_Q have been computed through numerical integration of Equation (2.2). In most cases prediction of the analytical model matches the corresponding observed CV_Q (MSRE = 0.07). This points to the models ability to reasonably capture the streamflow variability and its inter-seasonal dynamics across different climatic and landscape settings. The value of MSRE of mean discharge when all seasons at the eleven test catchments are considered is equal to 0.13. Given the complexity of processes involved in the hydrologic response of a catchment, model performances are deemed satisfactory.

2.6 Discussion

The method presented here is structurally able to provide a reasonable estimation of streamflow regimes based on limited information about climate and landscape. This encouraging outcome

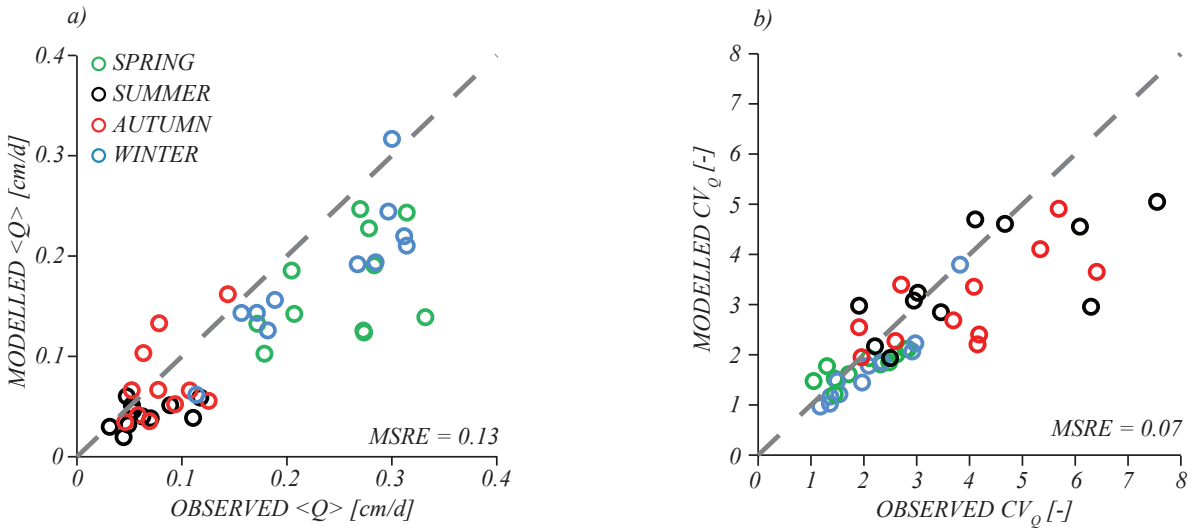

Fig. 2.9: Observed vs. modeled (a) $\langle Q \rangle$ and (b) CV_Q for all seasons at the eleven considered test catchments. The dashed line represents the 45 degree line (perfect fit). The MSRE value associated with each variable is also mentioned.

provides the opportunity for a number of potential applications such as evaluation of anthropogenic alteration of flow regimes or the prediction of hydrologic shifts induced by climate change. However, it should be noted that the stochastic streamflow model presented in this paper is best suited to describe flow regimes of pristine catchments with a contributing area smaller than a few thousand square kilometers, where streamflow dynamics result from the interaction between intermittent precipitation inputs and soil drainage. Although extensions to different settings (such as snow-dominated, urbanized or seasonally dry catchments) have been proposed [*Schaefli et al.,* 2013; *Müller et al.,* 2014; *Mejia et al.,* 2014], their predictive power in the absence of discharge measurements must be assessed. Moreover, the estimate of the model parameters based on climate and landscape requires the introduction of additional assumptions and parameters that may reduce the accuracy of the flow regime predictions. In the set of cases explored here, model performances were satisfactory, but more research is recommended to explore the reliability of the approach in a wider array of case studies.

The accuracy of the estimate of a (i.e. the degree of non-linearity of the hydrologic response) based on catchment morphology may be affected by the resolution of DEM. Moreover, the estimated value of a might depend on the drainage density and its spatial patterns [*Mutzner et al.,* 2013], which can be difficult to asses on experimental grounds, especially for large catchments. Moreover, the application to relatively flat catchments may be problematic due to lack of accuracy of automatically extracted networks and the dominant role played by hydrological features. An accurate estimation of the frequency of flow producing events (λ) may be challenging in presence of small-scale geologic heterogeneity. Also, the reliability of the water balance estimate is influenced by the type of model used. Our results suggest that suitably calibrated physically-based models perform better than empirical methods (such as Budyko), but require data from nearby sites or large-scale regional studies for their calibration. Where no information is available, empirical methods can be utilized, with increased uncertainty about the accuracy of the prediction. The estimation of α and K on the other hand is less precarious. The value of α is calculated from readily available long-term daily rainfall records, with little uncertainty. The

value of K is dependent on λ, α and a which makes the accuracy of its estimation dependent on the deviation of those parameters (Table 2.6). However, sensitivity of the analytical streamflow distribution to the parameter K is relatively low, particularly for values of a close to 2 [see *Botter et al.,* 2009]. This implies (and our result corroborate) that a rough estimate of the recession coefficient suffices for predicting $p(Q)$ with a reasonable accuracy.

2.7 Conclusion

A method is provided that allows for estimating the probability distribution of streamflows based on catchment scale climate and geomorphologic data. The approach employs a physically-based analytic model of streamflows with four parameters. It was shown that these parameters can be estimated in the absence of discharge time series, by exploiting climate data (precipitation, potential evapotranspiration) and information about the catchment morphology (DEMs).

The estimation procedure required the use of additional models, which were taken from the literature. A geomorphologic flow recession model was utilized to estimate parameters describing the recession behavior of the hydrograph, based on the topology of the stream network. A water balance model was used to predict the frequency of flow producing rainfall events. As the latter proves particularly important to predict the flow regime at a station, four existing water balance models were tested using rainfall and discharge data from 38 US catchments, characterized by diverse hydro-climatological characteristics. The best performing model (according to the Akaike selection criterion) was then used for the prediction of seasonal streamflow regimes in a disjointed set of eleven catchments within the considered study area.

The results demonstrated that the model is capable of capturing the streamflow regime reasonably well in most of the cases analyzed. This suggests the robustness of the approach in capturing the streamflow variability and its inter-seasonal dynamics across different climatic and landscape settings.

Our results suggest that the method has the potential for estimating the probability density function of river flows based on limited (and widely available) information on climate and landscape. The method has implications for a wide range of practical and scientific applications such as water resources management, ecological studies and flood risk assessment. Further efforts are needed to investigate the performance of the model in a wider array of catchments, and to test the applicability of the method in data-scarce regions. This is the objective of ongoing research.

Acknowledgments

The research leading to these results has received funding from the European Community's Seventh Framework Program (FP7/2007-2013 under grant agreement n265063). This study was also funded by the Swiss National Science Foundation (SNF, Projects No. 200021-149126). Additional support was provided by the Competence Center Environment and Sustainability (CCES) of the ETH domain in the framework of the RECORD and RECORD Catchment projects. Gianluca Botter acknowledges funding from project 60A09-4895/13 "Regimi idrologici e cambiamenti climatici". The EU project "SmartWater" is also acknowledged. Special thanks to i4 Consulting S.r.l. for their data management services.

2.8 Supplementary Information

2.8.1 Water Balance Models

In this section, the four water balance models utilized in this study are summarized.

The first model (WB1) represents the widely accepted empirical Budyko curve [*Budyko, 1974*]. The Budyko curve represents a very simple and effective way to estimate the annual runoff coefficient, based on rainfall and PET data. The runoff coefficient is estimated as a non-linear function of the 'Dryness Index' (D_I), defined as the ratio between annual average potential evapotranspiration and the annual average rainfall ($\langle PET \rangle / \langle P \rangle$). The analytical function of the Budyko curve reads:

$$\phi = 1 - \left[D_I (1 - e^{-D_I}) \, tanh\left(\frac{1}{D_I}\right) \right]^{0.5} \tag{S2.1}$$

In this model the only variable involved is D_I, which depends on rainfall and potential evapotranspiration. In our application rainfall is measured in climatic stations and the PET is derived from either the $MODIS$ or the $CGIAR$ dataset. Therefore, there are no parameters to be calibrated.

The second model (WB2) is a physically-based minimalist model, where the catchment water-storage is seen as a stochastic state variable that governs the water balance either point-wise or at the catchment scale [*Rodriguez-Iturbe et al.,* 1999; *Porporato et al.,* 2004; *Settin et al.,* 2007]. Soil moisture dynamics are interpreted and modeled at daily time scales, by conceptualizing the soil as a reservoir with a finite storage capacity (equal to nZ, where n is porosity and Z the rooting depth) intermittently filled by rainfall events in the form of random pulses with random depth. When soil moisture s exceeds a given threshold s_1 (an empirical parameter with a value between field capacity and complete saturation), the excess rainfall is lost by vertical drainage. Water losses occur via evapotranspiration (which is smaller than PET for $s < s_1$ due to water stress), drainage and surface runoff (when the soil is saturated). The mean runoff coefficient is written as [*Porporato et al.,* 2004]:

$$\phi = \frac{D_I \gamma^{\frac{\gamma}{D_I}} e^{-\gamma}}{\gamma \, \Gamma(\gamma / D_I, \gamma)} \tag{S2.2}$$

where $\Gamma(\cdot, \cdot)$ is the lower incomplete Gamma function, D_I is the Budyko's dryness index, and γ the maximum soil water storage available to plants normalized to the mean rainfall depth ($\gamma = \frac{(s_1 - s_w) nZ}{\alpha}$, with s_w representing the wilting point). D_I is calculated from climatic data, and rooting depth Z was calibrated. This model is particularly suited to be applied in association with the streamflow model used in this paper, which was originally conceived by coupling WB2 with a simplified hydrologic response model [*Botter et al.,* 2007a].

The third model (WB3) [*Milly,* 1994] is based on the hypothesis that the long-term water balance is determined by the local interaction of fluctuating water supply (precipitation) and demand (potential evapotranspiration), mediated by water storage in the soil. The partitioning of average annual precipitation into evapotranspiration and runoff is assumed to depend on the following factors: dryness index, the mean number of precipitation events per year, the ratio of

spatially averaged soil water holding capacity to the annual average precipitation, the spatial variability of storage capacity, and seasonality of precipitation and PET. The model postulates that in energy limited cases ($D_I < 1$) the dominant factor producing runoff is the excess of annual precipitation over annual potential evapotranspiration; in water limited cases ($D_I > 1$), instead, runoff is largely caused by forcing variability over time. The resulting analytical expression of the runoff coefficient reads [*Milly,* 1994]:

$$\phi = 1 - (1 - D_I) \sum_{j=0}^{\infty} \left[1 + j\gamma(D_I^{-1} - 1)k^{-1}\right]^{-k} {D_I}^j \qquad \texttt{for} \quad D_I < 1 \tag{S2.3}$$

$$\phi = 1 - (1 - D_I^{-1}) \sum_{j=0}^{\infty} \left[1 + (j+1)\gamma(1 - D_I^{-1})k^{-1}\right]^{-k} {D_I}^{-j} \qquad \texttt{for} \quad D_I > 1 \tag{S2.4}$$

where γ represents the normalized soil water storage and D_I is the dryness index. Spatial heterogeneity of soil properties is accounted for through the shape parameter k of the Gamma PDF that describes the spatial distribution of soil storage capacity. In WB3 the calibrated parameters were Z and k.

Model WB4 [*L'vovich,* 1979; *Ponce and Shetty,* 1995a, 1995b; *Sivapalan et al.,* 2011] is an annual water balance which is performed through a two-stage partitioning: first, annual precipitation P is decomposed into quick flow (S) and infiltration (termed catchment wetting, W). Subsequently, the resulting wetting is partitioned into slow flow (U) and an energy-dependent vaporization component (evaporation plus transpiration ET). This two-stages portioning can be written as $P = S + W$ and $W = U + ET$. The threshold values of P and W that must be exceeded before flow can occur are defined as $\lambda_s W_p$ and $\lambda_u PET$ respectively, where λ_s and λ_u are empirical parameters. W_p and PET are the upper bounds of $\langle W \rangle$ and $\langle ET \rangle$, which thus represent the potential wetting and the potential evapotranspiration of a catchment, respectively. Both the quick-flow and slow-flow components need to be combined to yield the total discharge in the stream ($Q = U + S$). The runoff equation is then expressed as [*Sivapalan et al.,* 2011]:

$$\phi = \frac{1 + \widetilde{\langle P \rangle}\varphi}{1 + \varphi + \widetilde{\langle P \rangle}\varphi} \tag{S2.5}$$

where $\varphi = \frac{PET - \lambda_u PET}{\langle P \rangle - \lambda_s W_p}$ and $\widetilde{\langle P \rangle} = \frac{\langle P \rangle - \lambda_s W_p}{(1 - \lambda_s) W_p}$.

This model was calibrated in different ways. Initially the 4 parameters (λ_s, λ_u, W_p, PET) were calibrated as in the original version of the model. Subsequently, in order to preserve the spatial variability of evapotranspiration, the available estimates of PET provided by the $MODIS$ and $CGIAR$ datasets (multiplied by a calibrated correction factor ξ) was included in the model formulation. Finally, with the goal of keeping the model viable for application in catchments where discharge measurements are lacking, the partitioning of P into S and W (whose application requires discharge data) was removed, thereby implying that all precipitation is turned into soil wetting. In this way the number of parameters to be calibrated is reduced to just one (λ_u). Given that the latter version of the model maximized model performance across the 38 calibration catchments, this was the method applied to WB4 as discussed in the results section.

3. PATTERNS OF STREAMFLOW REGIMES ALONG THE RIVER NETWORK: THE CASE OF THE THUR RIVER

Doulatyari, B.[12], A. Betterle[123], D. Radny[1], E. A. Celegon[4], P. Fanton[4], M. Schirmer[12], G. Botter[3] (2015), Patterns of streamflow regimes along the river network: the case of the Thur river, *Environ. Modell. Softw.*, Under Review.

Abstract

In this study, a modeling method which predicts the probability density function and the associated flow duration curve of streamflows based solely on catchment-scale climatic and morphological features, was applied point-wise along the river network of a test basin in north eastern Switzerland. A custom geo-database and a Web GIS platform were created for the management of data and application of the method. Model prediction for relevant flow statistics were validated at six subcatchment outlets with satisfactory results. Spatial patterns of flow regime exhibit a strong climatic signature, mostly driven by reduced rainfall amounts in the downstream areas. Specific discharge decreased with increasing contributing area. The seasonal variability of the streamflows shows a complex pattern, which is influenced by climatic gradients and by the structure of the river network. The framework presented here offers a novel and robust approach for assessing the spatial patterns of streamflows based on limited information.

3.1 Introduction

Streamflow dynamics and its seasonal variability are a central topic in hydrology with a broad impact on the environment and human activities. Water resource management policies, habitat characteristics and riverine biota are closely dependent on the availability and variability of streamflows [*Postel and Richter,* 2003; *Sabo et al.,* 2010; *Widder et al.,* 2014]. Streamflow statistics, such as the probability density function (PDF) of streamflows and flow duration curves (FDC), are a useful tool for summarizing the main features of the flow regime. They are frequently used for many civil and industrial purposes (e.g. hydropower production), environmental

[1] EAWAG Swiss Federal Institute of Aquatic Science and Technology, Department of Water Resources and Drinking Water, Duebendorf, Switzerland.
[2] University of Neuchâtel, The Centre of Hydrogeology and Geothermics (CHYN), Neuchâtel, Switzerland.
[3] University of Padova, Department ICEA and International Center for Hydrology "Dino Tonini", Padua, Italy.
[4] i4 Consulting S.r.l., via Barroccio dal Borgo 1, 35124 Padova, Italy

purposes (e.g. habitat restoration) and ecological studies [*Vogel and Fennessey,* 1995; *Ridolfi et al.,* 2006; *Poff et al.,* 2007; *Doulatyari et al.,* 2014].

Spatial patterns of flow regimes are the complex by product of diverse agents (climatic, geomorphic, land use and cover) and in turn affect various ecohydrological processes and dynamics along the river network. The role of flow regime in driving fish migration [*Tetzlaff et al.,* 2007, 2008], trophic chains [*Ceola et al.,* 2014], sediment transport [*Doyle and Shields* 2008], and water quality [*Benettin et al.,* 2015] has been well documented. The relationship between flow attributes and ecological functions of rivers becomes even more complicated in cases where the problem needs to be cast in a spatially explicit setting, because of the active movement of species along the network [e.g. *Ziv et al.,* 2012; *Mcluney et al.,* 2014; *Bertuzzo et al.,* 2012; *Muneepeerakul et al.,* 2007a]. In fact, spatial patterns of flow regimes influence the connectivity between nodes, with notable implication for river fragmentation [*Jaeger et al.,* 2014] and meta-population dynamics driven by movement. Likewise, the characterization of hydrological disturbance produced by complex water infrastructures and the identification of optimal trade-offs between anthropogenic and ecological uses of water resources, at the scale of entire river basins, needs to be rooted in a robust characterization of the natural spatial variability of flow regimes within riverine systems [*Botter et al.,* 2010a; *Ziv et al.,* 2012].

Despite recent advances in the characterization of flow regimes in spatially explicit settings [e.g. *Costa-Cabral et al.,* 2008; *Rigon et al.,*; *Formetta et al.,*; *Schaefli et al.,* 2014], the analysis and prediction of variability of flow duration curves along individual river networks still represents an area where research is needed. The ability to estimate flow statistics along the river network would highlight how spatial patterns of flow regimes are generated by the interplay between climatic and landscape heterogeneity.

This paper addresses two ambitious goals: (*i*) estimating seasonal streamflow duration curves at any arbitrary point along a river network based only on climate and landscape data; (*ii*) identifying spatial patterns of the underlying climatic and geomorphic drivers. A modeling method for prediction of flow duration curves, in the absence of discharge data, was recently proposed by *Doulatyari et al.,* [2015]. In this study we extend this method to provide point-wise estimates of flow regimes along the river network through customized geo-database and Web GIS platform that is capable of storing and analyzing data as well as model application. We believe this represents a novel and important development, particularly for assessment of spatial variability of water resources within complex river systems and the evaluation of catchment-scale impact of river regulation [*Lazarro et al.,* 2015]. The modeling method was tested on the Thur basin, located in Northeastern Switzerland. The Thur river is a highly monitored river, which is very well suited to analyze spatial patterns of flow regimes because of the availability of discharge data in a set of six nested discharge station spanning a wide range of contributing areas (from 16 to 1700 km^2).

This paper is organized as follows: section 2 presents the essential details about the study area. Section 3 summarizes the hydro-climatic data used in this study and the appropriate sources. The architecture of the geo-database and Web GIS platform and a brief description of the software used are also included here. Section 4 outlines the modeling approach as well as the theoretical framework used for estimating the four main model parameter. Results are presented in section 5. These include the validation of the model at six outlets (where discharge data were available), spatial patterns of model parameters and flow regimes, and scaling of recession parameters. Section 6 provides the overall conclusions and implication of this novel modeling method.

3.2 Study Area

The Thur river, a tributary of the Rhine river, has a length of approximately 130 km and is located in Northeast Switzerland (Figure 3.1). The Thur basin has an area of roughly 1700 km^2 and can be divided into two main morphologic regions: the upper pre-alpine section with the maximum altitude of 2500 $m.a.s.l.$ at Mount Säntis; and the Swiss plateau with altitudes of approximately 350 $m.a.s.l.$ in the lower catchment. The Thur valley aquifer, an important aquifer of Northeastern Switzerland, is located in the lowlands. The geology in the catchment consists of mainly limestone-dominated alpine headwaters, and Molasse sandstones, marls and Pleistocene unconsolidated sediments in the Swiss plateau [*Hayashi et al.,* 2012]. Precipitation ranges from 2500 $mm/year$ in the pre-alpine region to approximately $900 - 1000$ $mm/year$ [*Seiz and Foppa,* 2007] in the Swiss Plateau. Land use in the Thur basin is distributed as roughly 60% Agriculture, 30% Forest, and the rest barren land, surface waters, and urban areas [*Abbaspour et al.,* 2007; *Schneider et al.,* 2011].

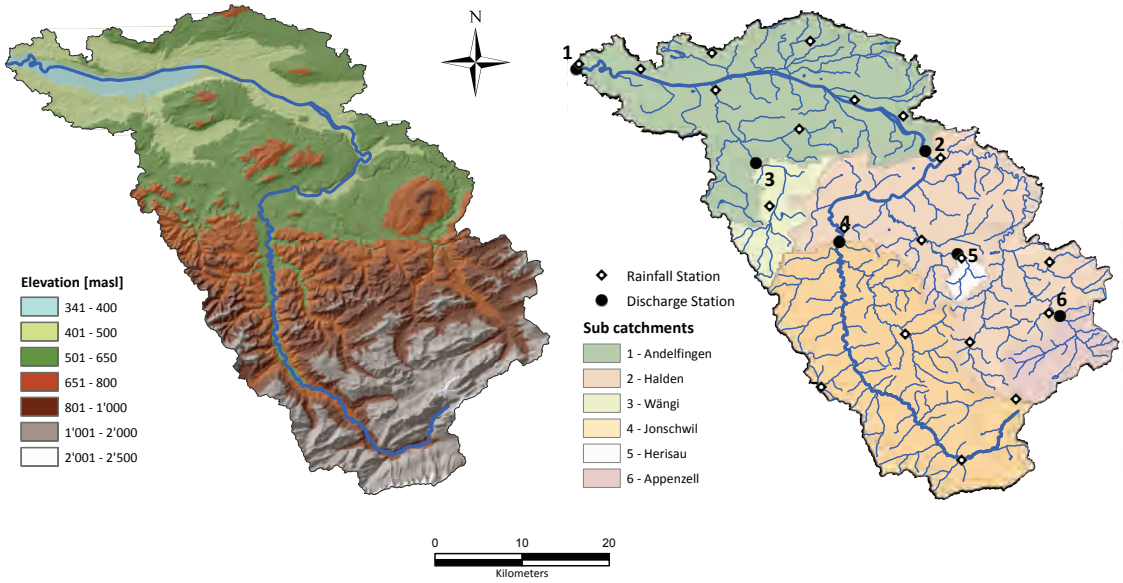

Fig. 3.1: (a) The digital elevation map of the Thur basin. The main morphological sections of the basin, the pre-alpine (to the south) and the Swiss plateau (to the north), are easily distinguished. (b) The Thur basin is divided into six sub-catchments. The corresponding gauging stations as well as 19 rainfall stations are marked on the map.

The hydrological regime of the Thur river has pre-alpine characteristics. The annual mean discharge is 53 m^2/s and discharge fluctuates rapidly in the entire course of the river, especially after heavy rainfalls in the upper catchment [*Cirpka et al.,* 2007]. The absence of lakes or other reservoirs along the Thur river is also noted. Long sections of the Thur were straightened and channelized in the 1890s in response to frequent flooding by the then meandering Thur river [*Kurth & Schirmer,* 2014]. However, flooding persisted and thus by the end of the 1980s first stretches of the river were restored as a flood protection measure. The restoration also aimed to provide recreational space and to improve the ecological condition of both the river and the floodplain [*Woolsey et al.,* 2007]. The effects of snow dynamics have been observed to be relevant in the headwaters catchment [*Seneviratne et al.,* 2012].

There are 19 evenly distributed rainfall stations as well as six discharge station in the Thur basin, spanning a whole range of contributing areas (Table 3.1, Figure 3.1). The discharge station Andelfingen represents the outlet for the entire basin. Suitable subsets of these discharge stations that represent a sequence of mutually nested sub-catchments (e.g. Jonschwil, Halden, Andelfingen) can be identified and therefore can be used to analyze the scaling of hydrological properties. A list of all rainfall stations within the boundaries of the Thur catchment is present in the Table S3.1.

Catchment and Discharge Station ID	**Tributary ID**	**Area** $[km^2]$	**X**	**Y**
Andelfingen	Thur	1700	693510	272500
Appenzell	Sitter	74	749040	244220
Halden	Thur	1085	733560	263180
Herisau	Glat	17	737270	251290
Jonschwil	Thur	493	723675	252720
Wängi	Murg	80	714105	261720

Tab. 3.1: List of all sub-catchments in the Thur basin. Station Andelfingen represents the outlet for the entire basin. The discharge station location is mentioned in the *CH1903 (LV03)* coordinate system.

3.3 Input Data: Sources and Management

Input data required by the model include potential evapotranspiration (PET), digital elevation map (DEM), and daily rainfall data. PET data were acquired from 'MODIS global evapotranspiration Project' (MOD16), available from the Montana University (`http://www.ntsg.umt.edu`), which includes a dataset providing PET at 1 km^2 resolution for 10^9 Million km^2 global vegetated land areas at 8-day, monthly and annual time resolution. The river network was estimated based on 25 m DEM obtained from the Federal Office of Topography, Switzerland (`http://www.swisstopo.admin.ch/`). Daily rainfall data at 19 rainfall stations throughout the Thur catchment were obtained from the Federal Office of Meteorology and Climatology, Switzerland (`http://www.meteoswiss.admin.ch/`). Long-term streamflow data were used to validate the results of the model in a set of outlets within the Thur river. Daily discharge data were provided by the Federal Office for the Environment, Switzerland (`http://www.bafu.admin.ch/`). All hydro-climatic data were obtained for the period of 1979 to 2012.

A geo-database with integrated automatic hydrological model simulations was created for the Thur basin. The hydrological and meteorological data mentioned above, and all rainfall and discharge stations throughout the catchment were incorporated. Other publicly available supplementary information, such as roads and aerial maps, were also included. The database offers a multi-user capable platform with a custom Web-GIS graphical user interface (GUI). The GUI allows for easy management and uploading of input data through various tools, functions and query capabilities. The various methods utilized for model parametrization (discussed in section 4) are incorporated in linked modules that allow for automatic analysis of the input data.

Figure 3.2 presents the overall structure of the database and Web-GIS platform (see Table S3.2 for more details). The database utilizes PostgreSQL for storing and retrieving data, and PostGIS for interactions with geospatial data. All data was gathered and then standardized for

format and units. Particular attention was required for identification and uniform treatment of datasets where no data was available in the time series in order to prevent inconsistencies. The application server is charged with data management and analysis. GeoServer acts as a middle layer between the database and the GUI. It also allows for central management and publishing of all data in different standard formats defined by Open Geospatial Consortium. The type of data (input or output) displayed in the GUI, coordinate reference system definition and re-projection, styling and labeling, and basic metadata information are also managed here. GeoWebCache is used to cache maps, from all publicly available data sources incorporated here, in order to accelerate and optimize map image delivery. Grass-GIS is used as a back-end web processing service to create functions for the various parameterization methods and integrate them in the overall framework. Since the Thur basin spans approximately 9 million pixels, functions were coded in a parallelized method to exploit multi-core CPU capabilities and to permit background execution. A PHP Rapid Application Development framework and GeoEXT were utilized in the implementation of Web-GIS platforms. All online published graphs were created on the fly through Dygraphs JavaScript charting library.

The development of the database and Web-GIS platform was a significant undertaking that incorporates many innovative techniques. The finished product offers a user friendly interface that emphasizes data visualization and intractability. Furthermore, it allows for online visualization of all data (input or output) as well as the option for exporting the data in appropriate file formats. Multiple streamflow model simulations with different parameterization can be run simultaneously and results are stored with unique identifiers. Other processes driven by streamflow dynamics and affected by its spatial variability (such as sediment transport, vegetation dynamics, solute transport) could be potentially incorporated as separate modules.

3.4 Methods

The seasonal PDF of daily streamflows are predicted by an analytical mechanistic model, where the catchment-scale soil water balance is driven by stochastic rainfall and is modeled at daily timescale [*Botter et al.,* 2007a]. The catchment-scale storage-discharge relationship is considered to be non-linear and modeled as power law. The steady-state PDF of daily specific (by unit catchment area) streamflows (Q) is expressed as [*Botter et al.,* 2009]:

$$p(Q) \propto Q^{-a} \exp\left(-\frac{Q^{2-a}}{\alpha K(2-a)} + \frac{\lambda Q^{1-a}}{K(1-a)}\right) \tag{3.1}$$

The above mentioned streamflow model is characterized by four physically based parameters: λ and α represent, respectively, the average frequency and depth of rainfall, while K and a are the coefficient and exponent of the non-linear relation that defines flow recession. These parameters incorporate the various hydrologic, climatic and geomorphologic features of the catchment and have been estimated on seasonal basis. For detailed theoretical background and application of this model, the reader is directed to *Botter et al.* [2009], *Basso et al.* [2015], and *Doulatyari et al.* [2015]. The flow duration curve is expressed by the cumulative distribution function of Q and can therefore be calculated by integrating equation (3.1), with closed-form analytical expressions available only for special cases (e.g. $a \in \mathbb{N}$).

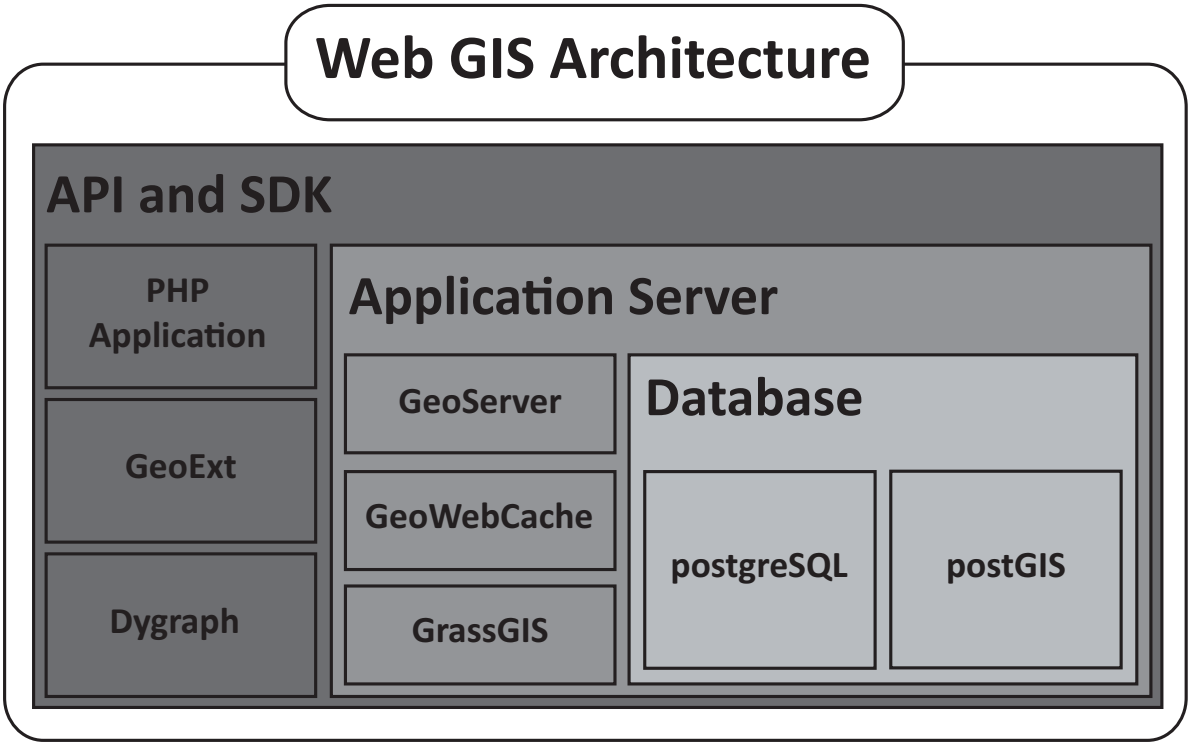

Fig. 3.2: Structure of the geo-database and Web GIS platform. The platform is built mainly from open source software.

Figure 3.3 outlines the overall modeling approach and the procedure used for estimating each parameter. In this section we discuss each module and elaborate on the modeling methods used. Hereon after, a "point" refers to a pixel along the river network.

In module (i), daily rainfall data (recorded at 19 climatic stations within the boundaries of the Thur basin) was interpolated and summed to create daily rainfall fields and estimate spatially distributed catchment scale rainfall statistics for individual seasons. The Inverse Distance Weighting (IDW) method, a built-in tool in the GRASS-GIS application, was adopted as the interpolation method with power parameter equal to 2 and using 12 nearest rainfall stations per interpolating point. This choice was made based on performance, computation time, and availability of the method as a free tool that can be easily incorporated in the data management system. Other methods can be chosen and implemented as per case study requirements or individual preference. However a detailed comparative study and bench marking is beyond the scope of this paper.

The frequency of rainfall events, λ_p was calculated for each point as the relative number of days in which the average rainfall in the upstream contributing area is larger than a given threshold (1 mm in this study). To this aim, the daily rainfall data were analyzed and for each day a raster of 0 or 1 values was created based on the rainfall field in the contributing area. If the upstream averaged rainfall was greater than the threshold then the value at that point was set to 1, otherwise it was 0 (i.e. it is not raining in the upstream area). For each point, the binary variable is then averaged over the number of days in the record to create seasonal rasters of λ_p. Moreover, the aforementioned rainfall fields were averaged over the number of time steps

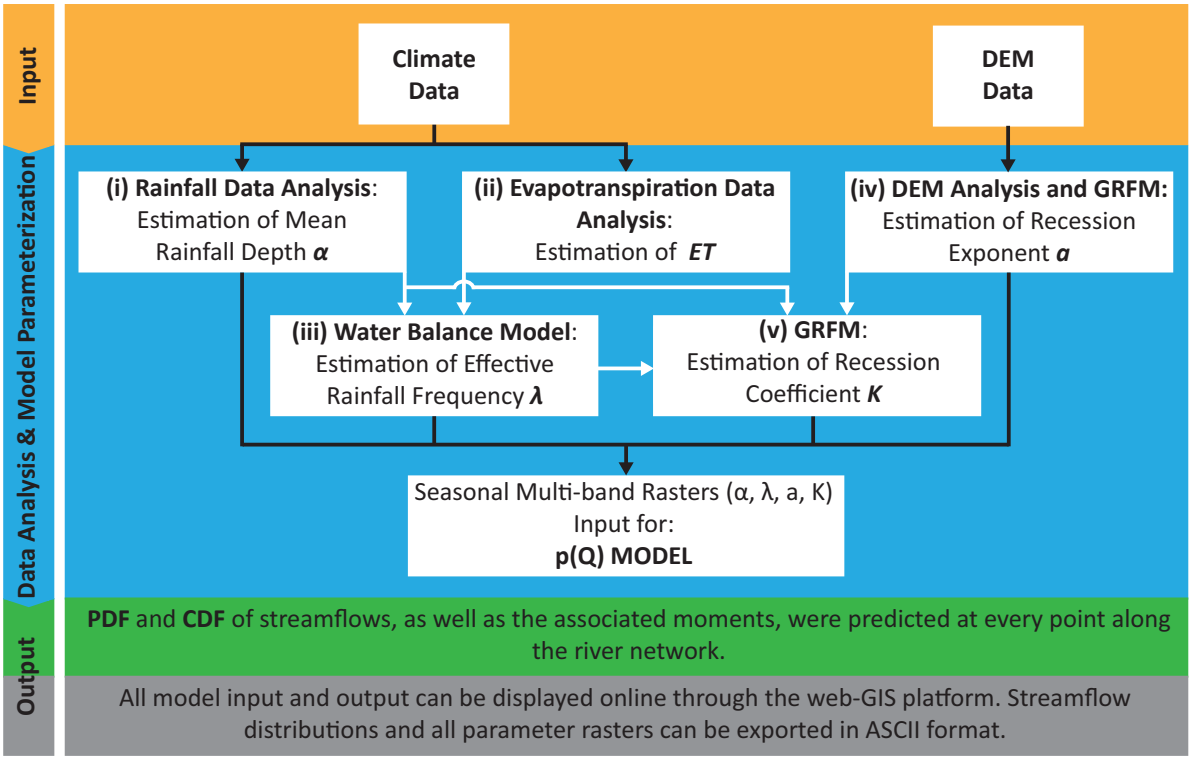

Fig. 3.3: Overall work-flow of the modeling approach. The four main model parameters are estimated at every point (i.e. every pixel along the river network).

and over the upstream contribution area of each point, to create seasonal cumulative rainfall fields ($\langle P \rangle$). Mean rainfall depth α was estimated point-wise as a ratio between the cumulative rainfall and frequency ($\alpha = \langle P \rangle / \lambda_p$). The observed values of α at the subcatchment outlets were calculated by averaging the daily rainfall values from all station in the contributing area for each outlet.

In module (ii), estimation of ET, MODIS seasonal PET rasters were cropped, re-sampled and geo-referenced according to DEM pixel dimension. Seasonal rasters of ET were created (using the Penman-Monteith method) and were averaged over the basin upstream for each point using GRASS-GIS tools.

Based on the streamflow model (Equation 3.1), the long-term mean of rainfall is expressed as $\langle P \rangle = \alpha \, \lambda_p$, and the specific discharge can be expressed as $\langle Q \rangle = \alpha \, \lambda$. The average seasonal runoff coefficient (the ratio of mean discharge to mean precipitation) is defined as $\phi = \langle Q \rangle \, / \, \langle P \rangle$. Hence, by combining the above equations, the frequency of effective rainfall events (rainfall events leading to discharge production) λ can be calculated as $\lambda = \phi \, \lambda_p$. The average seasonal runoff coefficient is estimated at every point by means of calibrated water balance models using precipitation statistics and ET data in the upstream contributing area. In module (iii), we use the physically-based analytical stochastic model of soil moisture dynamics presented by *Porporato et al.* [2004]. The mean runoff coefficient is written as:

$$\phi = \frac{D_I \gamma^{\frac{\gamma}{D_I}} e^{-\gamma}}{\gamma \, \Gamma(\gamma / D_I, \gamma)} \tag{3.2}$$

where $\Gamma(\cdot,\cdot)$ is the lower incomplete Gamma function, and $D_I = \langle PET \rangle / \langle P \rangle$ is the Budyko's dryness index, calculated from climatic data; γ represents the maximum soil water storage available to plants, normalized to the mean rainfall depth $\gamma = \frac{(s_1 - s_w)nZ}{\alpha}$ (s_1 is a proxy for field capacity, s_w is the wilting point, n is porosity). The rooting depth Z (assumed to be constant throughout the basin) was calibrated using observed mean discharge at the six outlets. It is important to note that Z represents the only calibrated parameter in the entire modeling method.

The a and K parameters were estimated based on analysis of the catchment DEM and the geomorphological recession flow model (GRFM) proposed by *Biswal and Marani* [2010]. This model stipulates that fluctuations of streamflows in time are linked to direct drainage into the active drainage network (ADN). Therefore, the recession equation $dQ/dt = K\,Q^a$ can be rewritten as [*Biswal and Marani,* 2014]:

$$\frac{N(l)}{A} \propto \left(\frac{G(l)}{A}\right)^a \tag{3.3}$$

where G is the length of the active drainage, $N(l) = dG(l)/dl$ is the number of links in the network at a distance l from the outlet, q is the flow generation rate per unit ADN length (constant), and A the catchment area. Based on this formulation, the recession exponent a is estimated through a least square regression relation between $G(l)$ vs. $N(l)$, which is in turned derived from the analysis of the DEM. The Thur basin DEM was analyzed by Grass-GIS tools in order to create the flow direction and flow accumulation rasters. The stream network was then extracted from the flow direction raster using a flow accumulation threshold of 0.09 km^2, in module (iv).

The recession coefficient K (module (v)) is estimated as a function of mean discharge ($\alpha\lambda$) and the recession exponent a such that [*Doulatyari et al.,* 2015]:

$$K = \theta(\alpha\lambda)^{1-a} \tag{3.4}$$

where θ is a constant dependent on the speed at which the ADN contracts towards the outlet. The value of θ was empirically found to be relatively constant throughout the seasons across the Thur basin. Hence, it was assumed to be equal to 0.2 d^{-1} in this study.

It is important to note that, according to the modeling method chosen, the patterns of flow regime along the river network emerge directly as a result of the aggregation of spatial heterogeneity of climate properties along the flow directions (driven by network topology itself), and are not dependent on external calibration procedures.

3.5 Results and Discussion

3.5.1 Model performance

The agreement between modeled and observed PDFs and CDFs was assessed through visual inspection. This was further quantified by comparing modeled and observed moments of the PDF, and by computing half the integral difference between the analytical and observed flow PDFs [*Botter et al.,* 2013]. The accuracy of the model estimates for the parameters and selected flow statistics was also analyzed through the Mean Squared Relative Error (MSRE).

Subcatchment Name	Season	Model Estimates				Observed			
		$\alpha[cm]$	$\lambda[\frac{1}{d}]$	$K[\frac{cm^{(1-a)}}{d^{(2-a)}}]$	$a[-]$	$\alpha[cm]$	$\lambda[\frac{1}{d}]$	$K[\frac{cm^{(1-a)}}{d^{(2-a)}}]$	$a[-]$
Andelfingen	*Spring*	0.54	0.48	1.35	2.41	0.56	0.54	1.02	2.53
	Summer	0.74	0.33	1.46	2.41	0.75	0.33	1.31	2.20
	Autumn	0.63	0.30	2.02	2.41	0.60	0.32	2.24	2.42
	Winter	0.50	0.46	1.60	2.41	0.50	0.45	1.11	2.30
Appenzell	*Spring*	0.88	0.46	0.60	2.29	0.86	0.58	0.49	2.03
	Summer	1.17	0.37	0.55	2.29	1.14	0.46	0.78	2.20
	Autumn	1.06	0.31	0.77	2.29	1.02	0.32	1.26	2.31
	Winter	0.94	0.42	0.61	2.29	0.92	0.28	0.78	2.00
Halden	*Spring*	0.64	0.48	0.78	2.22	0.62	0.60	0.53	2.17
	Summer	0.88	0.36	0.75	2.22	0.85	0.39	1.00	2.16
	Autumn	0.76	0.32	1.05	2.22	0.71	0.34	1.44	2.23
	Winter	0.60	0.45	0.90	2.22	0.58	0.43	0.96	2.17
Herisau	*Spring*	0.71	0.39	0.28	1.56	0.72	0.47	0.32	1.33
	Summer	1.01	0.30	0.27	1.56	1.03	0.32	0.49	1.53
	Autumn	0.81	0.25	0.34	1.56	0.74	0.34	0.34	1.20
	Winter	0.58	0.36	0.33	1.56	0.55	0.51	0.55	1.70
Jonschwil	*Spring*	0.72	0.48	0.91	2.42	0.78	0.61	0.46	2.24
	Summer	0.98	0.37	0.85	2.42	1.07	0.37	0.78	2.09
	Autumn	0.86	0.32	1.22	2.42	0.90	0.31	1.08	2.09
	Winter	0.72	0.45	0.99	2.42	0.76	0.37	0.87	2.14
Wängi	*Spring*	0.62	0.37	0.70	1.98	0.66	0.35	1.26	2.54
	Summer	0.78	0.24	0.84	1.98	0.86	0.19	1.84	2.46
	Autumn	0.73	0.23	0.95	1.98	0.67	0.24	2.42	2.60
	Winter	0.59	0.36	0.76	1.98	0.59	0.41	1.00	2.42

Tab. 3.2: Estimated seasonal values of model parameters at all sub-catchments in the Thur Basin. Here, Observed refers to values calculated from observed discharge and averaging of observed rainfall time series. The Model columns refer to values estimated by the method outlined in section 4.

The seasonal values of α, λ, a and K, estimated using only climate and landscape data (columns under Model Estimates heading), as well as their observed values (columns under Observed heading), based on discharge data, are presented in Table 3.2. The estimated values of α are in very good agreement with the observed values at all points ($MSRE = 0.003$). The estimates of λ also show good performance in almost all cases ($MSRE = 0.032$). The largest discrepancies occur in Appenzell and generally during the winter season. Appenzell is located in the highest elevations in the basin where snow accumulation and melting (which are not explicitly considered in the model formulation) may impact the seasonal water balance. The over estimated value of λ during winter (accumulation) and under estimation during the spring and summer (melting) also point in this direction. The estimates of a, despite being independent of the season, show very good performance across the basin ($MSRE = 0.017$). The gently sloping topography (in most sub-catchments) of the Thur basin potentially contributes to the good performance of the GRFM in estimating the recession exponent. The model estimates of K on the other hand show variable performances across the different sub-catchments and seasons ($MSRE = 0.137$). This could be potentially a result of the contrast between the underlying assumptions of GRFM with regards to the amount of water drained from the subsurface and the setting of the Thur basin, where groundwater dynamics may significantly impact recessions.

Figure 3.4 presents the observed (bars) and modeled (solid line) seasonal streamflow PDFs at Andelfingen and Appenzell outlets. The shape of the observed probability distribution is well captured by the model. Both sub-catchments demonstrate hump-shaped PDFs across all seasons

which is consistent with geographical location and climate of the Thur basin. The associated observed (circles) and modeled (solid line) CDFs are presented in the insets of Figure 3.4. In order to better represent the behavior of the curves for large streamflows the results are shown in the logarithmic scale. Apart from a small downward shift in the modeled winter CDFs as compared to the observed distributions, the shape of the CDF is well represented by the model.

Figure 3.5 shows the observed and modeled PDFs, and their associated CDF, for the summer season at the remaining four outlets (Halden, Herisau, Jonschwil, Wängi). Similar to the previous figure, all sub-catchments demonstrate a hump-shaped streamflow PDF. The model reasonably captures the shape of the streamflow PDFs and CDFs in all cases. However a slight underestimation of the small and intermediate discharge events is noted.

The ability of the model to reproduce observed flow statistics was tested by comparing the observed and modeled moments of the analytical PDF (calculated through numerical integration of Equation 3.1). Figure 3.6 shows the modeled seasonal mean discharge $\langle Q \rangle$ and coefficient of variation of daily flows CV_Q at all sub-catchments plotted against the corresponding observed values. The model estimations of mean discharge are in good agreement with the corresponding observed values.

It is noteworthy to mention that the analytical formulation for variance of Q is divergent in case where $a > 2$. In order to overcome this issue the upper limit of integration was set equal to the maximum observed specific discharge [*Lague et al.,* 2005]. While the underlying physical causes of this phenomenon requires further study, this method provided the most reasonable approach for network-scale studies of this type, where CV_Q is calculated for a very large number of sites. The effect of the divergence of the variance of $p(Q)$ on the variability of sample CV_Q is explored in the supplametntry information. The plot for CV_Q shows some scattering, but over all model performance if judged satisfactory considering that no parameter has been calibrated using the observed discharge variability.

3.5.2 Spatial patterns of model parameters

Figures 3.7 and 3.8 present the spatial patterns of α and λ across the basin for all seasons, respectively. The pre-alpine section of the basin receives larger amount of rainfall throughout the year as compared to the Swiss plateau. The rainfall events are less frequent but more intense during the summer, and the opposite is true for the winter season. The seasonal pattern of λ is very well correlated with that of α. The spatial pattern of λ in the main channel shows a weak increase from the headwaters to the basin outlet, which can be attributed to localized storms that involve only a fraction of the overall contributing area. Conversely, the value of λ in the first-order streams of the Swiss plateau is markedly smaller than that of all other streams with similar size because of the reduced amount of rainfall in this region.

Figures 3.9 and 3.10 display the spatial distribution of a and K across the river network. Note that, as per GRFM assumptions, the value of a is presumed to be constant across the seasons. The value of a is larger in the main channel as compared to the smaller tributaries, and an increasing trend towards the sub-catchment outlets is apparent within individual reaches. Furthermore, a shift in value after the merging of major tributaries is noticeable. These patterns

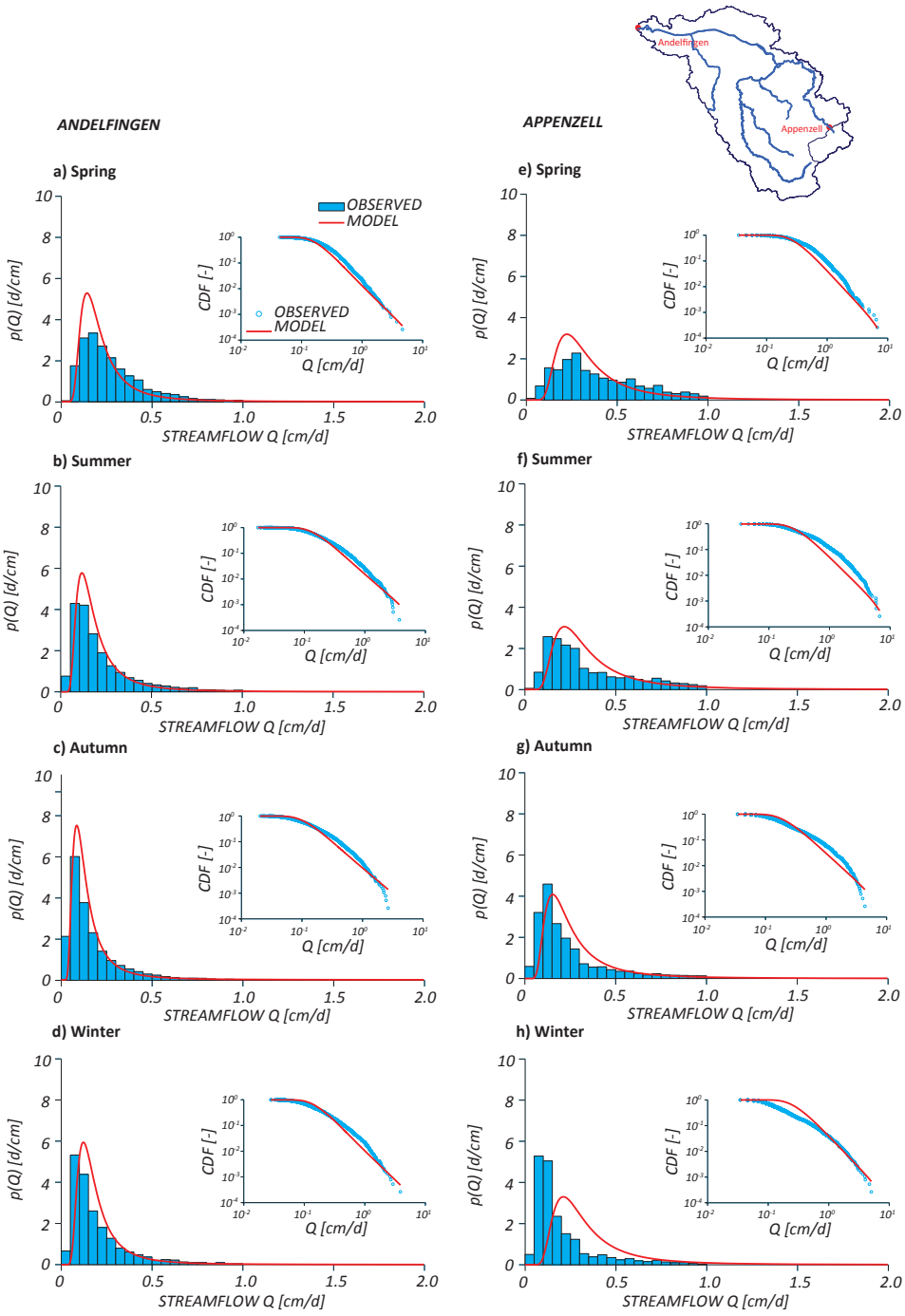

Fig. 3.4: Observed (bars) and modeled (solid lines) PDFs for all seasons at Andelfingen (a-d) and Appenzell (e-h) subcatchment outlets. The insets show the associated observed (circles) and modeled (solid line) CDFs for each plot on a loglog scale. The integral difference between modeled and observed PDFs is equal to (a) 0.166, (b) 0.254, (c) 0.309, (d) 0.303, (e) 0.210, (f) 0.260, (g) 0.294, and (h) 0.534.

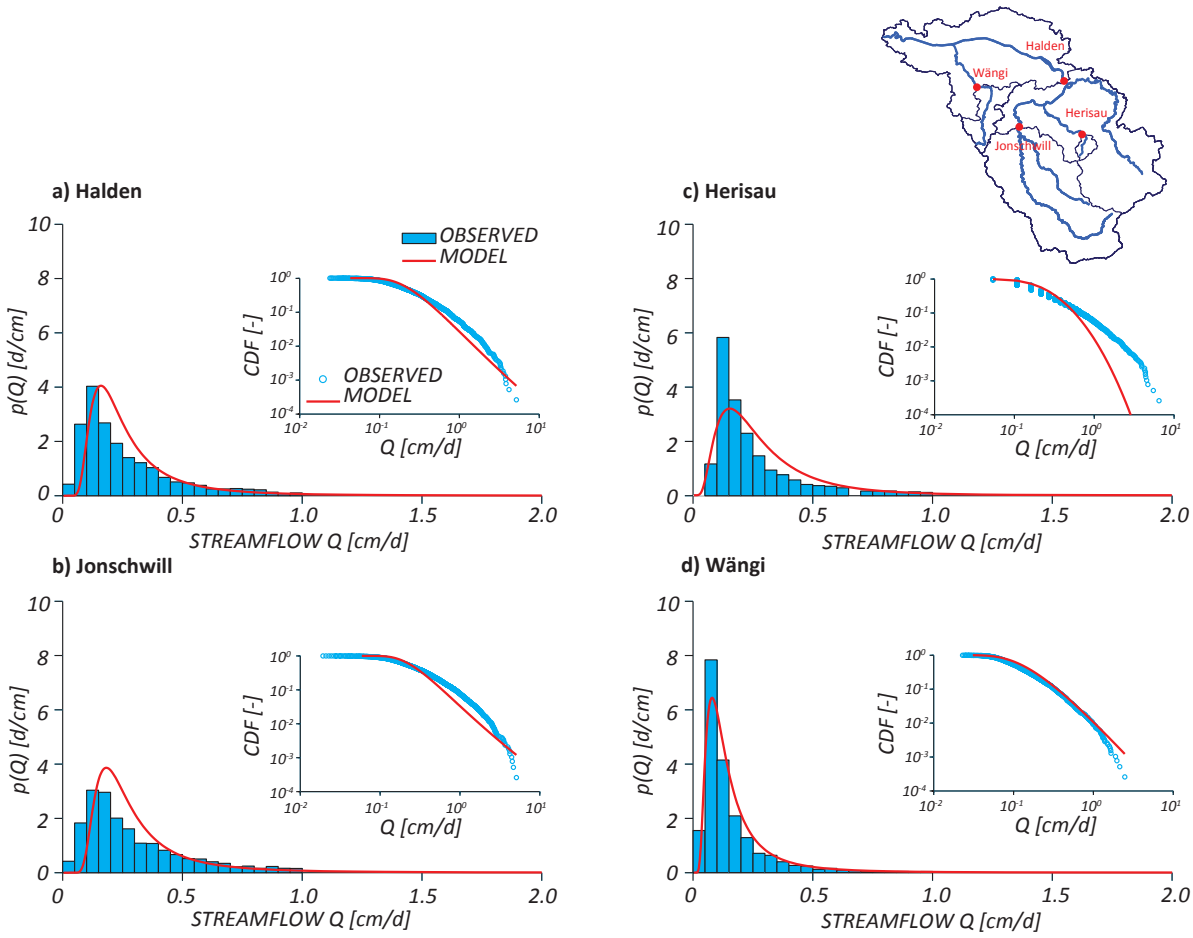

Fig. 3.5: Observed (bars) and modeled (solid lines) PDFs for summer season at (a) Halden, (b) Herisau, (c) Jonschwil, and (d) Wängi. The associated CDF plots (insets) are on a loglog scale. The integral difference between modeled and observed PDFs is equal to (a) 0.278, (b) 0.238, (c) 0.259, and (d) 0.278.

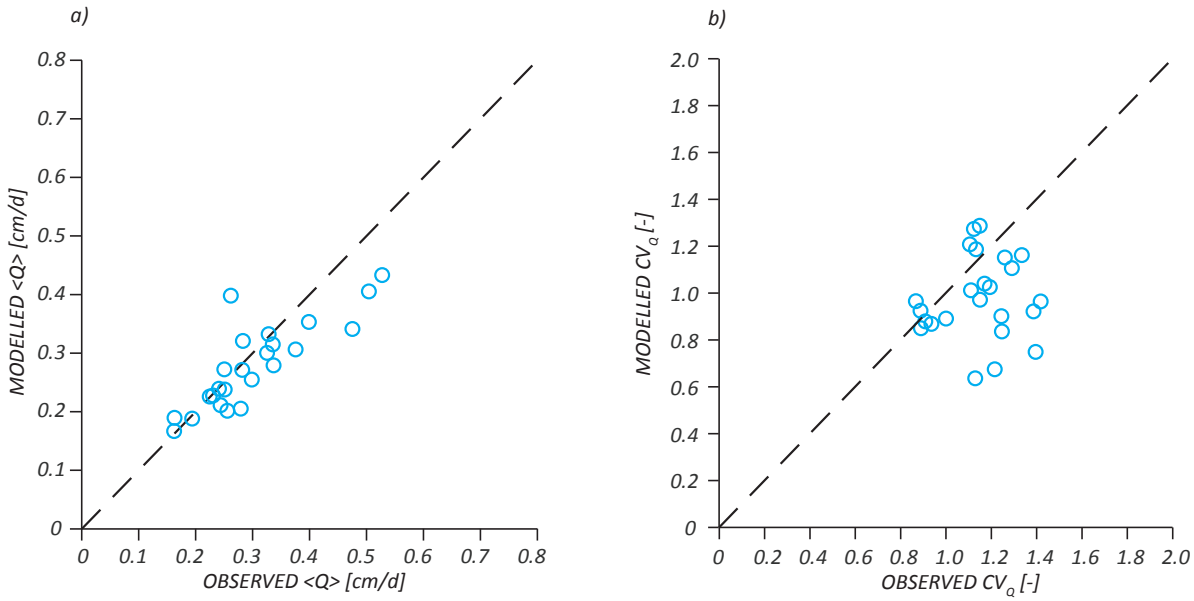

Fig. 3.6: Observed vs. modeled (a) $\langle Q \rangle$ ($MSRE = 0.030$) and (b) CV_Q ($MSRE = 0.049$) for all seasons and sub-catchments in the Thur basin. The dashed line represents the 45 degree line (perfect fit).

point to an overall increase in non-linearity in the main channel moving towards the basin outlet. This could be a by-product of increasing heterogeneity in the hydrologic response of the different sub-catchments that contribute to the streamflows at the outlet of larger basins [*Harman et al.,* 2009b]. K shows an increasing trend from the headwaters towards the basin outlet across the seasons. This is a possible byproduct of the negative correlation between a and K. The map highlights that the values of K are larger in autumn, which is the driest season of the year. In fact, K is inversely proportional to the catchment wetness (see Equation 3.4).

The spatial variability of flow regimes is the by product of the network-scale variability of these four parameters, which is discussed in the next section.

3.5.3 Spatial patterns of flow regimes

Seasonal multi-band rasters (composed of all the model parameters) were used to estimate streamflow distributions and flow statistics for every point along the river network. Figures 3.11 and 3.12 present the spatial pattern of $\langle Q \rangle$ and CV_Q across the basin for each season. The spatial patterns of $\langle Q \rangle$ show a decreasing trend from the pre-alpine section towards the plateau, while the seasonal patterns mirror the seasonality of the climate. This points to the climatic gradient being the main driver. Figure 3.12 shows a complex pattern of CV_Q from upstream to downstream which is the result of two contrasting effects: (i) the increase of a with increasing size of contribution area, which leads to enhanced variability of Q in larger catchments; and (ii) the increase of λ and decrease of α with increase in size of the contributing area, which instead tends to reduce the flow variability in larger catchments. Overall the range of CV_Q along the network is quite narrow, particularly in the main channel of the Thur river. The summer and autumn

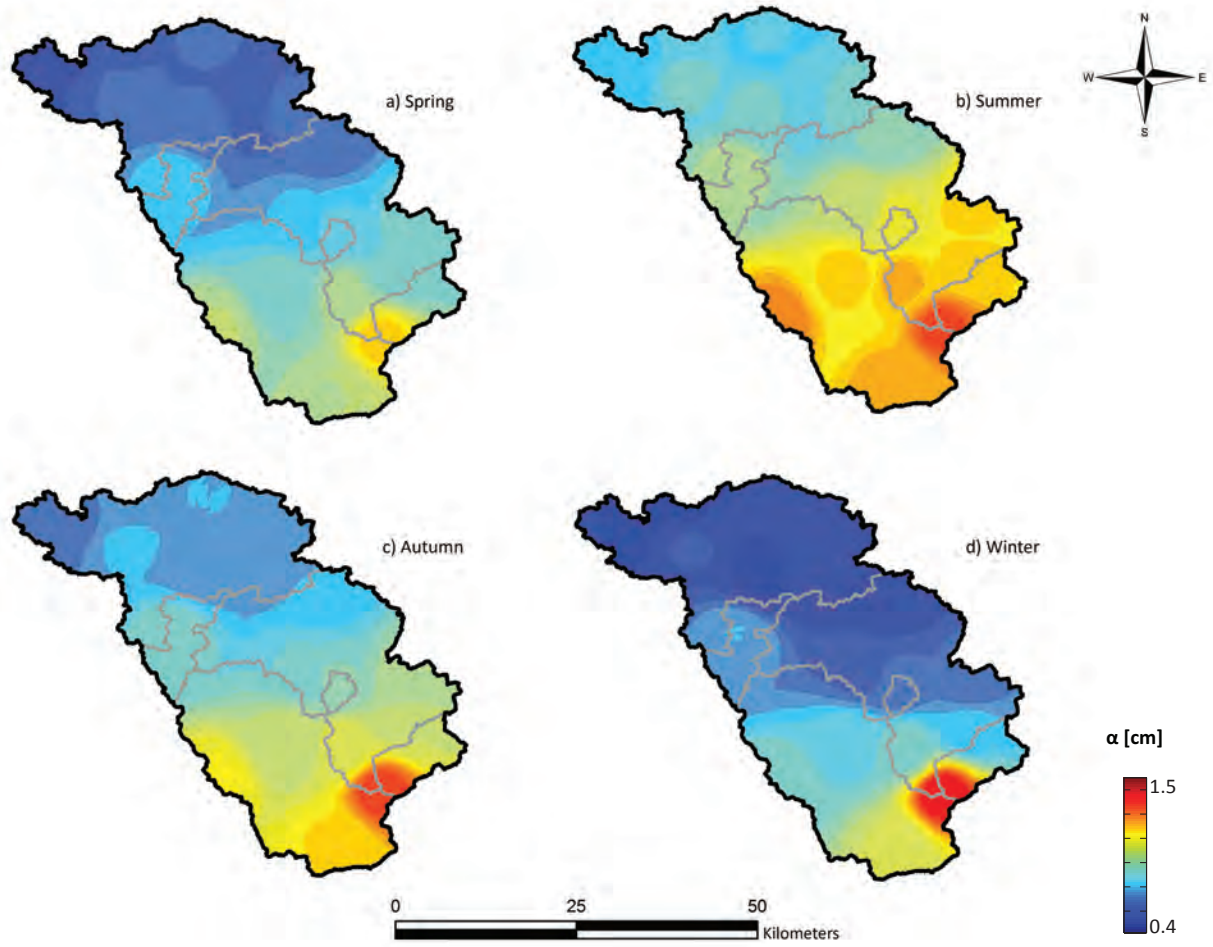

Fig. 3.7: Spatial patterns of α across the Thur basin during all seasons.

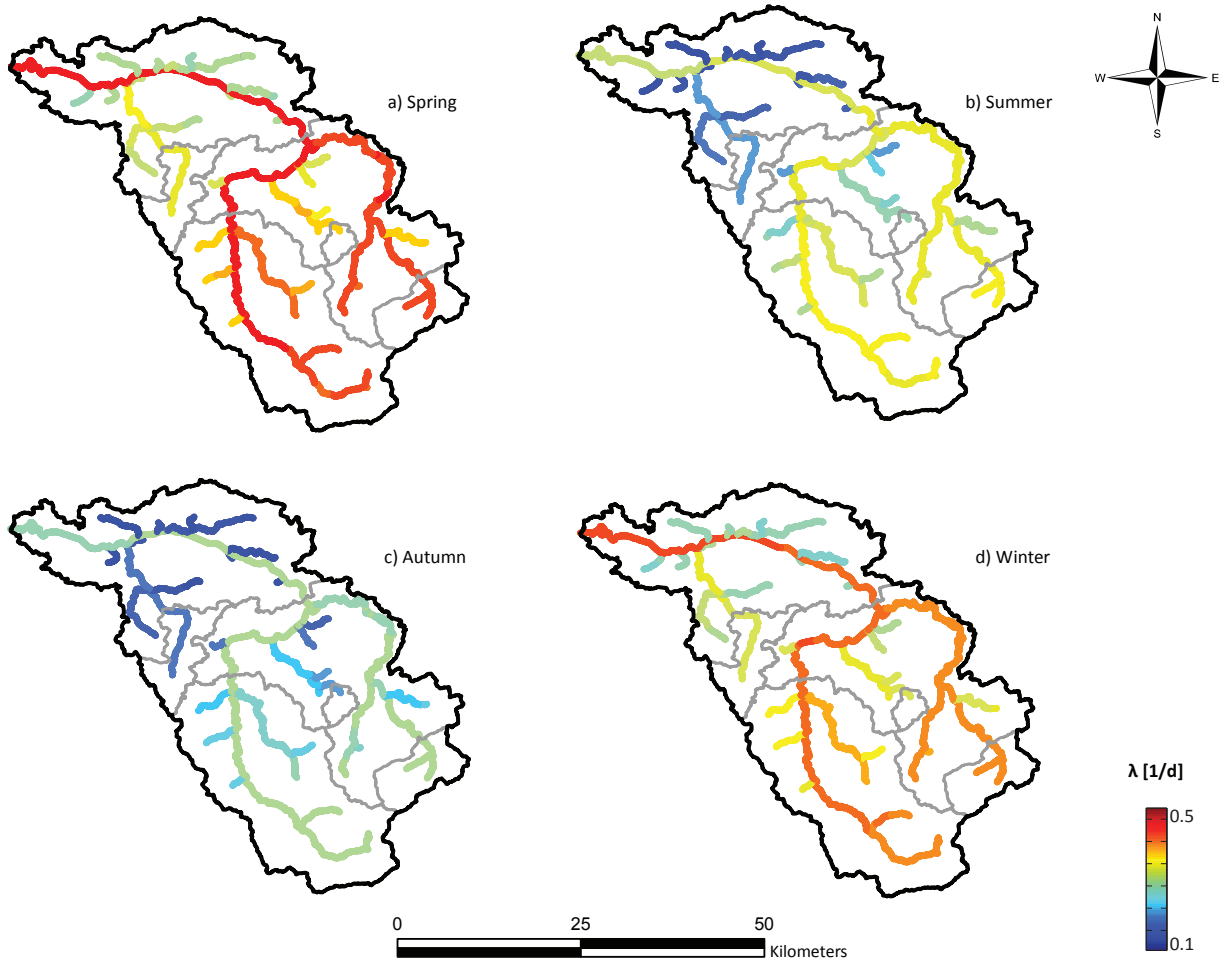

Fig. 3.8: Spatial patterns of λ across the Thur basin during all seasons.

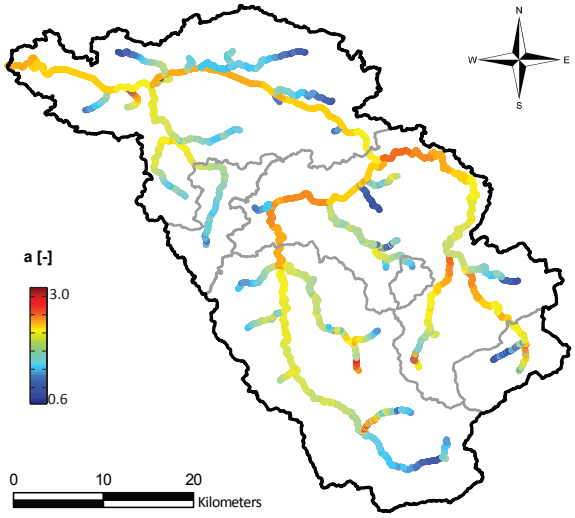

Fig. 3.9: Spatial patterns of a across the Thur basin during all seasons.

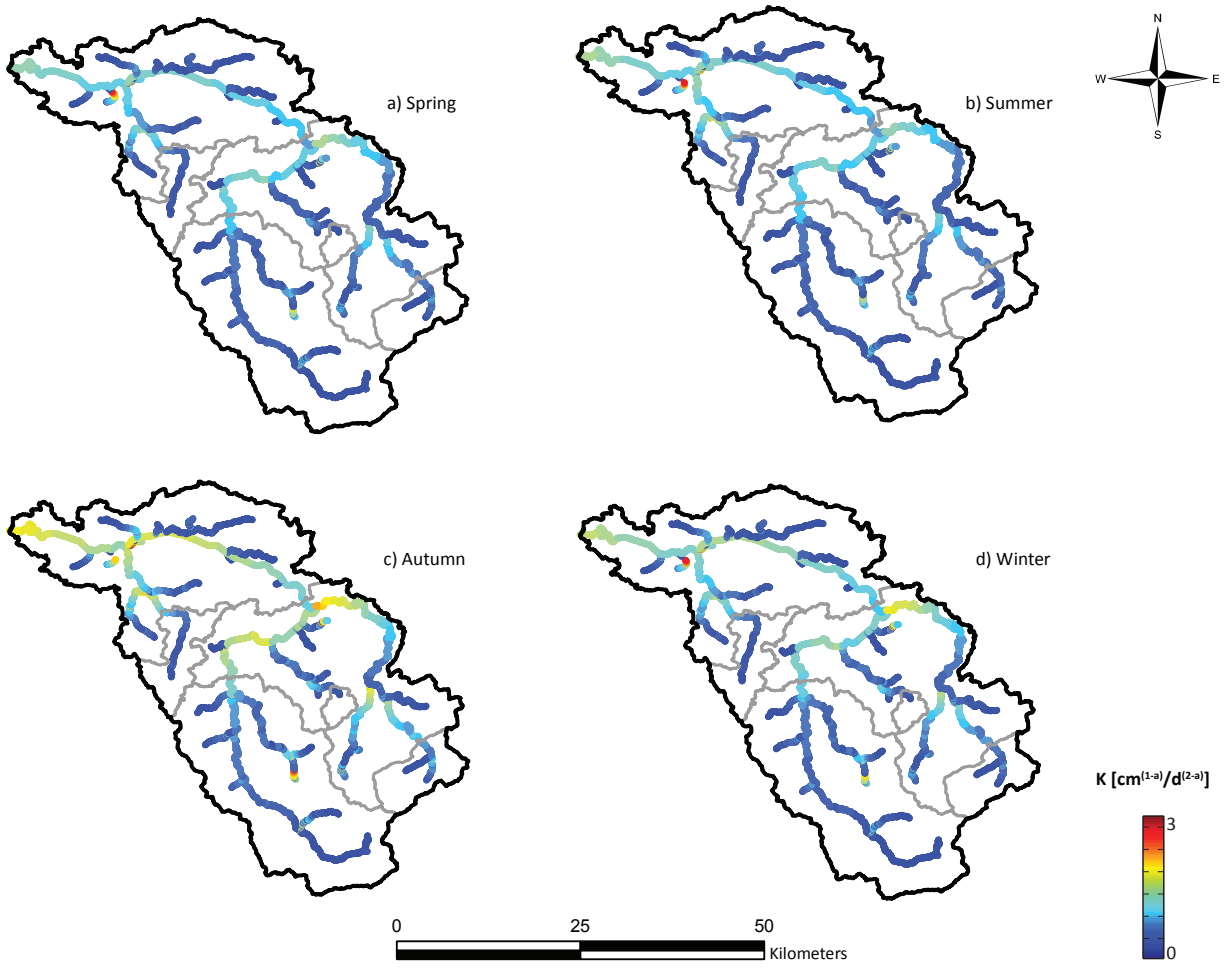

Fig. 3.10: Spatial patterns of K across the Thur basin during all seasons.

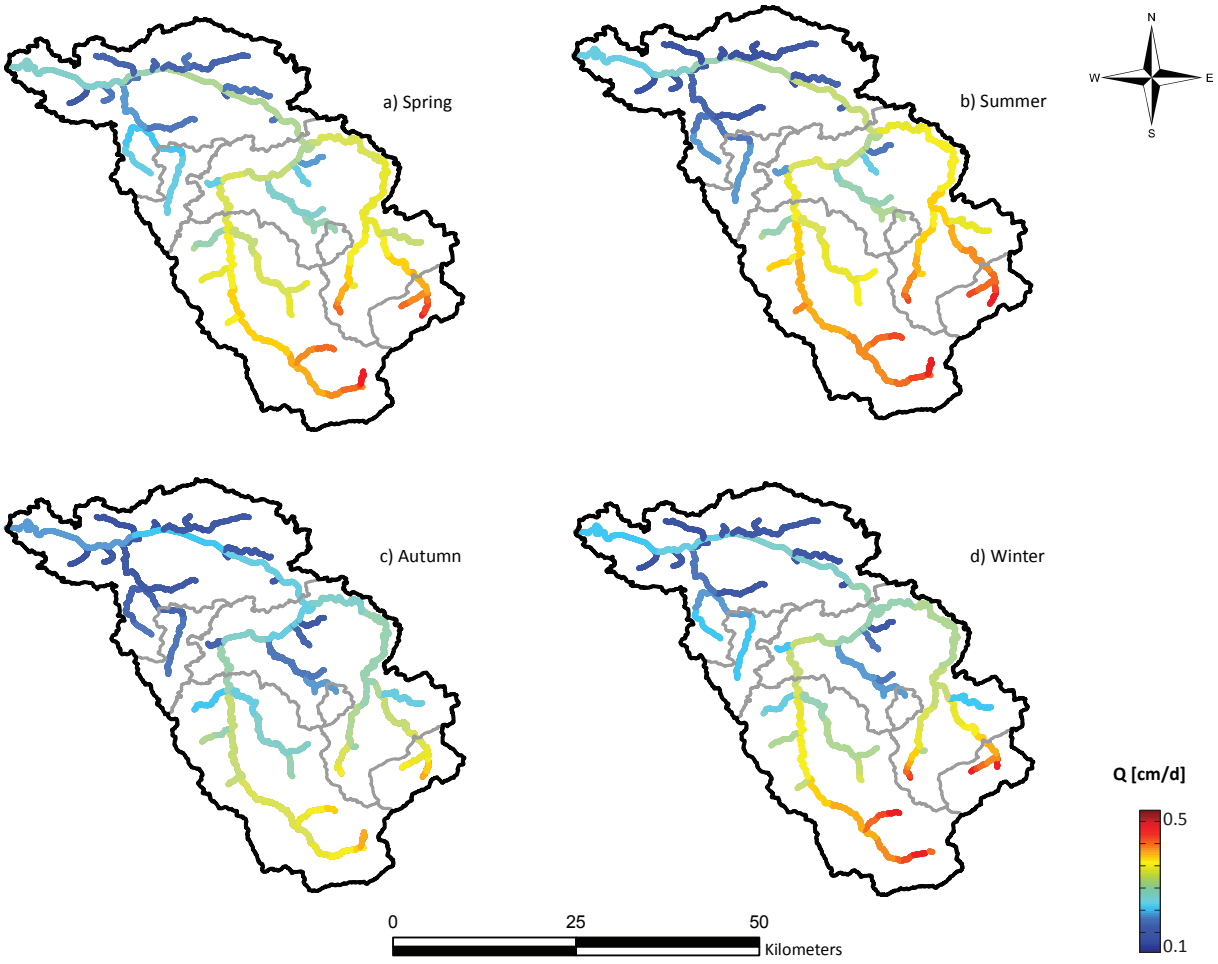

Fig. 3.11: Spatial patterns of specific discharge ($\langle Q \rangle$) across the Thur basin during all seasons.

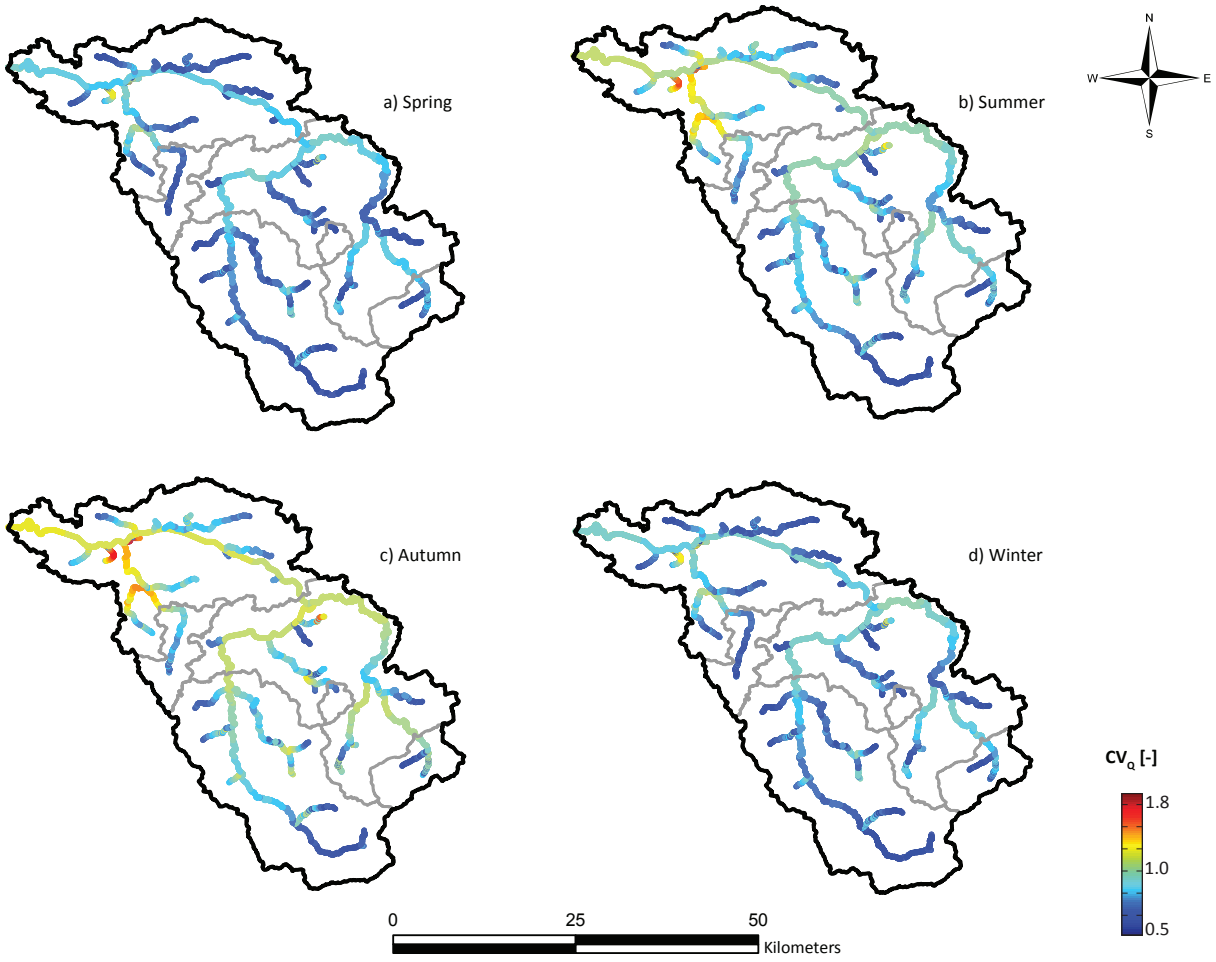

Fig. 3.12: Map shows the distribution of CV_Q throughout the Thur basin during all seasons.

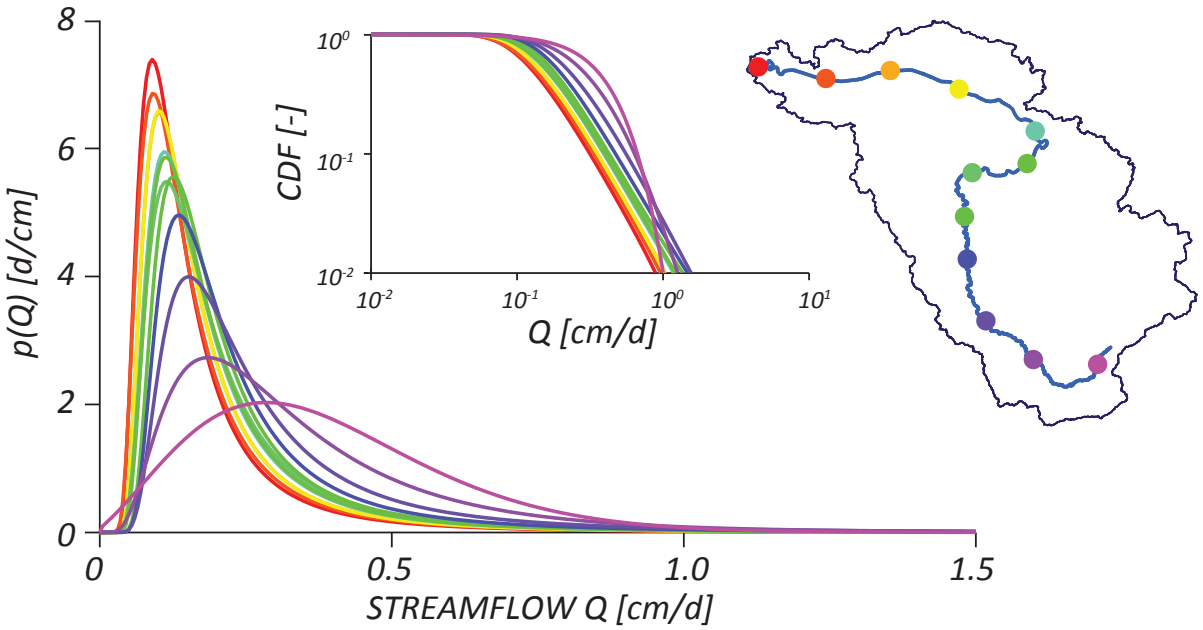

Fig. 3.13: The pattern of flow regime along the main channel of the Thur river (from headwaters in Jonschwill to the catchment outlet in Andelfingen) depicted through the model estimated PDFs and CDFs of streamflows. The CDF plot is in a loglog scale.

seasons display larger values of CV_Q overall. These model outcomes point to larger variability of discharge in seasons with smaller frequency of events and larger rainfall intensity.

The pattern of streamflow regime along the river network is highlighted in Figure 3.13. 12 model estimated PDFs and CDFs of specific discharge (by catchment area) for the autumn season along the main channel of the Thur river, as well as the sample location along the network, are depicted here. Congruous to previous results, the spatial patterns of the hydro-climatic drivers (α and λ), lead to a decreasing trend of mean specific discharge and an increase of the PDF mode, from the headwaters towards the basin outlet. The joining of major tributaries along the channel can modulate the extent and the speed at which these changes occur. In agreement with observed data, a shift in the tail of the PDF from exponential (in the upstream location) to power-law (downstream) is noticeable on the CDF plot. This is in line with *Basso et al.* [2015], who have linked the emergence of heavy-tails to enhanced non-linearity of the catchment hydrologic response (regardless the underlying hydro-climatic regime), especially in cases where the recession exponent a is larger than 2. Hence, in this basin the range of variability of streamflow is not reduced with increasing contributing area, with implication to flooding potential in the lower regions of the Thur river.

3.5.4 Scaling of recession parameters

The results presented in the previous section show that the Thur catchment depicts pronounced inter-seasonal and spatial patterns in the climatic and recession drivers. While the climatic parameters show a strong seasonal pattern that seems to dominate the streamflow dynamics, the role of the recession parameters is more nuanced. This is particularly true in the cases

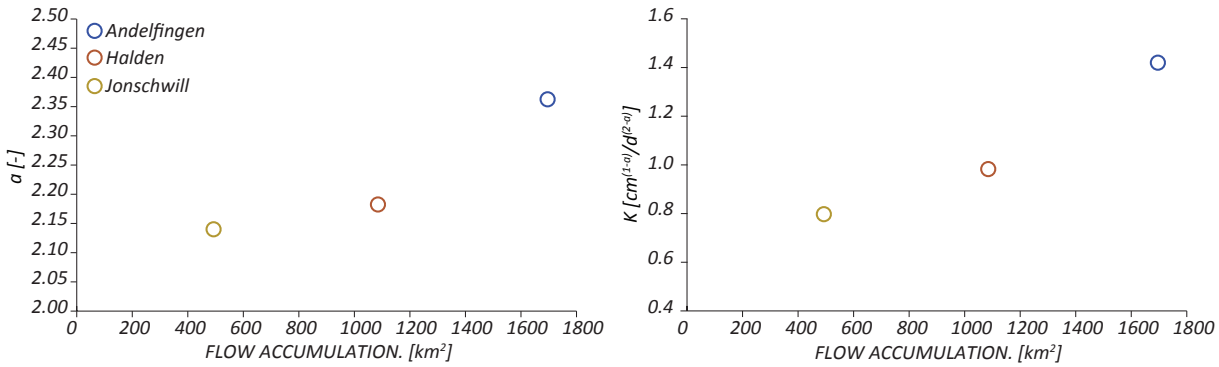

Fig. 3.14: Observed values of the (a) recession exponent a and (b) coefficient K with respect to the contributing area for a set of nested sub-catchments in the Thur basin. Each point represents the averaged annual value for the sub-catchments.

where (as in this study) the catchment response shows pronounced non-linearity. The scaling of the recession parameters with respect to contributing area is an interesting question which would help the prediction of flow regimes through the extrapolation of discharge time series recorded in catchments featured by much smaller (or larger) contributing areas. While empirical power law relations have been proposed in the literature to link hydrograph's properties to catchment size, experimental data seems to show contradicting results. From this perspective, the available discharge data from the Thur basin and modeling exercise performed here offer a unique opportunity to investigate emerging scaling laws.

Figure 3.14 presents the observed values of the recession exponent a and coefficient K versus the flow accumulation area for the set of nested sub-catchments: Jonschwil, Halden, and Andelfingen (see Figure 3.1b). These sub-catchments represent the contribution areas containing the main channel of the Thur river. Note that, the observed points have been derived from observed seasonal recessions and represent the average annual values for each subcatchment. The results show an increasing pattern for both parameters, which highlights the observed increase in non-linearity in catchment response with increasing contribution area. This is in agreement with the findings of *Harman et al.* [2009b], who related the increasing degree of non-linearity to heterogeneity of hydrologic response among different landscape units. This may also be the case for the Thur river, where strong spatial climatic gradients possibly enhance the internal heterogeneity of the hydrograph timescale.

The model estimated values of a and K for every point along the river network are plotted against flow accumulation area in Figure 3.15 and Figure 3.16, respectively. In order to better focus on the scaling patterns of recession parameters in the nested set of catchments considered, points corresponding to small contributing areas ($< 50\ km^2$), which are present throughout the basin, have been omitted from the figures. The figures are organized with the largest subcatchment on top to the smallest at the bottom.

In both cases, the large heterogeneity of data present in the smaller contributing areas is sharply reduced with increasing size. The discontinuities in the modeled points, and the corresponding "jumps" in model estimates of a and K, occur where different tributaries merge and is consistent between the scaling patterns of both parameters. After each drop, the value increases again along single river reaches. This is because of the network becoming more elongated with

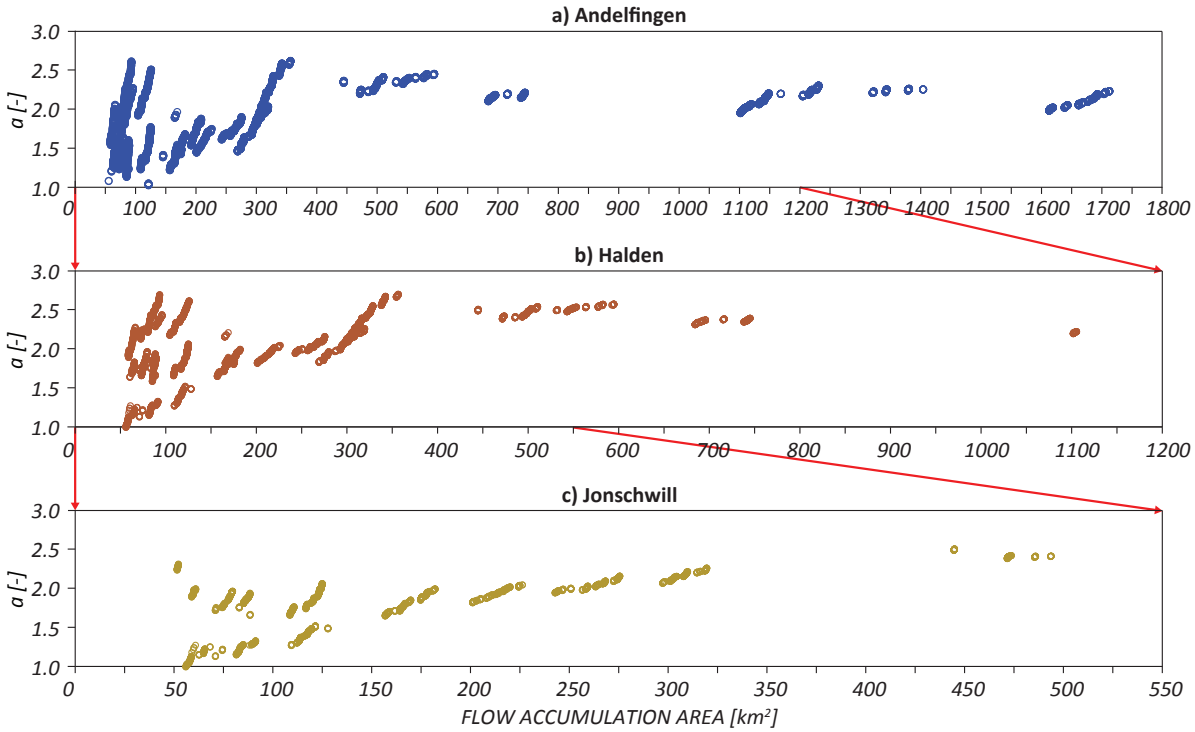

Fig. 3.15: Model estimates of the recession exponent a versus the contributing area for a set of nested sub-catchments (a) Andelfingen, (b) Halden, and (c) Jonschwil.

increasing contributing area, which increases the non-linearity in the relationship between N and G in (3.3). However, the slope of increase is reduced with increasing size. Overall, with increasing size there is a non-homogenous increasing pattern in the degree of non-linearity of the system, in agreement with observed data.

3.6 Conclusion

In this study a modeling method for estimating flow duration curves, in the absence of discharge data, was used to estimate streamflow distributions point-wise along the river network in the Thur basin, located in northeastern Switzerland. The model proved capable of capturing, in a satisfactory manner, the seasonal dynamics of streamflows observed at six gauging stations after calibration of a single parameter pertaining to the water balance component of the model. The model was able to reproduce observed streamflow statistics ($\langle Q \rangle$ and CV_Q) reasonably well at these six stations. The strong seasonal patterns of the climatic parameters proved to be the dominant driver of streamflow dynamics. The spatial patterns of model parameters further highlighted the importance of the climatic drivers in determining the behavior of the flow regime along the river network. More frequent but much less intense events in the Swiss plateau lead to a decreasing trend of specific discharge with increasing contributing area. The seasonal variability of the streamflows showed a complex pattern which is influenced by climatic gradients and the increasing degree of non-linearity of the hydrologic response observed at larger spatial scales.

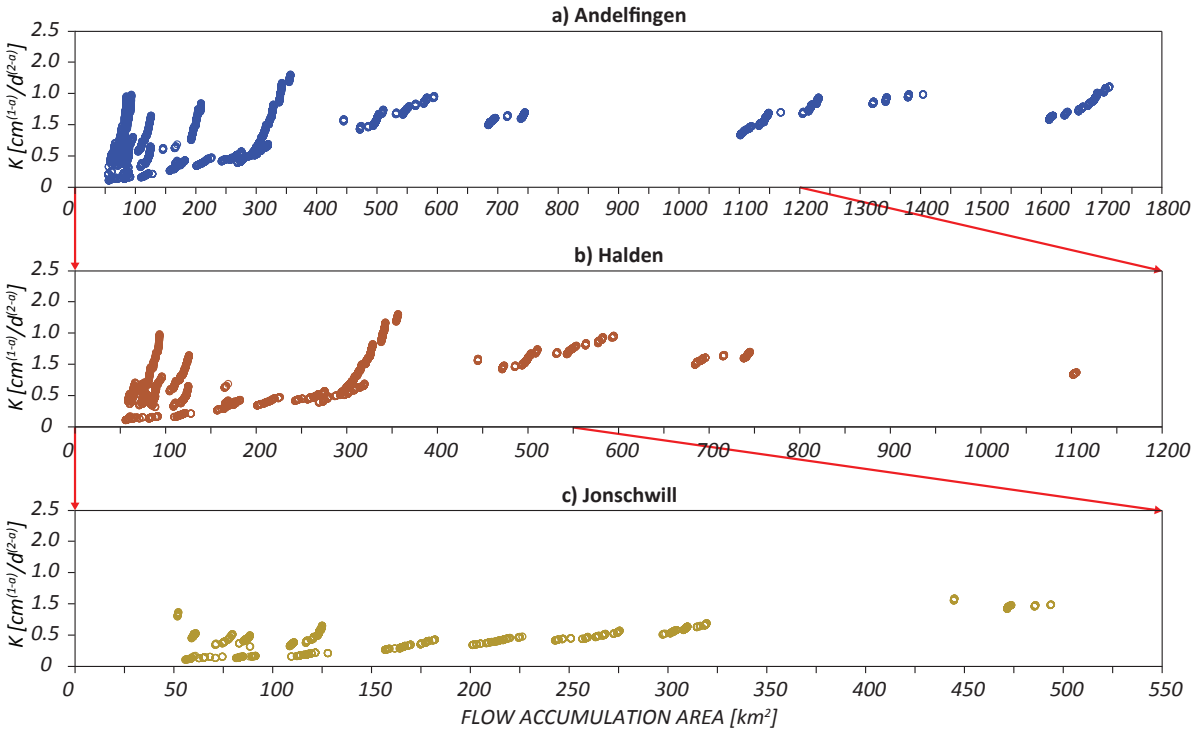

Fig. 3.16: Average annual model estimates of the recession coefficient K versus the contributing area for a set of nested sub-catchments (a) Andelfingen, (b) Halden, and (c) Jonschwil.

The increasing non-linearity in the catchment response with contribution area is possibly a by-product of the increasing heterogeneity of soil use and climate at larger scales, and generates power law tails in the streamflow distribution.

The data management and modeling approach presented here provide a valuable method to estimate long-term patterns of the flow regimes and predict streamflow statistics at any arbitrary point along the river network of a given basin with limited data requirements. This is a big step forward particularly for studying ecohydrological processes that require a spatially explicit representation of streamflow properties. The geo-database and Web GIS platform, encompassing the modeling approach, can be applied as a complete package to different catchments provided that the minimal data requirements are satisfied. The modular design employed in this platform allows for versatility in the type and number of methods used for estimating model parameters. It also provides the ability to consider multiple scenarios using different sets of data. Other processes driven by streamflows (such as sediment transport, habitat dynamics, chemical fluxes, etc.) might be incorporated in the future. Moreover, the approach can be used to assess the effect of changing climatic condition on the flow regime of a catchment, and the impacts of anthropogenic regulation on natural streamflow conditions. This study is the first step towards the development of a framework for comprehensibly describing catchment-scale ecohydrological processes using simple physically-based analytical models that do not require intensive calibration and computational burden.

Acknowledgments

The research leading to these results was funded by the Swiss National Science Foundation (SNF, Projects No. 200021-149126). Additional support was provided by the Competence Center Environment and Sustainability (CCES) of the ETH domain in the framework of the RECORD and RECORD Catchment projects. Gianluca Botter acknowledges funding from project 60A09-4895/13 "Regimi idrologici e cambiamenti climatici". Special thanks to Stefano Basso for his indispensable support.

3.7 Supplementary Information

3.7.1 Rainfall Stations

Name	X	Y	Min annual value [cm]	Max annual value [cm]	Mean annual average	Mean annual cumulative sum
Affeltrangen	719069	265660	0	9.37	0.27	99.02
Andelfingen	693809	273070	0	12.15	0.24	87.93
Appenzell	747734	244475	0	13.40	0.45	163.04
Bischofszell	735324	262285	0	10.91	0.28	102.42
Eeschlikon	715694	256830	0	10.27	0.34	125.00
Flawil	733139	252930	0	14.30	0.34	124.71
Frauenfeld	709479	270170	0	12.86	0.29	104.15
Herisau	737729	250830	0	11.75	0.38	138.97
Illhart	720328	275760	0	12.26	0.27	99.11
Kalchrain	709058	274350	0	14.32	0.27	97.35
Niederneunforn	700859	272510	0	11.26	0.24	87.42
Ricken	721599	236075	0	15.21	0.50	181.81
Säntis	744100	234900	0	18.67	0.70	245.01
Starkenbach	737699	227600	0	15.40	0.52	188.34
Stpeterzell	731249	242140	0	13.68	0.44	160.91
Sulgen	731024	267175	0	9.60	0.28	101.99
Teufen	747809	250410	0	13.45	0.42	151.88
Urnäsch	738679	241230	0	12.00	0.48	175.49
Weinfelden	725424	268935	0	11.74	0.26	96.44

Tab. S3.1: List of all rainfall gauging stations and their location in the *CH1903 (LV03)* coordinate system.

3.7.2 Database Architecture

Module	Software	Notes
API and SDK	Scriptcase RAD v.7	PHP Rapid Application Development is used for server side PHP web interface development [http://www.scriptcase.net].
	GeoEXT	OpenLayers and ExtJS libraries; Web application for composing and publishing maps. [http://trac.geoext.org]
	Dygraphs	Application for graph development. [http://dygraphs.com]
Application Server	GeoServer	GeoServer is an open source server software written in Java that allows users to share and edit geo-spatial data. It publishes data from any major spatial data source using open standards. GeoServer is the reference implementation of the Open Geospatial Consortium (OGC) Web Feature Service (WFS) and Web Coverage Service (WCS) standards, as well as a high performance Web Map Service (WMS). [http://docs.geoserver.org]
	GeoWebCache	GeoWebCache is a Java web application used to cache map tiles from a variety of sources such as OGC Web Map Service (WMS). It implements various service interfaces (such as WMS-C, WMTS, TMS, Google Maps KML, Virtual Earth) in order to accelerate and optimize map image delivery. It can also recombine tiles to work with regular WMS clients. [http://geowebcache.org/]
	GRASS-GIS	GRASS-GIS has been integrated into the framework for conducting hydrological functions in a multi-user environment: per process customized environment variables (data directory, location, mapset); per process grass execution control (start, stop, abort). [http://grass.osgeo.org]
Database	PostgreSQL	PostgreSQL is an object-relational database management system (ORDBMS) with an emphasis on extensibility and standards-compliance. As a database server, its primary function is to store data (securely and supporting best practices), and retrieve it later, as requested by other software applications. It is a free and open source software, released under the terms of the PostgreSQL License, a permissive free software license. [https://wiki.postgresql.org]
	PostGIS	PostGIS is a spatial database extender for PostgreSQL object-relational database. It adds support for geographic objects allowing location queries to be run in SQL. In addition to basic location awareness, PostGIS offers many features rarely found in other competing spatial databases such as Oracle Locator/Spatial and SQL Server. [http://postgis.net]

Tab. S3.2: A brief overview of software used in the geo-database and Web GIS platform is presented here.

3.7.3 Variability of sample CV_Q for distributions with infinite variance

In section 5 we discussed the divergence of the analytical formulation of variance based on Equation 3.1. The coefficient of variation of daily streamflows CV_Q is an important indicator for the behavior of the flow regimes. Hence, the impact of this divergence on variability of sample CV_Q was further explored through a Monte Carlo method. For each season at each of the six sub-catchment outlet a 40 year randomized synthetic time series of discharge was created based on observed values of the four main model parameters (λ, α, a, K). This was repeated 100 times and streamflow statistics were then calculated at each outlet. The moments of the analytical PDF were calculated through numerical integration (3.1) and results were averaged. Figure S3.1 depicts the variability of estimated seasonal CV_Q at each outlet by means of box-plots . The observed value of CV_Q (blue line) is also shown. In most cases, the observed value of CV_Q fall within the predicted range of variability produced by the model. The poor performance of Herisau, while noticeable, is expected. The analytical formulation of variance in this case is in fact convergent, since the value of the recession coefficient a is less than 2. This can instead be attributed to a poor representation of the recession dynamics at low flow conditions and very high flows for this sub-catchment. Furthermore, the results in the winter are generally less robust than the other seasons which is associated with the lower performance of the water balance model in this season.

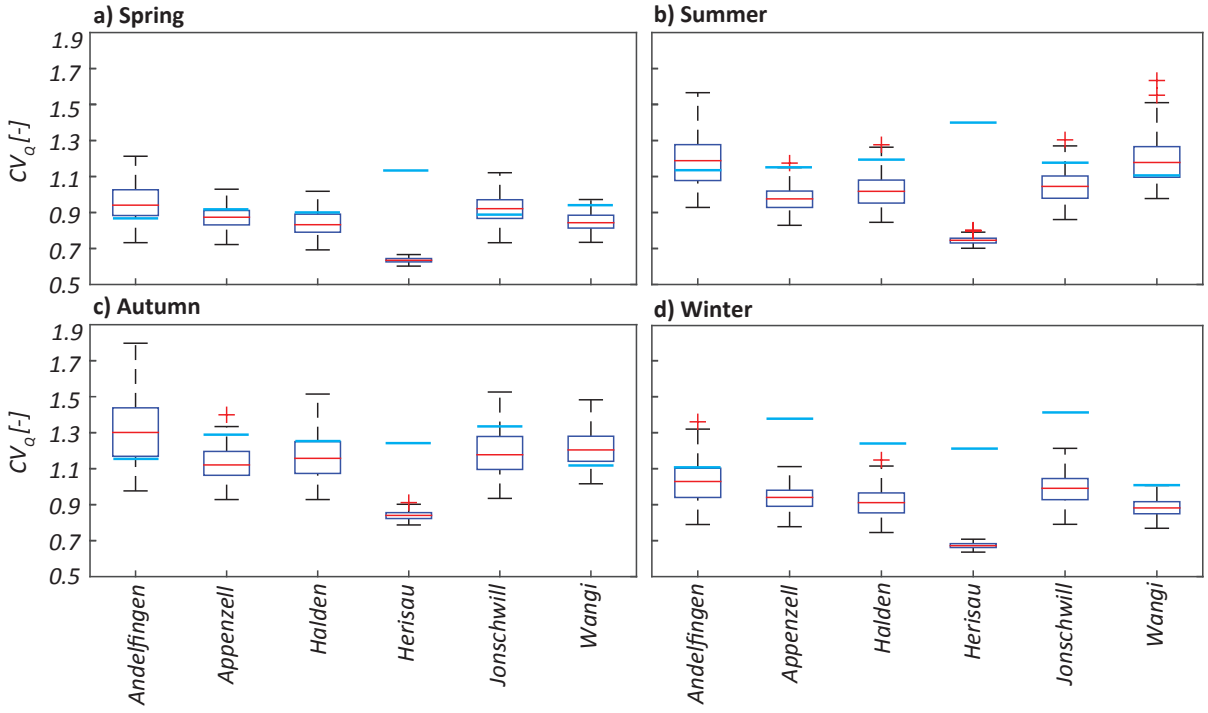

Fig. S3.1: The box plots show the 25%, 50% and 75% quartiles as well as the entire range of observed values across the seasons for all six sub-catchments. The blue lines represent the value of CV_Q calculated based on the observed discharge time series.

4. RIVER FLOW REGIMES AND VEGETATION DYNAMICS ALONG A RIVER TRANSECT

Doulatyari, B.[12], S. Basso[12], M. Schirmer[12], G. Botter[3] (2014), River flow regimes and vegetation dynamics along a river transect, *Adv. Water. Res.*, 73, 30-43, doi: 10.1016/j.advwatres.2014.06.015.

Abstract

Ecohydrological processes occurring within fluvial landscapes are strongly affected by natural streamflow variability. In this work the patterns of vegetation biomass in two rivers characterized by contrasting flow regimes were investigated by means of a comprehensive stochastic model which explicitly couples catchment-scale hydroclimatic processes, morphologic attributes of the river transect and in-stream bio-ecological features. The hydrologic forcing is characterized by the probability distribution (PDF) of streamflows and stages resulting from stochastic precipitation dynamics, rainfall-runoff transformation and reach scale morphologic attributes. The model proved able to reproduce the observed PDF of river flows and stages, as well as the pattern of exposure/inundation along the river transect in both regimes. Our results suggest that in persistent regimes characterized by reduced streamflow variability, mean vegetation biomass is chiefly controlled by the pattern of groundwater availability along the transect, leading to a marked transition between aquatic and terrestrial environments. Conversely, erratic regimes ensure wider aquatic-terrestrial zones in which optimal elevation ranges for species with different sensitivity to flooding and access to groundwater are separated. Patterns of mean biomass in erratic regimes were found to be more sensitive to changes in the underlying hydroclimatic conditions, notwithstanding the reduced responsiveness of the corresponding flow regimes. The framework developed highlights the important role played by streamflow regimes in shaping riverine environments, and may eventually contribute to identifying the influence of landscape, climate and morphologic features on in-stream ecological dynamics.

4.1 Introduction

Natural streamflow variability is currently recognized as a major driver for most processes occurring in fluvial landscapes. The whole range of streamflows, their temporal fluctuations and their

[1] EAWAG Swiss Federal Institute of Aquatic Science and Technology, Department of Water Resources and Drinking Water, Duebendorf, Switzerland.
[2] University of Neuchâtel, The Centre of Hydrogeology and Geothermics (CHYN), Neuchâtel, Switzerland.
[3] University of Padova, Department ICEA and International Center for Hydrology "Dino Tonini", Padua, Italy.

interactions with groundwater contribute to the determination of form and functioning of riverine ecosystems [*Poff et al.,* 1997; *Lytle and Poff,* 2004; *Schneider et al.,* 2011]. The study of interconnections among hydrological and biological dynamics has gained importance in recent years [e.g. *Laio et al.,* 2001a; *Porporato et al.,* 2001; *Rodriguez-Iturbe et al.,* 2001; *Guswa,* 2005; 2008; *Rodriguez-Iturbe et al.,* 2009; *Thompson and Katul,* 2012] because of the increasing awareness of the interconnected role of these processes in preserving and restoring healthy environments necessary for the provision of humanly valued ecosystem services.

In fluvial environments, one important focus is on the riparian vegetation dynamics at the reach scale. Streamflow variability plays a crucial role in the dynamics of riparian plant communities and the associated ecological processes [*Auble et al.,* 1994; *Tockner et al.,* 2000; *Nilsson and Svedmark,* 2002]. In particular, flooding and groundwater availability are key controls in riparian vegetation dynamics [*Hupp and Osterkamp,* 1985; *Bradley and Smith,* 1986; *Mahoney and Rood,* 1998; *Bendix and Hupp,* 2000; *Lite et al.,* 2005; *Perona et al.,* 2009a]. The state of flooding is characterized as the duration of time when a point along the river transect is inundated by the stream. Flooding can affect riparian vegetation both in a positive (providing nutrients, moisture and seeds) and a negative (uprooting, sediment removal, anoxia, and burial) manner (for more details on the impact of flooding on vegetation see *Yanosky* [1982]; *Kozlowski* [1984]; *Osterkamp and Costa* [1987]; *Hupp* [1988]; *Naiman and Decamps* [1997]; *Friedman and Auble* [1999]; *Naumburg et al.* [2005]). However, the detrimental impacts of flooding are more severe and typically outweigh potential beneficial effects. In contrast, when the point is exposed, vegetation (in particular phreatophyte species) can grow by accessing groundwater which fluctuates in correlation with streamflows. Therefore, the dynamics of riparian vegetation along a river transect is closely connected to the stochasticity of streamflows, which is in turn controlled by landscape, climate and morphologic features of the river and the contributing catchment.

The temporal variability of streamflows is typically described by means of the probability density function (PDF) of daily discharges, or the related flow duration curve [*Searcy, 1959*; *Vogel and Fennessey,* 1994; *Castellarin et al.,* 2007; *Doyle et al.,* 2005]. The prediction and characterization of streamflow distributions has been the goal of a large number of hydrologic studies which are based on statistical methods or process-based (numerical and analytical) models [*Vogel and Fennessey,* 1994; *Yokoo and Sivapalan,* 2011]. Recently, a stochastic analytical framework for linking the features of the streamflow distribution to climate and landscape attributes has been proposed [*Botter et al.,* 2007a; 2008; 2009]. This framework allows for a quantitative distinction between two different types of flow regimes (termed persistent and erratic), based on the ratio between mean inter-arrival of flow-producing rainfall events and the mean catchment response time [*Botter et al.,* 2013]. Persistent regimes are characterized by a small range of streamflows (reduced variability), while erratic regimes are characterized by a wider range of streamflows (enhanced variability) that results from the alternation between intense floods and prolonged droughts.

The impact of the stochastic fluctuations of streamflow on the dynamics of riparian vegetation has been previously explored. *Camporeale and Ridolfi* [2006] presented the most comprehensive process-based stochastic model of riparian vegetation dynamics and investigated the role of flow variability in vegetation distribution along a riparian transect through modeling the hydrological noise as dichotomic noise. *Camporeale and Ridolfi* [2007] further developed the model to investigate the effect of hydrological fluctuations on noise-induced stability and bi-modality in vegetation biomass dynamics along a riparian transect. This model was extended to investigate

the scaling of the riparian width at watersheds scale by *Muneepeerakul et al.* [2007b], and utilized by *Perona et al.* [2009b] to investigate riparian vegetation dynamics in meandering and braided rivers. *Perona et al.* [2009a] developed a stochastic approach for studying sediment-vegetation dynamics driven by stochastic flood disturbances at a flood plain scale. *Tealdi et al.* [2011] explored the effects of dam induced hydrological changes on total biomass along the transect. *Crouzy and Perona* [2012] developed a rigorous stochastic description of growth-uprooting that was validated through a flume experiment [*Perona et al.,* 2012]. More recently, *Tealdi et al.* [2013] investigated the role of the interspecific interactions, driven by a shot-noise hydrologic driver, on the distribution of the species along a river transect.

Here the approach of *Camporeale and Ridolfi* [2006] is adopted and, for the first time, complemented with the stochastic model of streamflows and stages developed by *Botter et al.* [2007a; 2010b], with the goal of analyzing the signature of catchment-scale hydro-climatic processes and river flow regimes in the patterns of vegetation biomass. The model is then applied to two catchments with opposing flow regimes: (*i*) the Boite, located in north eastern Italy (persistent), and (*ii*) the Youghiogheny, in MD USA (erratic). A detailed process-based analysis of the role played by hydrologic variability as the driver and limiting factor for vegetation growth along a river transect is presented. The main elements of novelty with respect to previous works are: a rigorous analytic formulation for the probability and mean duration of inundation/exposure, explicitly based on the climatic and hydrologic parameters is provided and validated against field data; based on this framework, the correlation scale of the hydrologic noise is properly defined such that it changes along the river transect according to the underlying flow variability rather than being assumed to be constant as in previous studies [*Camporeale and Ridolfi,* 2006]. The relative role of flooding and groundwater access in mean vegetation biomass is then explored through an analytic index that quantifies the deviation from carrying capacity. The impact of long-term variability of climate on the mean vegetation biomass along the transect is analyzed.

4.2 Model Outline

A general representation of the ecohydrological processes driving the riparian vegetation dynamics is depicted in Figure 4.1, which presents the temporal variation of streamflows, stages and vegetation biomass (left) and the associated PDF for each variable (right). The stochastic fluctuation of the streamflows is controlled by climatic and landscape features of the contributing watershed (expressed by the PDF of streamflows). The temporal variability of river stages is, in turn, a mirror of these fluctuations since they result from the random sequence of flow pulses delivered from the contributing catchment, suitably modulated by the morphological features of the transect. For a given point, vegetation biomass alternates between growth (when the site is exposed) and decay (when the site is inundated). The length of the exposure/inundation time as well as vegetation specific features determine the extent of growth and decay. We can therefore express the dynamics of vegetation along a river transect by means of coupling catchment-scale hydroclimatic processes, morphologic attributes of the river transect and vegetation specific biological features. In this section we outline the analytical frame work utilized to model these processes.

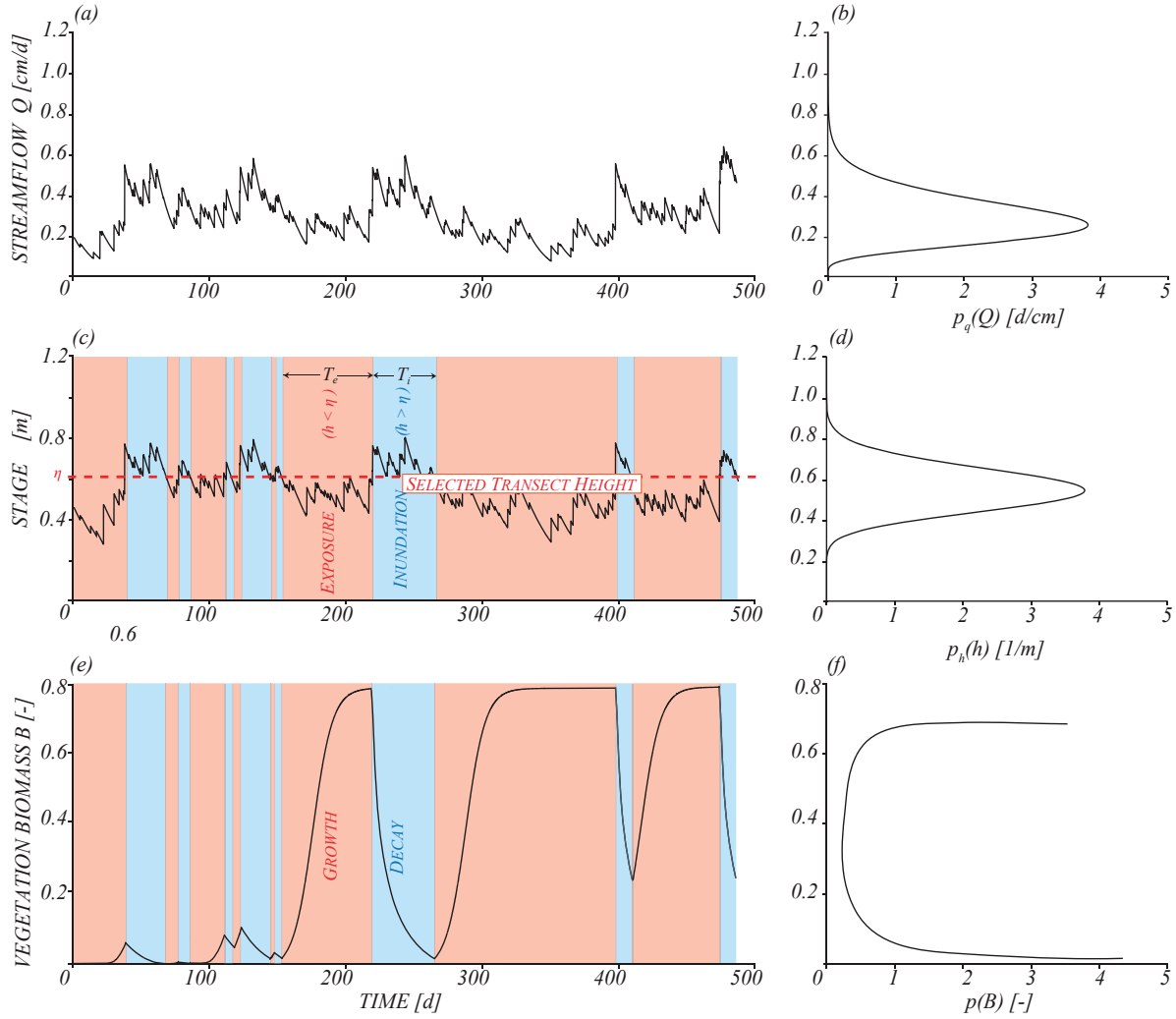

Fig. 4.1: Temporal dynamics of streamflows, stages and vegetation biomass (left) and the associated PDF for each variable (right). Vegetation biomass alternates between growth and decay based on the stochastic patterns of exposure/inundation for a given point along the river. This pattern is a mirror of stochastic fluctuation of the streamflows, which is determined by climatic and landscape features of the contributing watershed.

The flow regime defines the river flow variability and is embodied by the streamflow PDF. Here, the flow regime is characterized by means of a recent analytical mechanistic model [*Botter et al.,* 2007a] based on a catchment-scale soil water balance forced by stochastic rainfall which is modeled (at daily timescales) as a marked Poisson process with frequency λ_p and exponentially distributed depths with average α [*Rodriguez-Iturbe et al.,* 1999; *Porporato et al.,* 2004; *Botter et al.,* 2007a]. Accordingly, the specific (per unit catchment area) streamflow (Q) is composed of instantaneous jumps corresponding to rainfall events filling the soil water deficit in the root zone (taking place with frequency $\lambda < \lambda_p$) and the exponential decays between them. Therefore, the stochastic temporal dynamics of Q at a daily timescale (Figure 4.1a) can be described as:

$$\frac{dQ\,(t)}{dt} = -K_T Q\,(t) + \xi_Q(t) \tag{4.1}$$

where the first term on the right-hand side represents the deterministic exponential decay of Q between events (with rate K_T) and the second term represents the stochastic jumps induced by streamflow producing rainfall events (Figure 4.1a). The inter-arrival time of events and the jumps themselves are exponentially distributed, with means $1/\lambda$ and α respectively. The resulting PDF of specific streamflows (Figure 4.1b) is expressed by a Gamma distribution [*Botter et al.,* 2007a]:

$$p_q(Q) = \frac{\Gamma\left(\frac{\lambda}{K_T}\right)^{-1}}{\alpha K_T}\left(\frac{Q}{\alpha K_T}\right)^{\frac{\lambda}{K_T}-1}\exp\left(-\frac{Q}{\alpha K_T}\right) \tag{4.2}$$

where Γ is the complete gamma function (see the supplementary information for more details on the model). According to equation (4.2), the coefficient of variation of Q is given by $CV_Q = \sqrt{\frac{K_T}{\lambda}}$, thereby allowing the identification of two distinct regimes: when $\lambda > K_T$ the frequency of the events contributing to streamflow is large compared to the recession time scale and $CV_Q < 1$, implying that the flow variability is reduced (persistent regime). Conversely, when $\lambda < K_T$ the frequency of flow-producing events is small and $CV_Q > 1$, meaning that the flow variability is enhanced (erratic regime).

The stochastic fluctuations of Q control the temporal variability of stage h. The functional relationship between streamflow Q and stage h (above a certain datum h_0), for a fixed cross section, is usually estimated through a power law relationship $h = aQ^b$ (otherwise known as the discharge rating curve) where a and b are dependent on the cross section morphology [*Leopold and Maddock,* 1953; *Stall and Fok,* 1968; *Chow et al.,* 1988]. The stochastic temporal dynamics of h at a daily timescale (Figure 4.1c) can therefore be derived from the equation (4.1) as:

$$\frac{dh\,(t)}{dt} = -bK_T h\,(t) + \xi_h(t) \tag{4.3}$$

Much like the streamflows, here the first term on the right-hand side represents the deterministic exponential decay of h between events (with rate bK_T) and the second term represents the stochastic jumps induced by streamflow producing rainfall events. The frequency of ξ_Q and ξ_h is the same (and equal to λ), while the distribution of the sizes of the jumps is different. The PDF of stage h (Figure 4.1d) can be obtained from the PDF of the streamflows using the derived-distribution approach [*Botter et al.,* 2010b]:

$$p_h\,(h) = \frac{\theta\Gamma\left(\frac{\lambda}{K_T}\right)^{-1}}{b}\,(\theta h)^{\frac{\lambda}{K_T b}-1}\exp\left[-\,(\theta h)^{\frac{1}{b}}\right] \tag{4.4}$$

$p_h(h)$ is a generalized gamma distribution with shape parameters $\frac{\lambda}{K_T}$ and $\frac{1}{b}$, and scale parameter $\theta = a^{-1}(\alpha K_T)^{-b}$, which represents the inverse of the stage observed when the discharge is equal to the mean jump produced by the streamflow producing event ($Q = \alpha K_T$). Therefore the PDF of stage h is presented explicitly in terms of climatic and landscape controls (λ, α, K_T) and morphological features of the cross section (a, b).

Riparian vegetation dynamics along the river transect is studied by means of the model developed by *Camporeale and Ridolfi* [2006], which depicts the growth and decay of riparian vegetation driven by varying water table and river stages. Here, we utilize this model with some modifications (described later in the text), which allow for a more direct analysis of the impact of the flow regime on riparian vegetation dynamics. In contrast to *Camporeale and Ridolfi* [2006],

here the symbol * indicates unit-less parameters. Moreover, stage and elevation dependencies have been made explicit throughout the formulation to emphasize the location dependence of each parameter. Other notations from the original paper (such as α) have been modified in order to avoid confusion with similar parameters used in the analytic formulas of flow regime and river stage.

The major effect of the stochastic nature of stage dynamics on riparian vegetation is the random alternation, at any site along the transect, between exposure (during which vegetation is allowed to grow) and inundation (during which vegetation is removed by flooding, see Figure 4.1). The shifting between the exposure and inundation states is modeled as a Dichotomic Markov process where each of the two available states have a random (exponentially distributed) duration. In this model the overall vegetation biomass of a single phreatophyte species is considered while inter-specific interactions are neglected. A steady state river morphology is considered and geomorphological processes (such as sedimentation and erosion) are neglected. Moreover, the time delay between the change in the river stage and the groundwater table is neglected. Based on the above assumptions the local stochastic dynamics of riparian vegetation at a certain elevation (Figure 4.1e) is modeled as a dichotomic process [*Camporeale and Ridolfi* 2007] in which biomass dynamics switch between growth (during exposure) and decay (during inundation). Mathematically:

$$\frac{dB}{dt^*} = \begin{cases} -\alpha_B(\eta^*)B & h^* \geq \eta^* \quad (a) \\ B\left(\beta(\eta^*) - B\right) & h^* < \eta^* \quad (b) \end{cases} \tag{4.5}$$

where $\eta^* = \frac{\eta}{<h>}$ and $h^* = \frac{h}{<h>}$ represent normalized transect height and stage, B is dimensionless vegetation biomass at a given point with normalized elevation η^* ($0 < B < 1$), β is the average carrying capacity and α_B expresses the average decay rate of vegetation α_d(scaled to a species specific growth rate α_g). Dimensionless time is represented in equation (4.5) as $t^* = \alpha_g t$.

Equation (4.5a) models the vegetation decay due to flooding. Therein, the values of $\langle\alpha_d\rangle$ and therefore α_B are modulated along the transect through stage fluctuations (see the supplementary information).

Equation (4.5b) captures the vegetation growth according to a generalized Verhulst-logistic function for a phreatophyte species tapping the groundwater [*Botkin et al., 1972*; *Camporeale and Ridolfi,* 2006]. $\beta(\eta^*)$ is the average carrying capacity, which is calculated based on the average availability of soil water within the root zone taking into account the stage fluctuations implied by the streamflow variability (see the supplementary information for more details on the model parameters). The carrying capacity is dependent on the vegetation-specific optimal groundwater depth, Z_r (the notation emphasizes the dependence on species-specific root properties).

Equation (4.5) is linked to the flow regime in two different ways: (i) indirectly, in the definition of the parameters $\alpha_B(\eta^*)$ and $\beta(\eta^*)$, whose expressions involve the stage PDF $p_h(h)$; (ii) directly, in the switching between inundation and exposure at a given elevation along the transect, which is a dichotomic process driven by streamflow variability. Formally (see section 3), the dichotomic noise is defined here through the inundation probability P_I and the correlation time of the noise τ, which can be interpreted as a measure of the memory of the process [*Ridolfi et al.,* 2011]. For a given probability of inundation P_I smaller values of τ imply shorter and more frequent flood

periods. P_I and τ embed all the dynamical features of the hydrologic forcing and will be formally linked to the flow regime in section 3.

This model (equation (4.5)) can be written in terms of a stochastic differential equation [*Kitahara et al.,* 1980] with a steady-state solution representing the long-term vegetation biomass PDF (Figure 4.1f) for a point along the transect [*Camporeale and Ridolfi* 2006]:

$$p(B) = \frac{N}{\alpha_B} B^{\frac{\beta(1-\alpha_B\tau^*)-(\alpha_B+\beta)P_I}{\alpha_B\beta\tau^*}} (\beta - B)^{\frac{P_I}{\beta\tau^*}-1} (\alpha_B + \beta - B) \tag{4.6}$$

where vegetation biomass is constrained between $[0, \beta]$, and N is the normalization constant. Dimensionless correlation time of the noise is represented in equation (4.6) as $\tau^* = \alpha_g\tau$. The PDF of vegetation can then be calculated for any given point along the transect based on α_B, β, P_I and τ^* provided that $\alpha_B P_I < \beta P_E$ (the convergence criterion for N), otherwise $p(B)$ converges to a Dirac delta distribution. This criterion is defined by parameters that are all location dependent, and thus it provides the lowest limit of the vegetated zone for a given transect and flow regime [*Camporeale and Ridolfi,* 2006].

4.3 Vegetation Dynamics in the Aquatic Terrestrial Transition Zone

Riparian vegetation dynamics take place within areas that are periodically inundated by streamflows. In this context, such areas are referred to as the aquatic/terrestrial transition zone (ATTZ) since they alternate between the aquatic and terrestrial environments [*Junk et al.,* 1989]. The pattern of switching between these conditions is a result of the variability of stages controlled by the river morphology and the underlying flow regime (Figure 4.1). This concept provides a clear framework for describing the impact of the hydrologic noise in a river transect. The diverse hydrologic conditions along the aquatic-terrestrial transition region can be described focusing on five interrelated attributes: probability of exposure P_E and inundation P_I, mean duration of exposure $\langle T_E \rangle$ and inundation $\langle T_I \rangle$, and the correlation scale of the dichotomic noise τ.

The probability of exposure $P_E(\eta)$ for a point along the river transect (i.e. for a specific elevation η) can be derived as a non-exceedance probability of the stage PDF evaluated for $h = \eta$. The analytical expressions for P_E, based on the stage PDF, is shown below:

$$P_E(\eta) = \int_0^\eta p(h)\, dh = \frac{\gamma\left(\frac{\lambda}{K_T}, (\theta\eta)^{\frac{1}{b}}\right)}{\Gamma\left(\frac{\lambda}{K_T}\right)} \tag{4.7}$$

where $\gamma(\cdot,\cdot)$ is the lower incomplete gamma function. Accordingly, the probability of inundation can be calculated as $P_I(\eta) = 1 - P_E(\eta)$. Under steady state conditions the mean duration of time spent in the exposure state $\langle T_E \rangle$ can be analytically derived using the crossing properties of stochastic processes driven by shot noise [*Masoliver, 1987*; *Laio et al.,* 2001b; *Porporato et al.,* 2001]. If we define $\eta = aQ_\eta^b$ as the streamflow corresponding to the critical condition $h = \eta$, the resulting expression for $\langle T_E \rangle$ as a function of Q_η is:

$$\langle T_E \rangle (Q_\eta) = \frac{P_E(Q_\eta)}{K_T Q_\eta p_q(Q_\eta)} \tag{4.8}$$

The above equation, expressing the mean duration of exposure in terms of Q_η, can be re-cast in terms of η by means of the power law mentioned above, and equations (4.2) and (4.7). The result is:

$$\langle T_E \rangle (\eta) = \frac{\gamma\left(\frac{\lambda}{K_T}, (\theta\eta)^{\frac{1}{b}}\right)}{K_T \left(\frac{\eta}{a}\right)^{\frac{1}{b}} (\alpha K_T)^{-\frac{\lambda}{K_T}} \left(\frac{\eta}{a}\right)^{\frac{1}{b}\left(\frac{\lambda}{K_T}-1\right)} \exp\left(-(\frac{\eta}{a})^{\frac{1}{b}}(\alpha K_T)^{-1}\right)} \tag{4.9}$$

The mean duration of inundation $\langle T_I \rangle$ for a point along the transect can be obtained with the same method as equation (4.9) and is shown below:

$$\langle T_I \rangle (\eta) = \frac{\Gamma\left(\frac{\lambda}{K_T}\right) - \gamma\left(\frac{\lambda}{K_T}, (\theta\eta)^{\frac{1}{b}}\right)}{K_T \left(\frac{\eta}{a}\right)^{\frac{1}{b}} (\alpha K_T)^{-\frac{\lambda}{K_T}} \left(\frac{\eta}{a}\right)^{\frac{1}{b}\left(\frac{\lambda}{K_T}-1\right)} \exp\left(-(\frac{\eta}{a})^{\frac{1}{b}}(\alpha K_T)^{-1}\right)} \tag{4.10}$$

The dynamics of the dichatomic noise are driven by fluctuations of the river stage and so the frequency and duration of exposure/inundation events change based on elevation along the transect. As a result, the correlation time of the hydrologic noise τ, which is defined as:

$$\frac{1}{\tau(\eta)} = \frac{1}{\langle T_E \rangle (\eta)} + \frac{1}{\langle T_I \rangle (\eta)} \tag{4.11}$$

shall be dependent on η. We avoid representing the resulting expression (which can be easily defined by combining equations (4.9), (4.10) and (4.11)) due to space limitations. Therefore, in contrast to previous works [*Camporeale and Ridolfi,* 2006], we relax the assumption that the correlation time of the noise is constant for all η and calculate the changing value of τ for every point along the transect. We will discuss this matter further in section 4.

The distribution of mean exposure/inundation times provides an accessible description of the hydrologic noise along the river transect (Figure 4.2a, b, c). Below the threshold η_{EP} (defined as $\langle T_E \rangle (\eta_{EP}) = 1$ day) the system experiences a near constant aquatic (inundated) environment with exposure pulses of typical duration shorter than one day. Similarly, above the threshold η_{FP} (defined as $\langle T_I \rangle (\eta_{FP}) = 1$ day) the transect has a terrestrial (exposed) environment with floods typically lasting less than one day. The zone between these two points (dichotomic region) is periodically flooded with decreasing probability as elevation from the bottom of the river bed increases. Therein, the average duration of the exposure and inundation period exceeds one day. These different conditions are a result of the variability of stages, which is in turn based on the underlying flow regime and river morphology. The analysis of stage crossing times provides a framework to properly characterize the hydrologic noise in terms of instantaneous shots or dichotomic noise [*Tealdi et al.,* 2013].

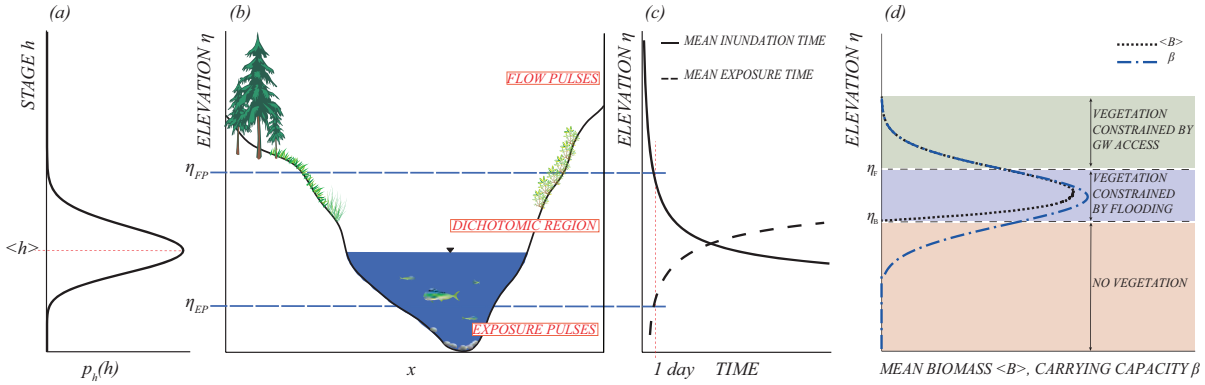

Fig. 4.2: (a) Probability density of the stages, (b) The river transect, (c) Distribution of mean exposure $\langle T_E \rangle$ and inundation $\langle T_I \rangle$ times along the river transect, (d) Distribution of mean vegetation biomass ($\langle B \rangle$, straight line) and carrying capacity (β, dashed line) along the transect. The exposure pulse region is the zone below η_{EP} where $\langle T_E \rangle < 1$ day. Similarly, the flow pulse region is the zone above η_{FP} where $\langle T_I \rangle < 1$ day. The average duration of exposure and inundation is larger than one day in the dichotomic region. There are three types of behavior depending on the position along the transect: no vegetation, vegetation constrained by flooding, and vegetation constrained by groundwater access. η_B represents the point where $\langle B \rangle = 0$, and η_F is the point where $\langle B \rangle$ converges to the value of the carrying capacity.

The analytical formulation allows for the calculation of the first moment of the vegetation PDF, which is stated here in a form simpler than previously provided by *Camporeale and Ridolfi* [2006]. The mean vegetation biomass for a point along the transect is expressed as:

$$\langle B \rangle = (1 + \alpha_B \tau^*) \frac{[\beta - (\alpha_B + \beta) P_I]}{1 - P_I + \alpha_B \tau^*} \tag{4.12}$$

provided that convergence criterion, $\alpha_B P_I < \beta P_E$, is satisfied. This formulation is advantageous (with regards to equation (4.12) in *Camporeale and Ridolfi* [2006]) since it allows for a more direct understanding of the role played by the various parameters involved (see below). All parameters in the expression above are driven by the statistical characteristics of the stage and are therefore dependent on the underlying streamflow regime.

In order to analyze the pattern of $\langle B \rangle$ along the transect it is constructive to introduce two new parameters (Figure 4.2d). η_F is the elevation above which the value of $\langle B \rangle$ is similar to the carrying capacity ($\langle B \rangle \approx \beta$), and η_B represents the lowest limit of the vegetated zone ($\langle B \rangle = 0$). It is interesting to note that η_B is independent of the correlation of the noise and it rather depends only on vegetation features (α_B, β) and the stage PDF (P_E, P_I).

It is possible to distinguish three patterns of behavior, depending on the elevation of the point considered along the transect (Figure 4.2d). The first zone, located below η_B, is characterized by the absence of vegetation. In this zone α_B is largest and P_I approaches one. In the second zone, located between η_B and η_F, the system switches between the inundation and exposure states frequently enough to constrain vegetation growth by flooding. Here β reaches a maximum, and mean vegetation biomass is also at its largest value. However, the decay caused by flooding constrains vegetation growth and thus $\langle B \rangle < \beta$. In the third area while P_I approaches zero, the value of $\langle B \rangle$ is comparable to the carrying capacity ($\langle B \rangle \approx \beta$). Consequently, mean vegetation biomass declines as the access of vegetation to groundwater is constrained.

Sensitivity analysis revealed that despite the changing value of τ along the transect, its relative impact on the overall mean vegetation biomass is not significant in the cases analyzed (see discussion in section 4). As a consequence, equation (4.12) can be further simplified to:

$$\langle B \rangle = \beta - \frac{\langle \alpha_d \rangle P_I}{\alpha_g P_E} \tag{4.13}$$

This formulation highlights the important role of groundwater access as a control for vegetation growth. One can then discuss $\langle B \rangle$ as the difference between maximum possible biomass (the carrying capacity) subtracted by the ratio between scaled decay and scaled intrinsic growth rates of the species. The scaling factors for decay and growth rates are represented by the time spent in the inundation (P_I) and exposure (P_E) states.

In order to better understand the impact of the hydrologic noise on the behavior of mean vegetation biomass, we developed the deficiency index defined as:

$$D_i = \frac{\beta - \langle B \rangle}{\beta} = \frac{\alpha_B P_I \left[(\beta + \alpha_B) \tau^* + 1 \right]}{\beta \left(1 - P_I + \alpha_B \tau^* \right)} \tag{4.14}$$

In physical terms, D_i represents the deviation from the maximum potential vegetation biomass along the transect due to flooding. In cases where the overall mean vegetation biomass is found to be unaffected by the terms associated with τ^* (see later discussion in section 3), the above expression can be further simplified into:

$$D_i = \frac{\alpha_B P_I}{\beta P_E} = \frac{\langle \alpha_d \rangle P_I}{\alpha_g \beta P_E} \tag{4.15}$$

In other words, the deficiency index can be thought of as the ratio between an effective decay rate ($\langle \alpha_d \rangle P_I$) and an effective growth rate ($\alpha_g \beta P_E$). The decay rate is scaled to the time spent in the inundation state (P_I) while the growth rate is scaled to the time spent in the exposure state (P_E) and the carrying capacity (β). D_i has a range of $[0 - 1]$. It is equal to 0 at η_F where vegetation biomass is not limited by flooding (P_I approaches 0) and increases to 1 at η_B where mean vegetation biomass approaches zero. It is intriguing to note that the concept expressed through the deficiency index is the same as the validity criterion for $\langle B \rangle$.

Based on equation (4.15), a general analytic expression for the deficiency index D_i can be derived by employing inherent properties of the gamma function:

$$D_i = \frac{\Gamma\left(\frac{\lambda_p}{K_T}\right)}{\Gamma\left(\frac{\lambda_p}{K_T} + b\right)} \frac{\Gamma\left(\frac{\lambda_p}{K_T} + b, (\theta\eta)^{\frac{1}{b}}\right) - \theta\eta\Gamma\left(\frac{\lambda_p}{K_T}, (\theta\eta)^{\frac{1}{b}}\right)}{\Gamma\left(\frac{\lambda_p}{K_T}, (\theta\eta_l)^{\frac{1}{b}}\right) - \Gamma\left(\frac{\lambda_p}{K_T}, (\theta\eta_h)^{\frac{1}{b}}\right)} \tag{4.16}$$

where $\Gamma(\cdot, \cdot)$ represents the upper incomplete gamma function, and η_l, η_h are the lower and upper bounds of the optimal range of groundwater for growth determined by Z_r (see the supplementary information).

4.4 Case Studies

The model described in the previous sections is applied (for the summer season) to the terminal reach of two different catchments characterized by contrasting flow regimes: the Boite (persistent,

$CV_Q = 0.37$) and Youghiogheny (erratic, $CV_Q = 1.4$) river basins. The Boite river is a tributary of the Piave river, located in the Dolomites region in north eastern Italy. It drains a catchment of 313 km^2 at Cancia, with an average discharge of 12.7 m^3/s. Observed rainfall, streamflow and stage data (at daily time scale) from the summer months (June-August) of the period 1986-2008 were utilized. The Youghiogheny River, a tributary of the Monongahela River, is located near Oakland (MD) in the United States. It drains an area of 347 km^2 and has an average discharge of 3.6 m^3/s. Observed rainfall, streamflow and stage data (at daily time scale) from the summer months of the period 1993-2012 were utilized.

Figure 4.3 illustrates the comparison between the analytical (solid line, equation (4.2)) and observed (bars) streamflow PDF during the summer season for both catchments. Parameters of the model were independently evaluated based on observed hydroclimatic data and not fitted to the observed distribution (see Botter et al., 2007b; 2007c; 2013 for more details on the parameter identification procedure). The theoretical gamma distribution provides a good fit to the streamflow PDF estimated based on the observed data in both regimes.

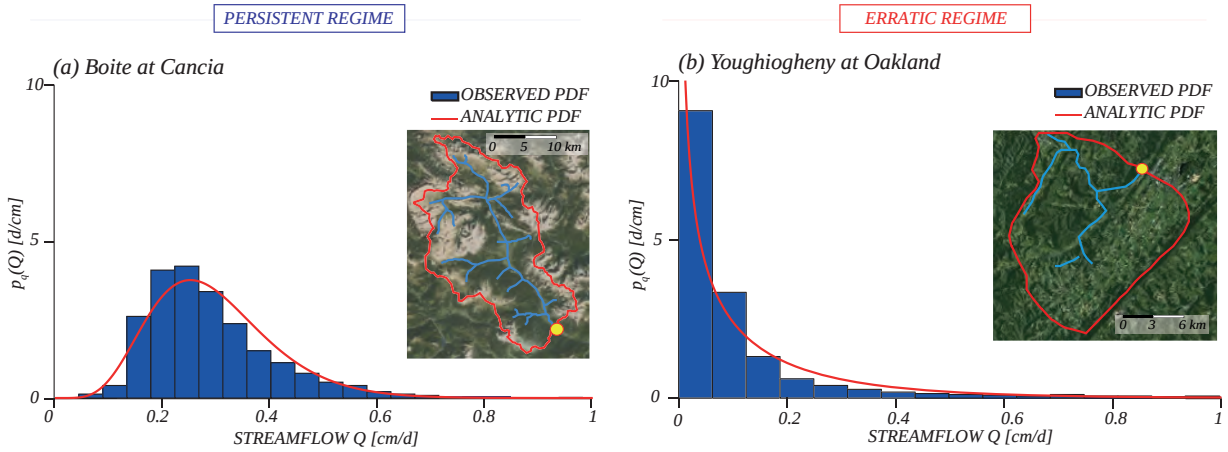

Fig. 4.3: Comparison between the analytical streamflow PDF (solid line) and the streamflow PDF estimated from summer season observed data (bars): (a) Boite River at Cancia, Italy ($\alpha = 0.65$ $[cm]$, $\lambda = 0.45$ $[d^{-1}]$ and $K_T = 0.066$ $[d^{-1}]$); (b) Youghiogheny River at Oakland, US ($\alpha = 0.91$ $[cm]$, $\lambda = 0.13$ $[d^{-1}]$ and $K_T = 0.28$ $[d^{-1}]$).

Figure 4.4 depicts the comparison between the analytical (solid line, equation (4.4)) and observed (bars) stage PDFs, and the shape of river transects at the catchment outlet. In addition the figure provides a comparison of the analytical and observed values of the average duration of exposure $\langle T_E \rangle$ (dashed line and squares) and inundation periods $\langle T_I \rangle$ (solid line and circles). The river transects feature a complex morphology and represent the most recent measurements available. The analytical stage PDFs provide a good fit to the observed stage PDFs and capture the overall variability stages for both catchments. It should be noted that in this model we utilize fixed mean values for rating curve parameters a and b. These fixed values are not always capable of capturing the frequent changes of the river morphology prevalent in some systems. The poor agreement between the analytical and observed stage PDFs close to zero for the erratic regime (Figure 4.4b) can be attributed to this.

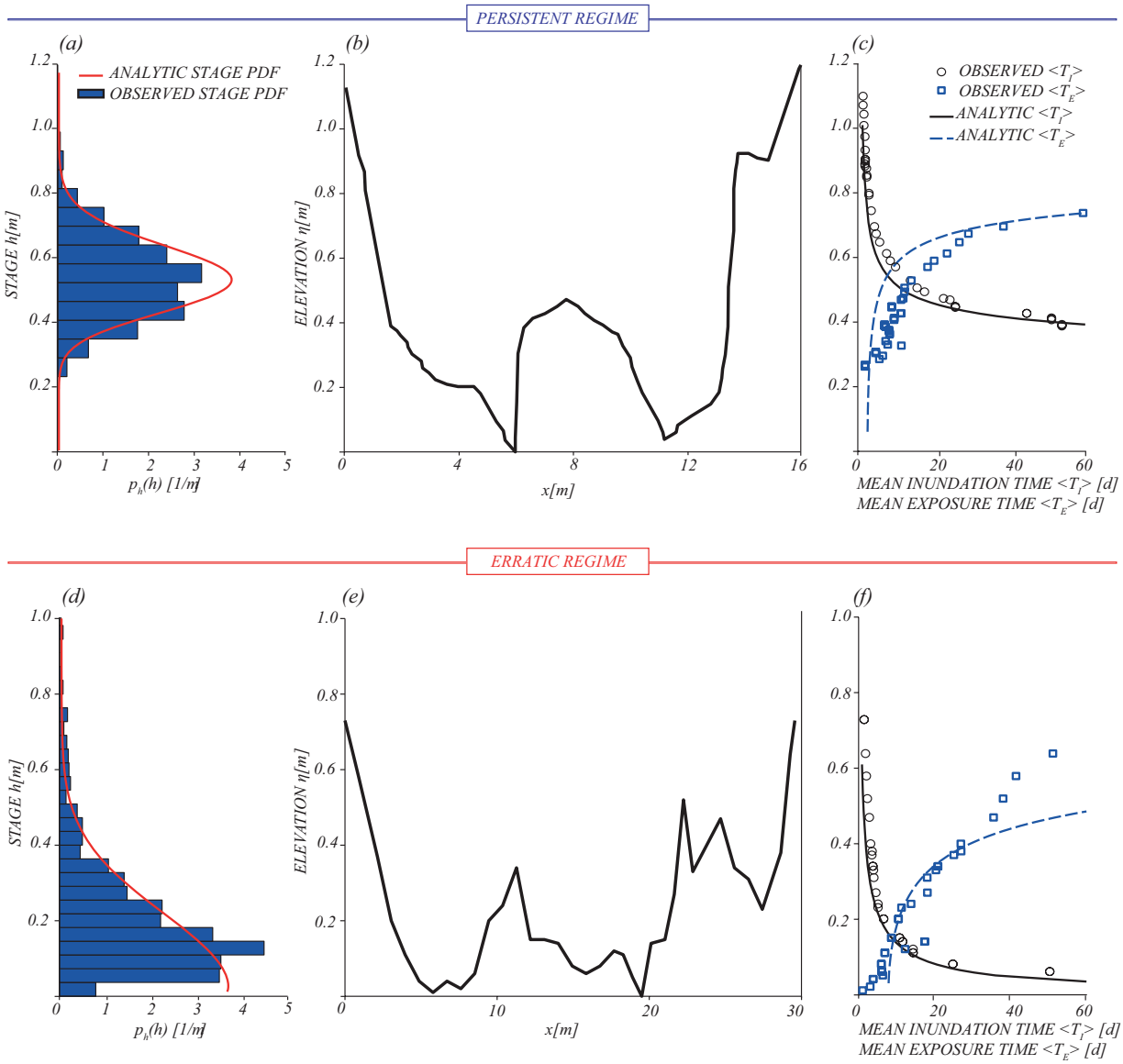

Fig. 4.4: (a,b) Comparison between the analytical (solid line) and observed (bars) stage PDFs, (c,d) river transect at the catchment outlet, (e,f) comparison of the analytical and observed mean duration of inundation $\langle T_I \rangle$ (solid line, circles) and exposure $\langle T_E \rangle$ (dashed line, squares). Rating curve parameters are $a = 1.03$ $[m(d/cm)^b]$, $b = 0.498$ $[-]$ for the Persistent regime (Boite River) and $a = 0.61$ $[m(d/cm)^b]$, $b = 0.49$ $[-]$ for the erratic regime (Youghiogheny River).

The agreement between the observed mean duration of exposure/inundation periods and the corresponding analytical estimates is reasonable, despite a systematic underestimation of $\langle T_E \rangle$ for the persistent regime. also note that some scattering appears in the data, for the low and high elevations, due to the limited size of the sample considered. The distribution of $\langle T_I \rangle$ is similar in both regimes. However, the exposure pulse zone (where exposure events last less than one day) is wider in the persistent regime. In contrast, in the erratic regime, the exposure pulse region is smaller owing to the longer recessions of streamflows and the higher probability of low flows. The poor agreement between the analytic and observed values of $\langle T_E \rangle$ of the erratic regime for low elevations is consistent with the behavior of the analytical stage PDF, where the observed

probability of stages close to zero is not accurately captured. The flow pulse region (where inundation events last less than one day) is limited to the edges of the transect, where high elevation makes the effect of flooding less important. Hence the representation of the hydrologic forcing in terms of dichotomic noise (upon which the analytical model of vegetation dynamics used in this paper relies) proves meaningful in these cases.

In both regimes $\langle T_E \rangle$ tends towards zero for low elevations, though it does so much faster in the persistent regime. The rapid decline indicates a dual behavior of mean vegetation biomass in the persistent regime, with no vegetation in the permanently inundated zone and undisturbed vegetation growth in the permanently exposed zone. This implies that biological succession is more likely to occur in the persistent regime. In erratic regimes instead, a large zone of the transect is characterized by a more dynamic exposure/inundation pattern leading to rapid growth and decay of vegetation. This promotes a distribution of vegetation along the transect according to the optimal elevation dictated by vegetation specific features.

The mean duration of exposure/inundation change with the elevation η due to fluctuations of the river stage (Figure 4.4). Consequently, the correlation time scale of the hydrologic noise τ shows a clear pattern along the transect. Figure 4.5 shows the observed and analytically calculated values of τ for both persistent and erratic regimes. These results confirm that τ does in fact change along the transect. In line with our previous assertion regarding equation (4.11), this change in τ was taken into account when calculating the mean biomass along the transect.

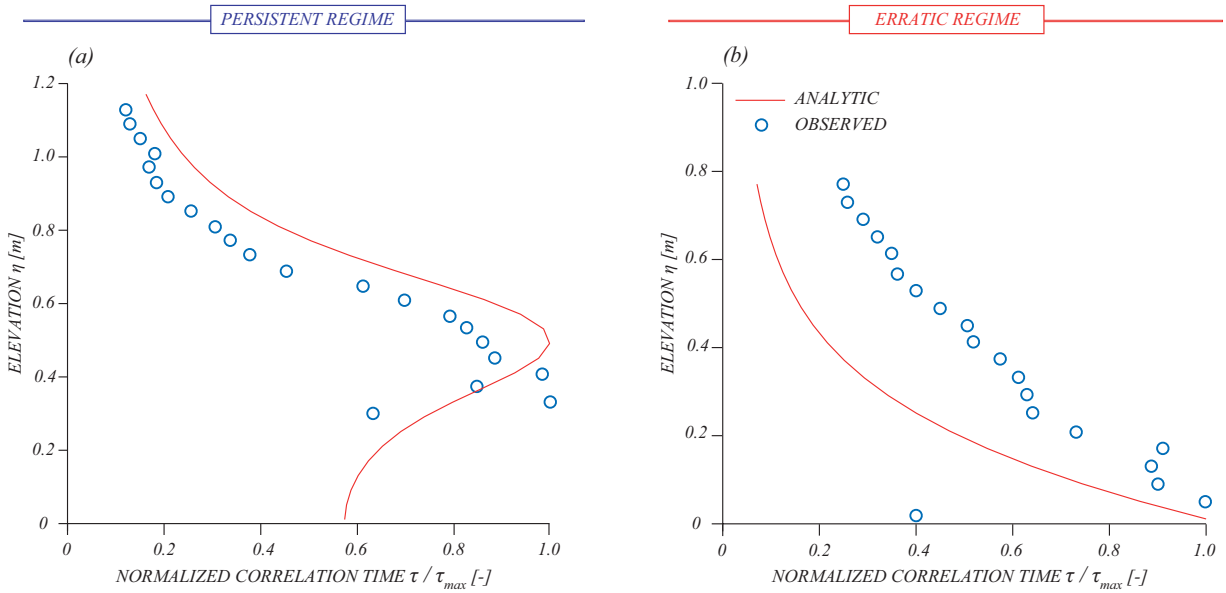

Fig. 4.5: Observed and analytical values of τ (suitably normalized by the corresponding maximum value of τ represented by τ_{max}) along the transect for both (a) persistent and (b) erratic regimes.

It is important to analyze the impact of vegetation specific parameters on the distribution of $\langle B \rangle$ along the transect in order to explore the different nature of the hydrologic noise in the two regimes. In line with *Camporeale and Ridolfi* [2006], the species-specific parameters considered here are the optimum depth of groundwater Z_r and the sensitivity to flooding k, which is related to the coefficient α_B in equation (4.5) (see the supplementary information). Figure 4.6 shows the

distribution of the carrying capacity β (dashed line) and the mean vegetation biomass (solid lines) for different values of $k = [0.28, 2.8, 10]$ and optimum depth of groundwater $Z_r = [0.1, 0.25, 0.5]m$. It is important to note that these values do not apply to any particular species. Rather they have been chosen from a range of possible values [*Camporeale and Ridolfi,* 2006; *Baskerville,* 1965; *Perry et al.,* 1969; *Young et al.,* 1980] in order to highlight the relevance of the different processes that control the distribution of vegetation biomass on a transect. In the zone where flooding is the limiting factor, the impact of the hydrologic noise is modulated by the value of k for different species. Where $\langle B \rangle$ is limited by access to groundwater, Z_r is the main control. The impact of flooding on vegetation is reduced with increasing Z_r. This is because, for larger values of Z_r, the optimal zone for the growth of a particular species is displaced to a higher elevation along the transect where flooding is less frequent. In the persistent regime, except for low optimum groundwater depths (Figure 4.6 a,b,c), the pattern of $\langle B \rangle$ along the transect remains relatively unchanged for different values of k. In the erratic regime (Figure 4.6 d,e,f), however, vegetation is still affected by flooding at similar optimum groundwater depths. The large variability of the streamflows in the erratic regime (owing to the larger ratio of λ/K_T) leads to a larger area along the transect where the distribution of $\langle B \rangle$ is impacted by flooding. Moreover, the peak of $\langle B \rangle$, for more sensitive species, is generally smaller as a result of the large variability of streamflows. In general, at large distances from the river base, the impact of flooding is less severe and thus access to groundwater becomes the limiting factor for vegetation growth. In contrast, at elevations closer to the river base, sensitivity to flooding (represented by k) is the dominant limiting factor. The value of k inversely effects the peak value and extent of $\langle B \rangle$, though its impact is more severe in the erratic regime. The enhanced sensitivity of vegetation biomass patterns to species-specific ecological attributes in erratic regimes promotes a heterogeneous distribution of riparian vegetation along the river transect, with disjointed elevation ranges for species with different Z_r and k.

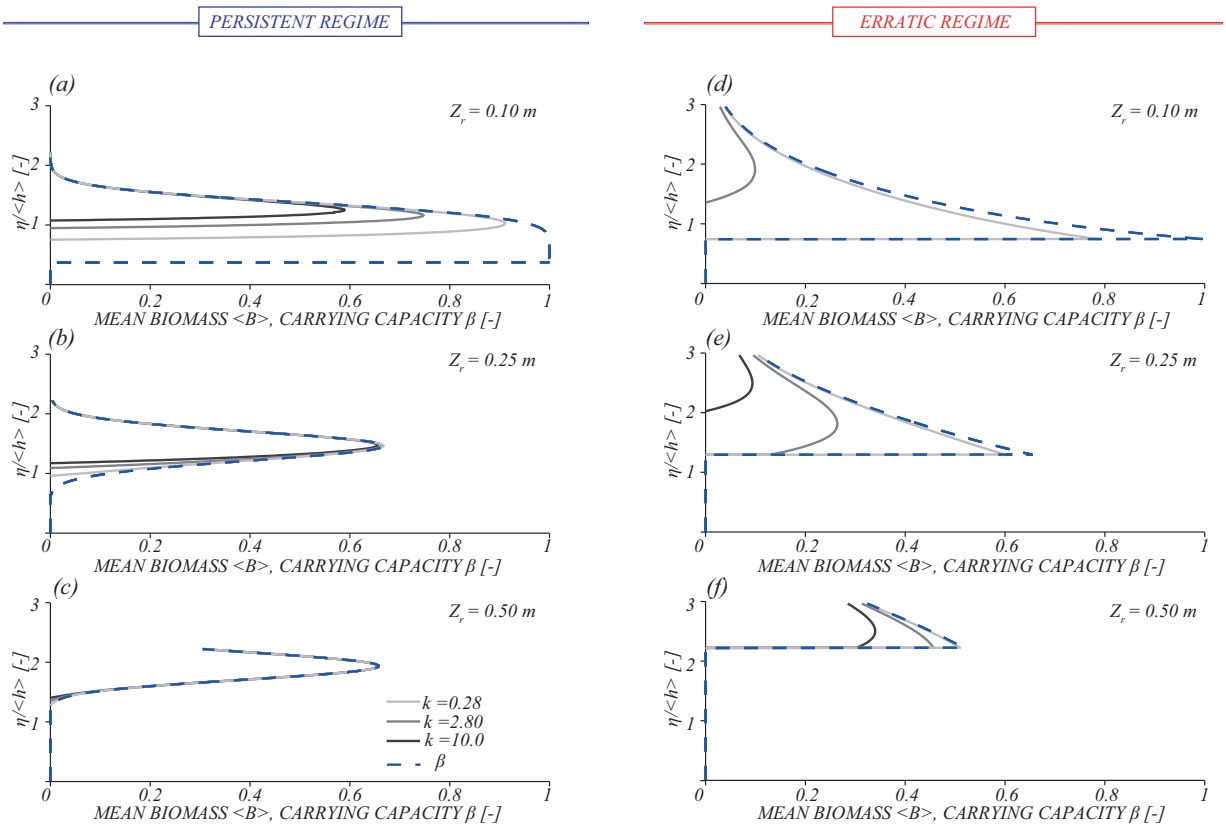

Fig. 4.6: Distribution of mean vegetation biomass ($\langle B \rangle$, solid lines) and carrying capacity (β, dashed line) along the transect for $k = [0.28, 2.8, 10]$ and $Z_r = [0.1, 0.25, 0.5]$ m in: persistent regime, Boite River (a,b,c), and erratic regime, Youghiogheny River (d,e,f). The values of Z_r considered are the same in both cases. The normalized values ($Z_r / < h >$) change in the two catchments based on the respective mean stage. Values of $Z_r / < h >$ are $[0.18, 0.45, 0.9]$ for the Boite river and $[0.4, 1, 2]$ for the Youghiogheny river.

The rigorous characterization of the correlation time scale of the hydrologic noise along the transect (Equation (4.11)) allowed for a suitable investigation of the role played by such parameter for the mean biomass. Despite the changing value of correlation time of the hydrologic noise along the transect, it was revealed that the relative impact of τ^* on the overall mean vegetation biomass is not significant in the cases analyzed, and limited to the zone where vegetation is constrained by flooding. The results presented in Figure 4.6 remained the same, when calculated based on equation (4.12) or (4.13). Therefore, previous results obtained based on the assumption that τ is constant along the transect and equal to the correlation time scale of streamflows [Camporeale et al., 2006] can be applied to most practical settings.

Figure 4.7 shows the distribution of D_i along the transect for the same range of k and Z_r considered previously. D_i is largest and equal to 1 at η_B and decreases thereafter to zero at η_F. The figure shows that in the persistent regime vegetation biomass quickly reaches the maximum potential (β) with increasing η^* regardless of underlying ecological parameters (k and Z_r). In the erratic regime the extent of the region impacted by flooding (where decay of D_i with respect to η^* is slower as k increases) is considerably larger. In both regimes the extent of the zone disturbed by flooding narrows with increasing Z_r. Therefore, the lowest limit of the vegetated zone is determined by Z_r, while k affects the rate of decrease of D_i along the transect.

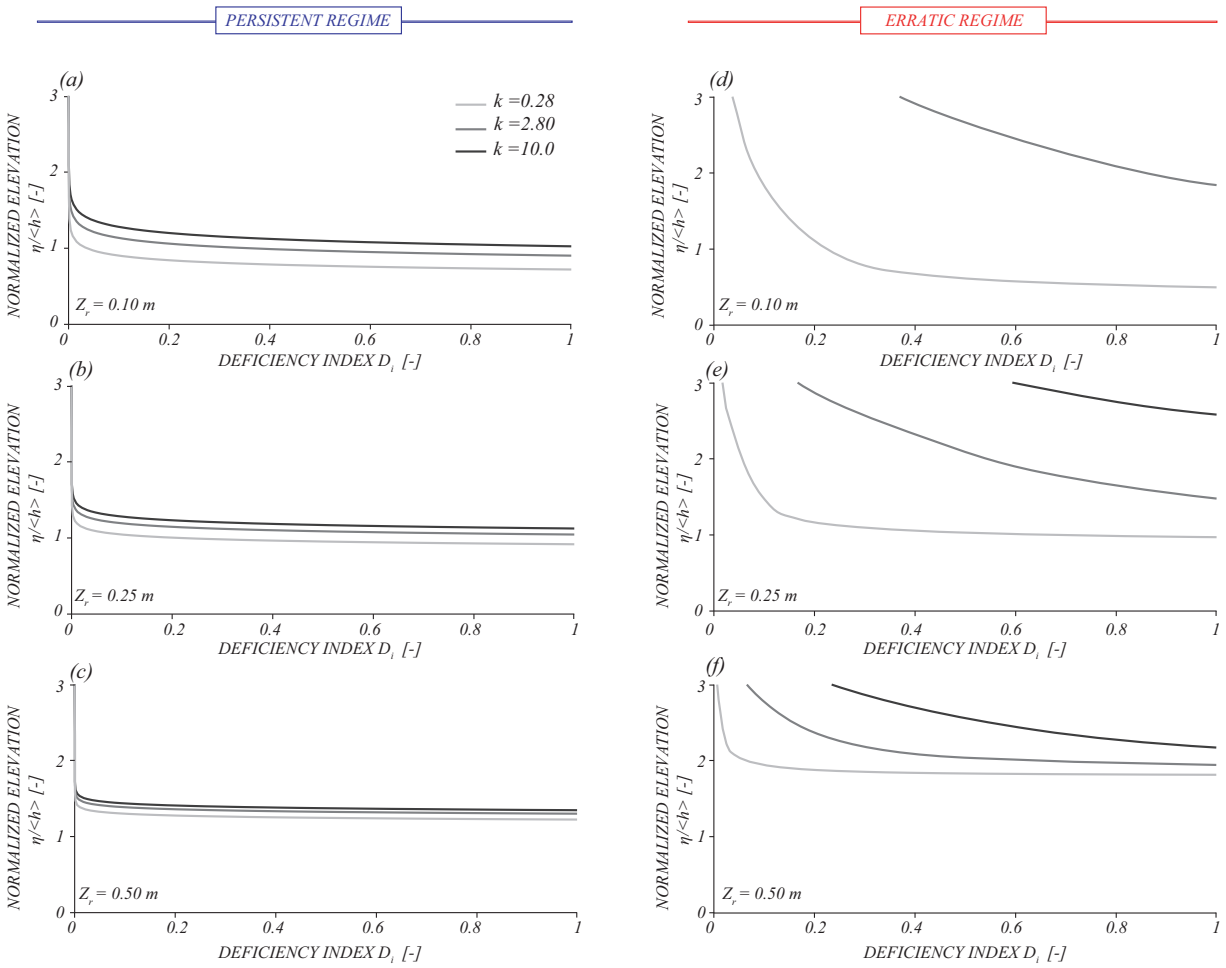

Fig. 4.7: Distribution of the deficiency index D_i along the transect for $k = [0.28, 2.8, 10]$ and $Z_r = [0.1, 0.25, 0.5]$. The cases considered are: Persistent regime, Boite River (a,b,c), Erratic regime, Youghiogheny River (d,e,f).

These results suggest that, despite competition and interspecific interactions not being taken into consideration within the framework, the dissimilar patterns of mean vegetation biomass in erratic (heterogeneous) and persistent (homogeneous) regimes may be of fundamental importance in explaining ecological gradients along aquatic terrestrial transition zones.

4.5 The Impact of Hydroclimatic Fluctuations

Thus far, we have explored the behavior of riparian vegetation in different flow regimes. However, the hydro-climatic parameters used in the model are temporally averaged values calculated from long-term historical data. It is equally interesting to investigate the impact of possible changes of climate/landscape properties on the patterns vegetation growth along the river transect.

The driving hydroclimatic parameters of the flow model are λ, α, and K_T (Equation (4.2)). In particular, the ratio λ/K_T is the indicator of the type of flow regime, with values less than

one suggesting an erratic regime and values greater than one representing a persistent regime. All three parameters may display significant long-term changes due to climate an landscape modification: inter-annual variability of the mean intensity of the events are specified by inter-annual fluctuations of α, while inter-annual changes in λ captures the combined effect of alteration in frequency and depth of precipitation as well as other parameters such as evapotranspiration. The inter-annual variability of K_T in turn captures the fluctuations in catchment-scale landscape response to rainfall events [*Botter et al.,* 2013].

In order to analyze the impact of possible long-term hydroclimatic fluctuations on flow/stage regimes and vegetation biomass, hypothetical scenarios were devised, where different values of α and λ/K_T within the range between the maximum and minimum observed values (Figure 4.8a, Figure 4.9a) were considered. In Figure 4.8, in particular, we analyze the effect of increasing rainfall depth α where the ratio λ/K_T (the shape parameter of the streamflow PDF) is kept constant and equal to that of the entire time series for each flow regime. This is tantamount to keeping the regime the same (i.e. persistent regime remains equally persistent), while increasing the amount of rain during wet days. Figure 4.8 depicts the PDF of streamflows (Figure 4.8b, f), stages (Figure 4.8c, g), as well as the mean biomass (Figure 4.8d, h) and deficiency index (Figure 4.8e, i) along the river transect for the persistent and erratic regimes. In the case of the persistent regime, changes in α produce a noticeable change in the distribution of streamflows and river stages (including the mean, variance, and the mode). The change of rainfall depth also produces an upward shift in the mean biomass along the transect, with a small reduction of the peak. In the erratic regime instead, the PDF of streamflows remain relatively unchanged. This is in line with observed reduced sensitivity of erratic flow regimes to changes in the climate [*Botter et al.,* 2013]. The shape of stage PDF in this case is not similar to the shape of flow PDF due to the reduced derivatives of $p_h(h)$. This is especially true for low stage values, where the performance of the analytical model is quite poor (see Figure 4.4). The increase in rainfall increased the area of impact of the hydrologic noise along the transect (Figure 4.8h). As a consequence, the shift and reduction of peak mean biomass is more noticeable in the erratic regime (where the effect of flooding is larger) compared to the persistent regime.

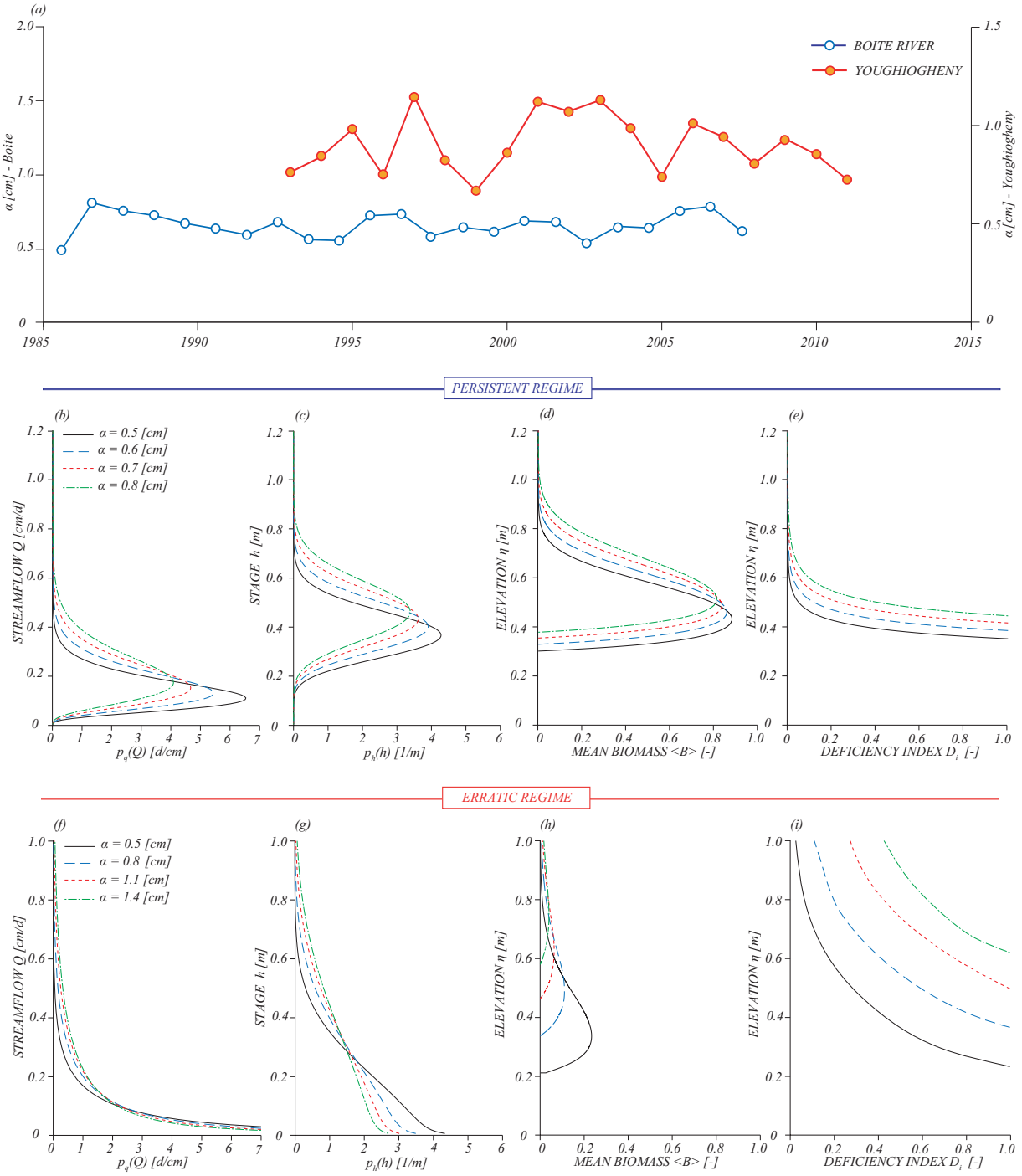

Fig. 4.8: Effect of increasing rainfall depth α on vegetation biomass along the transect. The ratio λ/K_T is kept constant and equal to that of the entire time series for each flow regime. (a) temporal fluctuations of observed values of α, (b,f) PDF of streamflows, (c,g) PDF of stages, (d,h) mean biomass, (e,i) deficiency index along the river transect for the persistent and erratic regimes. $\alpha = [0.5, 0.6, 0.7, 0.8]$ and $\lambda/K_T = 4.21$ for the persistent regime, and $\alpha = [0.5, 0.8, 1.1, 1.4]$ and $\lambda/K_T = 0.46$ for the erratic regime. Vegetation specific parameters were kept the same ($Z_r = 0.1[m]$ and $k = 2.8$) for all scenarios. The choice of values was deliberate as to allow a better visualization of the results. Nevertheless, similar patterns can be obtained with different parameter combinations.

Changes in the climate can also lead to significant shifts in the type of flow regime. Figure 4.9a depicts the temporal fluctuations of λ/K_T for both cases considered in this study. It is interesting to note that in the erratic regime, the ratio exceeds the threshold $\lambda/K_T = 1$ in some cases. This indicates that the catchment does not always follow an erratic behavior. Figure 4.9 depicts the PDF of streamflows (Figure 4.9 b, f), stages (Figure 4.9 c, g), as well as the mean biomass (Figure 4.9d, h) and deficiency index (Figure 4.9e, i) along the river transect for the observed range of λ/K_T. In the persistent regime, the increasing value of the ratio λ/K_T is depicted with smaller variance in the PDF of streamflows and stages. The reduced variability of streamflows limits the vegetation growth to a smaller area with larger peaks, approaching the maximum potential biomass (carrying capacity). The effect of an increase in the ratio λ/K_T on the mean biomass is overall weak specially in extremely persistent regimes. This can be more readily recognized in the deficiency index curves, where a sharp transition from 0 to 1 is observed. A similar trend can be observed in the erratic regime. However, the effect of changes in the type of flow regime is enhanced in this case, with larger shifts of mean biomass and extremely low peaks of $\langle B \rangle$ in cases where $\lambda/K_T < 1$. Note that when $\lambda/K_T = 1.4$, the streamflow PDF is indeed no longer of the erratic type. At the other extreme, when $\lambda/K_T = 0.1$, the stage PDF is also monotonic. In this case no vegetation is present along the entire transect.

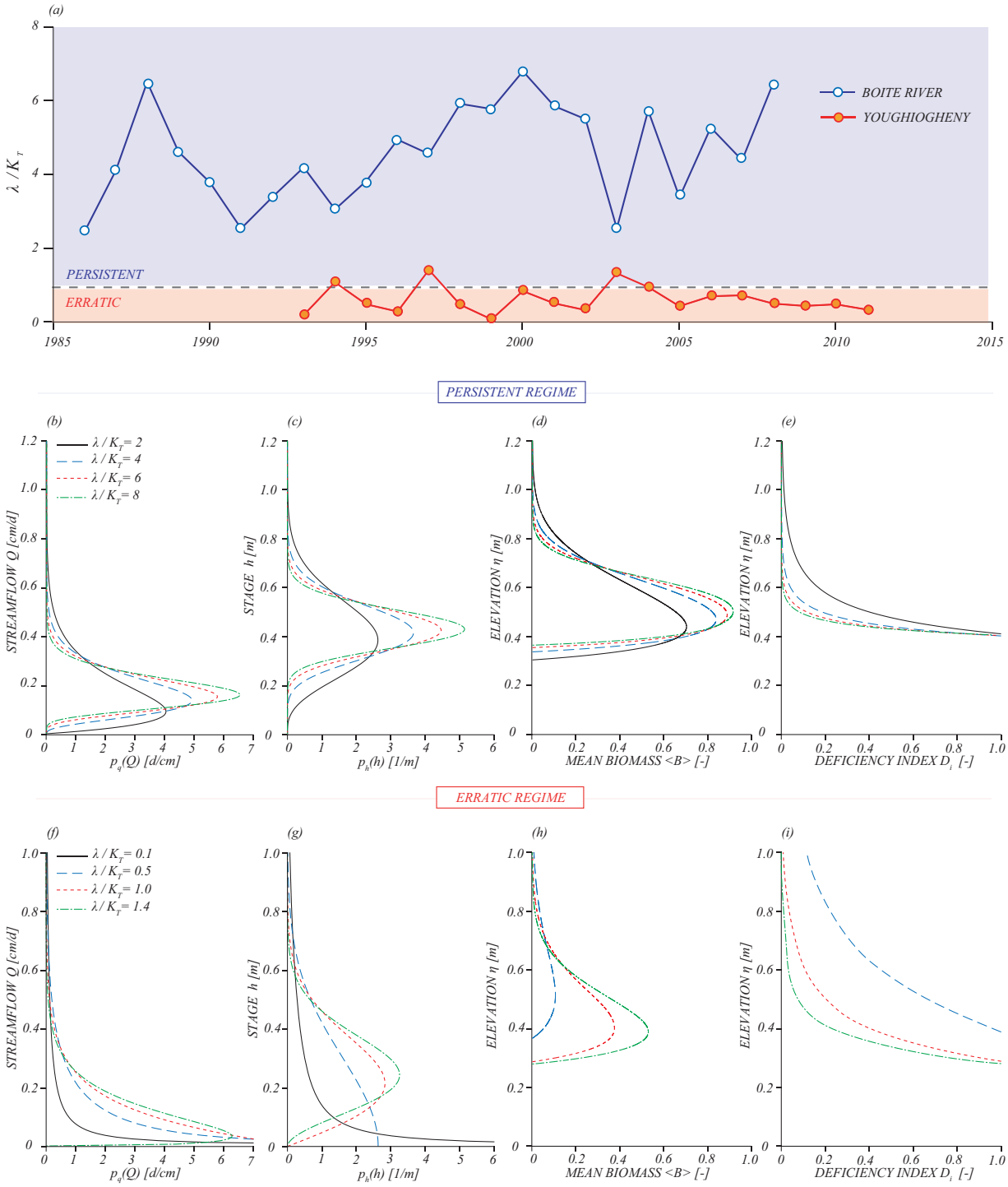

Fig. 4.9: Effect of shifts in flow regime on vegetation biomass along the transect. (a) temporal fluctuations of observed values of λ/K_T, (b,f) PDF of streamflows, (c,g) PDF of stages, (d,h) mean biomass, (e,i) deficiency index along the river transect for the persistent and erratic regimes. $\alpha = [1.37, 0.68, 0.46, 0.34]$ and $\lambda/K_T = [2, 4, 6, 8]$ for the persistent regime, and $\alpha = [4.19, 0.84, 0.42, 0.29]$ and $\lambda/K_T = [0.1, 0.5, 1.0, 1.4]$ for the erratic regime. Vegetation specific parameters were kept the same ($Z_r = 0.1[m]$ and $k = 2.8$) for all scenarios.

These results indicate that changes in the climate can amplify existing conditions (i.e. regime

becomes more persistent), and in some instances lead to a shift between erratic and persistent regimes. In the previous section we elaborated on the significance of vegetation specific parameters in the distribution of mean biomass. The measure of sensitivity to flooding and optimum groundwater depth make some species suited to a particular flow regime. Thus, a shift in the type of flow regime can be detrimental to some vegetation, especially riparian species in erratic regimes, which appear to be most sensitive to hydroclimatic change. This becomes doubly important since previous studies [*Botter et al.,* 2010a; *Destouni et al.,* 2013] have shown that anthropogenic changes in the river system can lead to human-induced shifts in flow regimes.

4.6 Conclusion

This paper explored the legacy of river flow regimes and reach morphology on patterns of mean vegetation biomass along complex river transects. To this aim we employed a stochastic model of streamflows, stages and riparian vegetation dynamics that explicitly couples catchment-scale hydroclimatic processes, morphologic attributes of the river transect and in-stream bio-ecological features. The stochastic model was able to reproduce the observed distribution of mean exposure and inundation times along the transect reasonably well, thereby providing a robust tool for characterizing the hydrologic noise in riparian areas. The different behaviors observed in erratic and persistent flow regimes allow this hydrologic distinction to be used as a framework for understanding the patterns of riparian vegetation and, in particular, the role of flooding as a limiting factor for vegetation growth. The hydrologic noise, in concurrence with ecological attributes, defines the lowest bound for vegetation in both regimes. In persistent regimes, where variability in streamflow is low, the spatial pattern of vegetation along the river transect is primarily determined by groundwater access. The pronounced vertical gradients of mean inundation and exposure times lead to a noticeable transition between aquatic and terrestrial environments and a narrow vegetated zone with homogeneous vegetation patterns. On the contrary, the large variability of streamflows in erratic regimes, reflected by a slower decline in mean duration of exposure, leads to a wider zone impacted by flooding. The erratic regime exhibits vegetation patterns whose peaks are separated based on the underlying ecological properties (sensitivity to flooding and access to groundwater). Moreover, under changing climatic patterns, the large area of impact of the hydrologic noise leads to a more noticeable shift and reduction of mean biomass in the erratic regime compared to the persistent regime. Notwithstanding the simplicity used to describe the analyzed phenomena, the proposed model allowed us to highlight the pivotal role of the flow regime in determining the different distributions of the riparian vegetation along a river transect in persistent and erratic regimes.

Acknowledgments

The research leading to these results has received funding from the European Community's Seventh Framework Program (FP7/2007-2013 under grant agreement n265063). The US Geological Survey, the National Climatic Data Center, and the Italian Regional Agency for Environmental Protection of the Veneto Region are acknowledged for providing hydrological and hydrometeorological data. We would like to particularly thank the USGS staff in Oakland (MD) for their

exceptional support. Additional backing was provided by Eawag, the Competence Center Environment and Sustainability (CCES) of the ETH domain in the framework of the RECORD (Restored Corridor Dynamics) and RECORD Catchment projects. Gianluca Botter and Stefano Basso acknowledge funding from research grant CPDA105501.

4.7 Supplementary Information

4.7.1 Flow Regime

In this paper, the flow regime was characterized by means of an analytical mechanistic model [*Botter et al.,* 2007a] based on a catchment-scale soil water balance forced by stochastic Poisson rainfall (modeled at daily timescales) with frequency λ_p and exponentially distributed precipitation depths with average α [*Rodriguez-Iturbe et al.,* 1999; *Porporato et al.,* 2004; *Botter et al.,* 2007a]. The portion of rainfall contributing to streamflows is identified by the set of events providing sufficient water to fill the water deficit created by plant transpiration in the root zone and drive the soil water content in the region above its retention capacity. The distribution of streamflow-producing rainfall events is also assumed to follow a Poisson process characterized by frequency λ [*Botter et al.,* 2007a]. This frequency is smaller than that of overall rainfall ($\lambda < \lambda_p$), since not all rainfall events lead to generation of streamflow, and it can be calculated based on information regarding climate, soil and vegetation cover of the basin (Equation (S3) in *Botter et al.,* [2013]). The excess water is assumed to be instantaneously released from the upper soil to deeper layers, and contributed to the streamflow as subsurface runoff. The subsurface storage of the catchment is thought of as a linear reservoir with an exponential unit hydrograph and mean response time equal to K_T^{-1}. Under the above assumptions, the specific (per unit catchment area) streamflow Q (Figure 4.1a) is made up of instantaneous jumps corresponding to each effective rainfall depth and exponential decays between the events, as stated by equation (4.1). The three parameters λ, α, and K_T that define the streamflow PDF (equation (4.2)) are estimated as follows: α is the mean depth of precipitation during rainy days; K_T can be deduced from recession analysis; λ is operationally calculated based on the mean observed $\langle Q \rangle$ as $\lambda = \frac{\langle Q \rangle}{\alpha}$.

4.7.2 Riparian Vegetation Dynamics

Here we provide a more comprehensive description of the parameters used in the vegetation model developed by *Camporeale and Ridolfi* [2006]. The local stochastic dynamics of riparian vegetation were modeled as:

$$\frac{dB}{dt} = \begin{cases} -\alpha_d(\eta, h)\, B^n & h \geq \eta \qquad (a) \\ \alpha_g\, B^m \left(V_c(\eta, h) - B\right)^p & h < \eta \qquad (b) \end{cases} \tag{S4.1}$$

where B is dimensionless vegetation biomass at an elevation η along the transect and $0 < B < 1$. Equation $(S4.1a)$ models the vegetation decay due to flooding. $\alpha_d(\eta, h)$ is the coefficient quantifying the damage caused to vegetation by flooding and its value is modulated along the transect through stage fluctuations ($\alpha_d = K\,(h - \eta)\,/\,\langle h \rangle$). K is a decay coefficient and for convenience it is assumed to be equal to $0.0028 d^{-1}$ in all cases [*Camporeale and Ridolfi,* 2006].

Equation ($S4.1b$) captures the vegetation growth according to a generalized Verhulst-logistic function for a phreatophyte species tapping the groundwater [*Botkin et al., 1972*; *Camporeale and Ridolfi,* 2006]. α_g is a vegetation specific constant representing the intrinsic rate of growth [*Kot,* 2001]. n, m and p are vegetation specific numerical constants and are set equal to one for simplicity [*Camporeale and Ridolfi,* 2006]. $V_c(\eta, h)$ is the carrying capacity (similarly to *Camporeale and Ridolfi* [2006] defined as the maximum attainable biomass and it is dependent on the position of the groundwater depth with respect to elevation of the point considered. It is recognized that plant growth is significantly reduced for groundwater levels that are too low (water stress) or too high (anoxia). Hence, for simplicity we assume the value of the carrying capacity to be maximum ($V_c(\eta, h) = 1$) when the water table (obtained based on observed river stage data at a daily time scale) falls within a given range (η_l , η_h) around the optimum groundwater depth Z_r, and zero elsewhere. The bounds of this optimum range of groundwater depth that allow vegetation growth are defined as $\eta_l = \eta - Z_r - \delta$ and $\eta_h = \eta - Z_r + \delta$, where δ is assumed to be 0.1 m for simplicity.

In order to facilitate the derivation of an analytical expression for the PDF of vegetation biomass, a dimensionless and temporally averaged formulation of the above equation is preferred. To that end a temporally averaged value for the decay coefficient and the carrying capacity are defined as follows:

$$\langle \alpha_d \rangle (\eta) = \frac{1}{P_I(\eta)} \int_{\eta}^{\infty} \alpha_d(\eta, h)\, p_h(h)\, dh \tag{S4.2}$$

$$\langle V_c \rangle (\eta) = \frac{1}{P_E(\eta)} \int_{0}^{\eta} V_c(\eta, h)\, p_h(h)\, dh \tag{S4.3}$$

where P_I and P_E are the probability of inundation and exposure. The notation on the left had side signifies the dependence on η. Equation (S4.1) can therefore be re-written in dimensionless terms as equation (4.5). α_B and β are defined as:

$$\alpha_B(\eta^*) = \frac{\langle \alpha_d \rangle}{\alpha_g} = k \langle h^* - \eta^* \rangle \tag{S4.4}$$

$$\beta(\eta^*) = \langle V_c \rangle \tag{S4.5}$$

Note that, parameter α_B and β are calculated for each point along the transect. k, defined here as $\frac{K}{\alpha_g}$, represents the sensitivity of specific vegetation to flooding.

5. CONCLUSIONS AND PERSPECTIVES

In this section, the main results from the previous three chapters are highlighted and elaborated on. Finally, the implications of this work as well as challenges and potential areas of improvement for continuing this research are presented.

5.1 Conclusions

The main objective of this Ph.D. thesis was to develop catchment-scale methods for providing a process-based description of flow regimes, their spatial variability and relevant ecological processes. Moreover, this work aimed at creating a modeling framework which could help in large scale management of water resources in a complex river network, particularly for areas faced with data scarcity.

To that end, a method was provided that allowed for estimating the flow duration curve based on catchment-scale climate (precipitation, potential evapotranspiration) and morphological data (DEMs). The method utilizes a physically-based analytic model of streamflows with four parameters, which incorporate the various hydrologic, climatic and geomorphologic features of the catchment (estimated on seasonal time scale). Model parameters were estimated through coupling of established water balance models with a geomorphologic flow recession model, in the absence of observed discharge time series. The water balance model was selected amongst four alternatives from literature, based on extensive performance ranking. The method was in turn applied to eleven test catchments distributed across the United States, east of the rocky mountains. The method was capable of capturing the shape of the flow duration curve and the seasonal dynamics of flow statistics reasonably well. Considering the limited and widely available data used for implementation of the method, the approach is a useful tool in water resources management and ecological studies.

Since the method proved able to successfully estimate flow duration curves in the absence of discharge data, it was further extended to be applied point-wise along river networks and predict the spatial patterns of the flow regimes. A custom geo-database and a Web GIS platform were created for the management of data, model parameterization and application of the method to the Thur basin, located in northeastern Switzerland. The performance of the method in replicating the model parameters and seasonal dynamics of streamflows, observed at the six subcatchment outlets with available discharge data, was assessed and judged to be satisfactory. The method also was able to capture observed streamflow statistics, mean specific discharge and the associated coefficient of variation, reasonably well. Strong seasonal patterns of rainfall were shown to be the major driver of streamflow variability in the Thur river. In particular, the climatic patterns were

marked by less intense rain events and higher ET downstream, which lead to a decreasing trend of specific discharge with increasing contributing area. These results highlighted the importance of the climatic drivers in determining the behavior of the flow regime along the river network. The non-linearity of the hydrologic response was shown to increase with contribution area possibly as a result of the increasing complexity of river network structure, possibly emphasized by the enhanced heterogeneity of land-use and climate at larger scales. The data management and modeling approach presented here provide a valuable method to estimate long-term patterns of the flow regimes and predict streamflow statistics at any arbitrary point along the river network of a given basin with minimal data requirements.

Streamflow variability is a major driver for many ecological processes in the riverine system. Among the various ecological processes, riparian vegetation dynamics are among the most relevant because of the role they play in biodiversity, water quality and sediment transport. Here, we explored the role of river flow regimes in determining patterns of mean vegetation biomass along complex river transects. The growth and decay of vegetation along a river transect was estimated through coupling of catchment-scale hydroclimatic processes, morphological attributes of the river transect and vegetation specific biological features. A coupled stochastic model of streamflows, stages and vegetation biomass was developed which allowed us to derive analytic expression for mean exposure and inundation times, and mean biomass along the transect. The model was applied to the terminal reach of two catchments with contrasting flow regimes. The results allow for using the hydrological distinction between flow regimes to be used as a tool for understanding the patterns of riparian vegetation. It was shown that erratic regimes are featured by wider aquatic-terrestrial transition regions, where the limitation to growth due to hydrologic noise plays a critical role. It was also shown that changing climatic condition have a significant impact on vegetation patterns along river reaches characterized by large flow variability. Despite the simplicity of growth and decay processes in this analysis, the proposed model highlighted the important role of flow regime variability in determining the different distributions of the riparian vegetation along river transects.

5.2 Implications and Outlook

The modeling methods presented in this Ph.D. thesis proved to be robust and satisfactory results were achieved. Nonetheless, they can be augmented in various ways in order to broaden the applicability and improve the outcomes. Here we will briefly discuss the areas in which the methods developed and tested in this thesis could be expanded, and the overall direction for continuation of this research.

The method discussed in chapter 2 performed exceedingly well, specially considering the minimal data requirements and in the absence of discharge data. The geomorphic model adopted for estimating the catchment-scale recession properties (GRFM), works best in gently sloping catchments due to the underlying assumptions regarding flow generation mechanisms. Other models with alternative conceptual models for relating flow recession to catchment geomorphic structure, have been presented in recent studies [*Mutzner et al.,* 2013]. Incorporating such models and conducting rigorous performance assessments would be fruitful for expanding the applicability of this method.

The geo-database and Web GIS platform presented in chapter 3 are the focal point of this research project. The framework is particularly relevant since it provides a complete modeling package that can be applied in different areas and climatic conditions, notably in areas where data acquisition is a limiting factor. It is recommended that the framework be tested at other locations with different climatic and topographic settings, in order to prove consistency of performance and find potential limits in suitability.

An intentional feature of the platform design was to allow for the addition of other pertinent processes (such as water quality, sediment transport and ecological processes) that should be considered in developing integrated water resources management strategies. Among the variety of available methods in the literature, some are better suited due to synergies provided by their comparable analytic structure and underlying assumptions. Recent works have tackled water quality issues through a similar modeling approach, which employ the concept of travel time distributions [*Benettin et al.,* 2015]. Moreover, novel methods for modeling sediment transport, which use the same analytical description of flow variability, have also been proposed [*Basso et al.,* (in press)]. Dynamics of riparian vegetation, presented in chapter 4, are strongly interconnected with sediment transport processes and erosion control mechanism. Furthermore, the dynamics of river stage, which were expressed explicitly in terms of the hydrologic forcing in chapter 4, have noteworthy implications for habitat suitability.

Changing climatic conditions can potentially cause sever stress on the availability of water resources. While floods and droughts are a point of immediate concern for many, the change in catchment-scale behavior of complex river networks is an important consideration for efficient management of water resources. The densely monitored Thur basin (test site discussed in chapter 3), provides an ideal location for studying the effect of changing climatic condition on the flow regime of a catchment. Synthetic rainfall patterns under different scenarios can be incorporated in the model and the outcomes compared. Finally, in the context of changing climate, the impact on snow dynamics and glacial melt on flow regimes (currently not explicitly incorporated in the model) should be explored and included in the framework.

In general, a rigorous study of ecohydrologic processes along the river network and assessing the impacts of anthropogenic regulation on natural streamflow conditions, require a spatially explicit representation of flow properties. The modeling framework presented in this thesis is uniquely capable of providing this information in an accurate and data efficient manner. The addition of other ecological and morphological processes to this framework (such as but not limited to the cases discussed above) will be a positive step in creating a comprehensive catchment-scale model for assessment and study of major processes relevant to human valued services in complex river networks.

BIBLIOGRAPHY

Abbaspour, K. C., J. Yang, I. Maximov, R. Siber, K. Bogner, J. Mieleitner, J. Zobrist, R. Srinivasan (2007), Modelling hydrology and water quality in the pre-alpine/alpine Thur watershed using SWAT, *J. Hydrol.*, 333, 2-4, 413-430, doi:10.1016/j.jhydrol.2006.09.014.

Akaike, H. (1974), A new look at the statistical model identification. *Trans. on Aut. Cont.*, 19 , 716-723, doi:10.1109/TAC.1974.1100705.

Allen, R., L. S. Pereira, D. Raes, M. Smith (1998), Crop evapotranspiration - Guidelines for computing crop water requirements, *FAO Irrigation and Drainage Paper*, 56, FAO, Rome.

Auble, G. T., J. M. Friedman, M. L. Scott (1994), Relating riparian vegetation to present and future streamflows, *Ecol. Appl.*, 4:544554, doi:10.2307/1941956.

Baskerville, G. L. (1965), Dry matter production in immature balsam fir stands, *For. Sci. Monogr.*, 9, 1 42.

Basso, S., M. Schirmer, G. Botter (2015), On the emergence of heavy-tailed streamflow distributions, *Adv. Water. Res.*, 82, doi:10.1016/j.advwatres.2015.04.013.

Basso, S., A. Frascati, M. Marani, M. Schirmer, and G. Botter (in press), Climatic and landscape controls on effective discharge, *Geophys. Res. Lett.*.

Bendix, J., and C. R. Hupp (2000), Hydrological and geomorphological impacts on riparian plant communities, *Hydrol. Process.*, 14: 29772990. doi: 10.1002/1099-1085(200011/12)14:16/17¡2977::AID-HYP130¿3.0.CO;2-4.

Benettin, P., J. W. Kirchner, A. Rinaldo, and G. Botter (2015), Modeling chloride transport using travel time distributions at Plynlimon, Wales, *Water. Resour. Res*, 51, 32593276, doi:10.1002/2014WR016600.

Berghuijs, W. R., R. A. Woods, M. Hrachowitz (2014), A precipitation shift from snow towards rain leads to a decrease in streamflow, *Nature Clim. Change*, 4(7): 583-586, doi:10.1038/nclimate2246.

Bertuzzo, E., L. Mari, L. Righetto, M. Gatto, R. Casagrandi, I. Rodriguez-Iturbe, A. Rinaldo (2012), Hydroclimatology of dual-peak annual cholera incidence: Insights from a spatially explicit model, *Geophys. Res. Lett.*, 39, L05403, doi:10.1029/2011GL050723.

Beven, K.J., and M.J. Kirkby (1979), A physically based, variable contributing area model of basin hydrology. *Hydro. Sci. Bull.*, 24, 4369. doi:10.1080/02626667909491834.

Biondi, D., G. Freni, V. Iacobellis, G. Mascaro, A. Montanari (2012), Validation of hydrological models: Conceptual basis, methodological approaches and a proposal for a code of practice, *Phy. Chem. Earth*, doi:10.1016/j.pce.2011.07.037.

Biswal, B., and M. Marani (2010), Geomorphological origin of recession curves, *Geophys. Res. Lett.*, 37, doi:10.1029/2010GL045415.

Biswal, B., and M. Marani (2014), Universal recession curves and their geomorphological interpretation, *Adv. Water. Res.*, doi:10.1016/j.advwatres.2014.01.004.

Biswal, B., and D. Nagesh Kumar (2013), A general geomorphological recession flow model for river basins, *Water. Resour. Res*, 49, doi:10.1002/wrcr.20379.

Biswal, B., and D. Nagesh Kumar (2014a), What mainly controls recession flows in river basins?, *Adv. Water Res.*, 65, 25-33, doi:10.1016/j.advwatres.2014.01.001.

Biswal, B., and D. Nagesh Kumar (2014b), Study of dynamic behaviour of recession curves,*Hydrol. Process.*, 28: 784792. doi: 10.1002/hyp.9604.

Booker, D. J., R. A. Woods (2014), Comparing and combining physically-based and empirically-based approaches for estimating the hydrology of ungauged catchments, *J. Hydro.*, doi:10.1016/j.jhydrol.2013.11.007.

Botkin, D. B., J. R. Wallis, J. F. Janak (1972), Some ecological consequences of a computer model of forest growth, *J. Ecol.*, 60(3), 849-872.

Botter, G., A. Porporato, I. Rodriguez-Iturbe, A. Rinaldo (2007a), Basin-scale soil moisture dynamics and the probabilistic characterization of carrier hydrologic flows: Slow, leaching-prone components of the hydrologic response, *Water. Resour. Res.* 43, doi:10.1029/2006WR005043.

Botter, G., A. Porporato, E. Daly, I. Rodriguez-Iturbe, and A. Rinaldo (2007b), Probabilistic characterization of base flows in river basins: Roles of soil, vegetation, and geomorphology, *Water Resour. Res.*, 43(6), doi: 10.1029/2006WR005397.

Botter, G., F. Peratoner, A. Porporato, I. Rodriguez-Iturbe, and A. Rinaldo (2007c), Signatures of large-scale soil moisture dynamics on streamflow statistics across US climate regimes, *Water Resour. Res.*, 43, W06404, doi:10.1029/2006WR005397.

Botter, G., S. Zanardo, A. Porporato, I. Rodriguez-Iturbe, A. Rinaldo (2008), Ecohydrological model of flow duration curves and annual minima. *Water. Resour. Res.*, 44, doi:10.1029/2008WR006814.

Botter, G., A. Porporato, I. Rodriguez-Iturbe, A. Rinaldo (2009), Nonlinear storage-discharge relations and catchment streamflow regimes, *Water. Resour. Res.* 45, doi:10.1029/2008WR007658.

Botter, G., S. Basso, A. Porporato, I. Rodriguez-Iturbe, A. Rinaldo (2010a), Natural streamflow regime alterations: Damming of the Piave river basin (Italy), *Water Resour. Res.*, 46, W06522, doi:10.1029/2009WR008523.

Botter, G., N. B. Basu, S. Zanardo, P. S. C. Rao, A. Rinaldo (2010b), Stochastic modeling of nutrient losses in streams: Interactions of climatic, hydrologic, and biogeochemical controls, *Water Resour. Res.*, 46, W08509, doi:10.1029/2009WR008758.

Botter, G., S. Basso, I. Rodriguez-Iturbe, A. Rinaldo (2013), Resilience of river flow regimes, *Proc. Natl. Acad. Sci.*, doi:10.1073/pnas.1311920110.

Botter, G. (2014), Flow regime shifts in the Little Piney creek (US), *Adv. Water Res.*, doi:10.1016/j.advwatres.2014.05.010.

Blöschl G. (2006), Rainfall-runoff modeling of ungauged catchments, *Encyclopedia of Hydrological Sciences*, 11:133, doi:10.1002/0470848944.hsa140.

Bradley, C. E., and D. G. Smith (1986), Plain cottonwood recruitment and survival on prairie meandering river floodplain, Milk river, southern Alberta and northern Montana, *Can. J. Bot.*, 64(7), 1433-1442, doi:10.1139/b86-195.

Brutsaert, W., and J. L. Nieber (1977), Regionalized drought flow hydrographs from a mature glaciated plateau, *Water. Resour. Res* 13(3), 637-644, doi:10.1029/WR013i003p00637.

Budyko, M. I. (1974), Climate and life. *Academic*, San Diego, California, 508 pp.

Bunn, S. E., and A. H. Arthington (2002), Basic principles and ecological consequences of altered flow regimes for aquatic biodiversity, *Environ. Manage.*, 30, 492507, doi:10.1007/s00267-002-2737-0.

Burnham, K. P., D. R. Anderson (2002), Model Selection and Multimodel Inference, *Springer*, New York, doi:10.1007/b97636.

Camporeale, C., and L. Ridolfi (2006), Riparian vegetation distribution induced by river flow variability: A stochastic approach, *Water Resour. Res.*, 42, W10415, doi:10.1029/2006WR004933.

Camporeale, C., and L. Ridolfi (2007), Noise-induced phenomena in riparian vegetation dynamics, *Geophys. Res. Lett.*, 34, L18406, doi:10.1029/2007GL030899.

Castellarin, A., R. M. Vogel, A. Brath (2004), A stochastic index flow model of flow duration curves. *Water. Resour. Res*, 40, W03104, doi:10.1029/2003WR002524.

Castellarin, A., G. Camorani, A. Brath (2007), Predicting annual and long-term flow-duration curves in ungauged basins, *Adv. Water Res.*, 30, 937-953, doi:10.1016/j.advwatres.2006.08.006.

Castiglioni, S., L. Lombardi, E. Toth, A. Castellarin, A. Montanari (2010), Calibration of rainfall-runoff models in ungauged basins: A regional maximum likelihood approach, *Adv. Water. Res.*, doi: 10.1016/j.advwatres.2010.04.009

Ceola, S., G. Botter, E. Bertuzzo, A. Porporato, I. Rodriguez-Iturbe, A. Rinaldo (2010), Comparative study of ecohydrological streamflow probability distributions, *Water. Resour. Res*, 46, W09502, doi:10.1029/2010WR009102.

Ceola, S., E. Bertuzzo, G. Singer, T. J. Battin, A. Montanari, A. Rinaldo (2014), Hydrologic controls on basinscale distribution of benthic invertebrates, *Water Resour. Res.*, 50, 29032920, doi:10.1002/2013WR01511.

Cheng, L., M. Yaeger, A. Viglione, E. Coopersmith, S. Ye, M. Sivapalan (2012), Exploring the physical controls of regional patterns of flow duration curves Part 1: Insights from statistical analyses, *Hydrol. Earth Syst. Sci.*, 16, 4435-4446, doi:10.5194/hess-16-4435-2012.

Chow, V. T., D. Maidment, L. Mays (1988), Applied Hydrology, 572, *McGrawHill*, New York.

Cirpka, O. A., M. N. Fienen, M. Hofer, E. Hoehn, A. Tessarini, R. Kipfer, P.K. Kitanidis (2007), Analyzing bank filtration by deconvoluting time series of electric conductivity, *Ground Water*, 45 (3), 318-328, doi:10.1111/j.1745-6584.2006.00293.x.

Constantz, J. (1998), Interaction between stream temperature, stream flow and groundwater exchange in alpine streams, *Water Resour. Res.*, 34(7), 16091615, doi:10.1029/98WR00998.

Costa-Cabral, M. C., J. E. Richey, G. Goteti, D. P. Lettenmaier, C. Feldktter, A. Snidvongs (2008), Landscape structure and use, climate, and water movement in the Mekong River basin, *Hydrol. Process.*, 22: 17311746, doi: 10.1002/hyp.6740.

Crouzy, B., and P. Perona (2012), Biomass selection by floods and related timescales. Part 2: Stochastic modeling, *Adv. Water Res.*, 39, 97-105, doi:10.1016/j.advwatres.2011.09.018.

Destouni, G., F. Jaramillo, C. Prieto (2013), Hydroclimatic shifts driven by human water use for food and energy production, *Nat. Cli. Change*, 3:213217, doi:10.1038/NCLIMATE1719.

Donohue, R. J., M. L. Roderick, T. R. McVicar (2007), On the importance of including vegetation dynamics in Budyko's hydrological model, *Hydrol. Earth Syst. Sci.*, 11(2), 983995, doi:10.5194/hess-11-983-2007.

Doulatyari, B., S. Basso, M. Schirmer, G. Botter (2014), River flow regimes and vegetation dynamics along a river transect. *Adv. Water. Res.*, doi: 10.1016/j.advwatres.2014.06.015.

Doulatyari, B., A. Betterle, S. Basso, B. Biswal, M. Schirmer, G. Botter (2015), Predicting streamflow distributions and flow duration curves from landscape and climate, *Adv. Water. Res.*, doi:10.1016/j.advwatres.2015.06.013.

Doyle, M. W., E. H. Stanley, D. L. Strayer, R. B. Jacobson, J. C. Schmidt (2005), Effective discharge analysis of ecological processes in streams, *Water Resour. Res.*, 41, W11411, doi:10.1029/2005WR004222.

Doyle, M. W., and C. A. Shields (2008), An alternative measure of discharge effectiveness, *Earth Surf. Process. Landforms*, 33: 308316. doi: 10.1002/esp.1543.

Formetta G., A. Antonello, S. Franceschi, O. David, R. Rigon (2014), Hydrological modelling with components: A GIS-based open-source framework, *Environ. Model. Softw.*, 55: 190-200, 1364-8152, doi:10.1016/j.envsoft.2014.01.019.

Friedman, J. M., and G. T. Auble (1999), Mortality of riparian box elder from sediment mobilization and extended inundation, *Regul. Rivers: Res. Mgmt.*, 15: 463476, doi: 10.1002/(SICI)1099-1646(199909/10)15:5¡463::AID-RRR559¿3.0.CO;2-Z.

Ganora, D., P. Claps, F. Laio, A. Viglione (2009), An approach to estimate nonparametric flow duration curves in ungauged basins. *Water. Resour. Res*, 45:W10418. doi:10.1029/2008WR007472.

Gregory, K. J., and D. E. Walling (1968), The variation of drainage density within a catchment, *Bull. Intn. Ass. Sci. Hydr.*, 13(2), 6168, doi:10.1080/02626666809493583.

Godsey, S. E. and J. W. Kirchner (2014), Dynamic, discontinuous stream networks: hydrologically driven variations in active drainage density, flowing channels and stream order, *Hydr. Proc.*, doi: 10.1002/hyp.10310

Gupta, H. V., T. Wagener, Y. Liu (2008), Reconciling theory with observations: elements of a diagnostic approach to model evaluation. Hydrological Processes, 22, 38023813, *Hydr. Proc.*, doi:10.1002/hyp.6989.

Guswa, A. J. (2005), Soil-moisture limits on plant uptake: An upscaled relationship for water-limited ecosystems, *Adv. Water Res.*, 28(6), 543-552, doi:10.1016/j.advwatres.2004.08.016.

Guswa, A. J. (2008), The influence of climate on root depth: A carbon cost-benefit analysis, *Water Resour. Res.*, 44, W02427, doi:10.1029/2007WR006384.

Harman, C., and M. Sivapalan (2009a), A similarity framework to assess controls on shallow subsurface flow dynamics in hillslopes, *Water. Resour. Res*, 45, W01417, doi:10.1029/2008WR007067.

Harman, C. J., M. Sivapalan, P. Kumar (2009b), Power law catchment-scale recessions arising from heterogeneous linear small-scale dynamics, *Water Resour. Res.*, 45, W09404, doi:10.1029/2008WR007392.

Hayashi, M., T. Vogt, L. Mchler, M. Schirmer (2012), Diurnal fluctuations of electrical conductivity in a pre-alpine river: Effects of photosynthesis and groundwater exchange, *J. Hydrol.*, 450451, 93104, doi:10.1016/j.jhydrol.2012.05.020.

Hrachowitz, M., H. H. Savenije, G. Blöschl, J. J. McDonnell, M. Sivapalan, J. Pomeroy, B. Arheimer, T. Blume, M. P. Clark, U. Ehret, F. Fenicia, J. E. Freer, A. Gelfan, H. V. Gupta, D. A. Hughes, R. W. Hut, A. Montanari, S. Pande, D. Tetzlaff, P. A. Troch, S. Uhlenbrook, T. Wagener, H. C. Winsemius, R. A. Woods, E. Zehe, C. Cudennec (2013), A decade of Predictions in Ungauged Basins (PUB) a review (2013), *Hydrolog. Sci. J.*, doi:10.1080/02626667.2013.803183.

Hupp, C. R. (1988), Plant ecological aspects of flood geomorphology and paleoflood history, In: V.R. Baker ,R.C. Kochel , P.C. Patton, editors. Flood geomorphology, *John Wiley & Sons*, New York, 335-356.

Hupp, C. R., and W. R. Osterkamp (1985), Bottomland vegetation distribution along passage creek, Virginia, in relation to fluvila landforms, *Ecology*, 66(3), 670-681, doi:10.2307/1940528.

Hurford, A. P., and J. J. Harou (2014), Balancing ecosystem services with energy and food security-Assessing trade-offs from reservoir operation and irrigation investments in Kenyas Tana Basin, *Hydrol. Earth Syst. Sci.*, 18, 32593277, doi:10.5194/hess-18-3259-2014.

Jaeger, K. L., J. D. Oldenb, N. A. Pellandc (2014), Climate change poised to threaten hydrologic connectivity and endemic fishes in dryland streams, *Proc. Natl. Acad. Sci.*, doi/10.1073/pnas.1320890111.

Jaramillo, F., and G. Destouni (2015), Developing water change spectra and distinguishing change drivers worldwide, *Geophys. Res. Lett.*, 41, 83778386, doi:10.1002/2014GL061848.

Junk, W. J., P. B. Bayley, R. E. Sparks (1989), The flood pulse concept in river-floodplain systems, p. 110-127, In D. P. Dodge [ed.] Proceedings of the International Large River Symposium, *Can. Spec. Publ. Fish. Aquat. Sci.*, 106.

Kirchner, J. W. (2009), Catchments as simple dynamical systems: Catchment characterization, rainfall-runoff modeling, and doing hydrology backward, *Water. Resour. Res*, 45, W02429, doi:10.1029/2008WR006912.

Kitahara, K., W. Horsthemke, R. Lefever, Y. Inaba (1980), Phase-diagrams of noise induced transitions - Exact results for a class of external colored noise, *Prog. Theor. Phys.*, 64(4), 1233-1247, doi: 10.1143/PTP.64.1233.

Kot, M. (2001), Elements of Mathematical Ecology, *Cambridge Univ. Press*, New York.

Kozlowski, T. T. (1984), Responses of woody plants to flooding, in Flooding and Plant Growth, *Academic press*, New York.

Kurth, A. M., and Schirmer, M. (2014) Thirty years of river restoration in Switzerland: implemented measures and lessons learned, *Environ. Earth Sci.*, 72(6), 2065 - 2079. doi: 10.1007/s12665-014-3115-y.

Laio, F., A. Porporato, C. P. Fernandez-Illescas, I. Rodriguez-Iturbe (2001a), Plants in water-controlled ecosystems: active role in hydrologic processes and response to water stress - IV. Discussion of real cases, *Adv. Water Resour.*, 24(7), 745-762, doi:10.1016/S0309-1708(01)00007-0.

Laio, F., A. Porporato, L. Ridolfi, I. Rodriguez-Iturbe (2001b), Mean first passage times of processes driven by white shot noise, *Phys. Rev. E*, 63(3), doi:10.1103/PhysRevE.63.036105.

Langbein, W. B. (1949), Annual runoff in the United States, *U.S. Geol. Surv.*, 52.

Lazzaro, G., and G. Botter (2015), Run-of-river power plants in Alpine regions: Whither optimal capacity?, *Water Resour. Res.*, 51, 56585676, doi:10.1002/2014WR016642.

Leopold, L. R., and T. Maddock (1953), The hydraulic geometry of stream channels and some physiographic implications, *U.S. Geol. Surv. Prof. Pap.*, 252.

Lite, S. J., K. J. Bagstad, and J. C. Stromberg (2005), Riparian plant species richness along lateral and longitudinal gradients of water stress and flood disturbance, San Pedro River, Arizona, USA, *J. Arid. Environ.*, 63(4), 785-813, doi:10.1016/j.jaridenv.2005.03.026.

Lytle, D., and N. L. Poff (2004), Adaptation to natural flow regimes, *Trends Eco. Evo.* 19(2), 94-100, doi:10.1016/j.tree.2003.10.002.

L'vovich, M.I. (1979), World Water Resources and Their Future, *Am. Geophys. Union*, doi: 10.1029/SP013.

Mahoney, J. M., and S. B. Rood (1998), Streamflow requirements for cottonwood seedling recruitment - An integrative model, Wetlands, 18(4), 634-645, doi:10.1007/BF03161678.

Masoliver, J. (1987), 1st-Passge times for non-markovian processes - shot noise, *Phys. Rev. A*, 35(9), 3918-3928, doi:10.1103/PhysRevA.35.3918.

McCluney, K. E., N. L. Poff, M. A. Palmer, J. H. Thorp, G. C. Poole, B. S. Williams, M. R. Williams, J. S. Baron (2014), Riverine macrosystems ecology: sensitivity, resistance, and resilience of whole river basins with human alterations, *Front. Ecol. Environ.*, 12: 4858. doi:10.1890/120367.

Mark, D. M. (1988), Network models in geomorphology, Chapter 4 in *Model. Geomorph. Sys.*, Edited by M.G. Anderson, John Wiley, 73-97.

Mejia, A., E. Daly, F. Rossel, T. Jovanovic, J. Gironas (2014), A stochastic model of streamflow for urbanized basins, *Water. Resour. Res*, doi:10.1002/2013WR014834.

Merz, R., and G. Blöschl (2004), Regionalisation of catchment model parameters. *Jour. Hydro.*, 287, 95123, doi:10.1016/j.jhydrol.2003.09.028

Milly, P. C. D. (1994), Climate, soil water storage, and the average annual water balance, *Adv. Water Resour.*, 30(7), 21432156, doi:10.1029/94WR00586.

Müller M. F., D. N. Dralle, S. E. Thompson (2014), Analytical model for flow duration curves in seasonally dry climates, *Adv. Water Res.*, doi:10.1002/2014WR015301.

Muneepeerakul, R., J. S. Weitz, S. A. Levin, A. Rinaldo, I. Rodriguez-Iturbe (2007a), A neutral metapopulation model of biodiversity in river networks, *J. Theor. Biol.*, 245, 351 363, doi:10.1016/j.jtbi.2006.10.005.

Muneepeerakul, R., A. Rinaldo, I. Rodriguez-Iturbe (2007b), Effects of river flow scaling properties on riparian width and vegetation biomass, *Water Resour. Res.*, 43, W12406, doi:10.1029/2007WR006100.

Mutzner R, E. Bertuzzo, P. Tarolli, S. V. Weijs, L. Nicotina, S. Ceola, N. Tomasic, I. Rodriguez-Iturbe, M. B. Parlange, A. Rinaldo (2013), Geomorphic signatures on Brutsaert base flow recession analysis, *Water. Resour. Res*, 49:546272. doi:10.1002/wrcr.20417.

Naiman, R. J., and H. Decamps (1997), The ecology of interfaces: Riparian zones, *Annu. Rev. Ecol. Syst.*, 28, 621-658.

Naumburg, E., R. Mata-Gonzalez, R. G. Hunter, T. McLendon, D. W. Martin (2005), Phreatophytic vegetation and groundwater fluctuations: A review of current research and application of ecosystem response modeling with an emphasis on Great Basin vegetation, *Environ. Manage.*, 35(6), 726-740, doi:10.1007/s00267-004-0194-7.

Nilsson, C., and M. Svedmark (2002), Basic principles and ecological consequences of changing water regimes: Riparian plant communities, *Environ. Manage.*, 30(4), 468-480, doi: 10.1007/s00267-002-2735-2.

Osterkamp, W. R., and Costa, J. E. (1987), Changes accompanying an extraordinary flood on a sand-bed stream, in Catastrophic flooding, edited by L. Mayer, and D. Nash, 201-224, *Allen & Unwin*, Boston.

Oudin, L., V. Andreassian, C. Perrin, C. Michel, N. Le Moine (2008), Spatial proximity, physical similarity, regression and ungagged catchments: a comparison of regionalization approaches based on 913 French catchments, *Water. Resour. Res*, 44, W03413, doi:10.1029/2007WR006240.

Perona, P., P. Molnar, M. Savina, P. Burlando (2009a), An observation-based stochastic model for sediment and vegetation dynamics in the floodplain of an Alpine braided river, *Water Resour. Res.*, 45, W09418, doi:10.1029/2008WR007550.

Perona, P., C. Camporeale, E. Perucca, M. Savina, P. Molnar, P. Burlando, L. Ridolfi (2009b), Modelling river and riparian vegetation interactions and related importance for sustainable ecosystem management, *Aquat. Sci.*, 71(3), 266-278, doi:10.1007/s00027-009-9215-1.

Perona, P., P. Molnar, B. Crouzy, E. Perucca, Z. Jiang, S. Mclelland, D. Wuthrich, K. Edmaier, R. Francis, C. Camporeale, A. Gurnell (2012), Biomass selection by floods and related timescales: Part 1. Experimental observations, *Adv. Water Resour.*, 39, 85-96, doi:10.1016/j.advwatres.2011.09.016.

Perry, T. O., H. E. Sellers, C. O. Blanchard (1969), Species-diversity and pattern-diversity in the study of ecological succession, *J. Theor. Biol.*, 10, 370383, doi:10.1016/0022-5193(66)90133-0.

Poff, N. L., J. D. Allan, M. B. Bain, J. R. Karr, K. L. Prestegaard, B. D. Richter, R. E. Sparks, J. C. Stromberg (1997), The natural flow regime, *Bioscience*, 47(11), 769-784, doi: 10.2307/1313099.

Poff N., J. Olden, D. Merrit, D. Pepin (2007), Homogenization of regional river dynamics by dams and global biodiversity implications, *Proc. Natl. Acad. Sci.*, 104 (14) 5732-5737, doi: 10.1073/pnas.0609812104.

Ponce, V. M., and A. V. Shetty (1995a), A conceptual model of catchment water balance: 1. Formulation and calibration, *Jour. hydr.* 173, 27-40, doi:10.1016/0022-1694(95)02739-C.

Ponce, V. M., and A. V. Shetty (1995b), A conceptual model of catchment water balance: 2. Application to runoff and baseflow modeling, *Jour. hydr.* 173, 4150, doi:10.1016/0022-1694(95)02745-B.

Porporato, A., F. Laio, L. Ridolfi, I. Rodriguez-Iturbe (2001), Plants in water-controlled ecosystems: active role in hydrologic processes and response to water stress - III. Vegetation water stress, *Adv. Water Resour.*, 24(7), 725-744, doi:10.1016/S0309-1708(01)00006-9.

Porporato, A., and L. Ridolfi (2003), Detecting determinism and nonlinearity in river-flow time series, *Hydr. Sci. Jour.*, vol 48(5) , 763-780, doi:10.1623/hysj.48.5.763.51457.

Porporato, A., E. Daly, I. Rodriguez-Iturbe, (2004), Soil water balance and ecosystem response to climate change, *Am. Nat.*, 164(5), 625-32, doi:10.1086/424970.

Postel, S., and B. Richter (2003), Rivers for Life: Managing Water for People and Nature, *Island Press*, Washington, DC.

Pumo, D., L. V. Noto, F. Viola (2013), Ecohydrological modelling of flow duration curve in Mediterranean river basins,*Adv. Water Resour.*, 52:31427, doi:10.1016/j.advwatres.2012.05.010.

Ridolfi L., P. DOdorico, F. Laio (2006), Effects of vegetation-water table feedbacks on the stability and resilience of plant ecosystems, *Water Resour. Res.*, 42, doi: 10.1029/2005WR004444.

Ridolfi, L., P. D'Odorico, F. Laio (2011), Noise-Induced Phenomena in the Environmental Sciences, *Cambridge Univ. Press*, Cambridge.

Rigon, R., G. Bertoldi, T. M. Over (2006), GEOtop: A Distributed Hydrological Model with Coupled Water and Energy Budgets, *J. Hydrometeor*, 7, 371388, doi: 10.1175/JHM497.1.

Rinaldo, A. (1991), Geomorphological Dispersion, *Water Resour. Res.*, 27(4), 513-525, doi:10.1029/90WR02501.

Rinaldo, A., G. K. Vogel, R. Rigon, I. RodriguezIturbe (1995), Can one gauge the shape of a basin?, *Water. Resour. Res.*, doi: 10.1029/95WR03290.

Rodriguez-Iturbe, I., A. Porporato, L. Ridolfi, V. Isham, D. R. Coxi (1999), Probabilistic modelling of water balance at a point: the role of climate, soil and vegetation, *Proc. Royal Soc. London*, doi:10.1098/rspa.1999.0477.

Rodriguez-Iturbe, I., A. Porporato, F. Laio, L. Ridolfi (2001), Plants in water-controlled ecosystems: active role in hydrologic processes and response to water stress - I. Scope and general outline, *Adv. Water Resour.*, 24(7), 695-705, doi:10.1016/S0309-1708(01)00004-5.

Rodriguez-Iturbe, I., R. Muneepeerakul, E. Bertuzzo, S. A. Levin, A. Rinaldo (2009), River networks as ecological corridors: A complex systems perspective for integrating hydrologic, geomorphologic, and ecologic dynamics, *Water Resour. Res.*, 45, W01413, doi:10.1029/2008WR007124.

Sabo, J. L., T. Sinha, L. C. Bowling, G. H. W. Schoups, W. W. Wallender, M. E. Campana, K. A. Cherkauer, P. L. Fuller, W. L. Graf, J. W. Hopmans, J. S. Kominoski, C. Taylor, S. W. Trimble, R. H. Webb, E. E. Wohln (2010), Reclaiming sustainable watersheds in the Cadillac Desert, *Proc. Natl. Acad. Sci.*, doi:107(50), 21263-21269.

Searcy, J. C. (1959), Manual of hydrology, 2, Low flow techniques, flow duration curves, *U. S. Geol. Surv. Water Supply Pap.*, 1542-A.

Seneviratne, S. I., I. Lehner, J. Gurtz, A. J. Teuling, H. Lang, U. Moser, D. Grebner, L. Menzel, K. Schroff, T. Vitvar, M. Zappa (2012), Swiss prealpine Rietholzbach research catchment and lysimeter: 32 year time series and 2003 drought event, *Water Resour. Res.*, 48, W06526, doi:10.1029/2011WR011749.

Settin, T., G. Botter, I. Rodriguez-Iturbe, A. Rinaldo (2007), Numerical studies on soil moisture distributions in heterogeneous catchments, *Water Resour. Res.*, 43, doi: 10.1029/2006WR005737.

Schaefli, B., A. Rinaldo, G. Botter (2013), Analytic probability distributions for snow-dominated streamflow, *Water Resour. Res.*, 49, 39363951, doi:10.1002/wrcr.2023.

Schaefli, B., L. Nictina, C. Imfeld, P. Da Ronco, E. Bertuzzo, A. Rinaldo (2014), a Spatially Explicit Hydrologic Response model for ecohydrologic applications, *Geosci. Model Dev.*, 7, 2733-2746, doi:10.5194/gmd-7-2733-2014.

Schneider, P., T. Vogt, M. Schirmer, J. Doetsch, N. Linde, N. Pasquale, P. Perona, O. A. Cirpka (2011), Towards improved instrumentation for assessing river-groundwater interactions in a restored river corridor, *Hydrol. Earth Syst. Sci.*, 15, 2531-2549, doi:10.5194/hess-15-2531-2011.

Seiz, G., and N. Foppa (2007), National Climate Observing System (GCOS Switzerland), *Publication of MeteoSwiss and ProClim*, 92, available online:`http://www.gcos.ch`.

Shaw, S. B., and S. J. Riha (2012), Examining individual recession events instead of a data cloud: Using a modified interpretation of dQ/dtQ streamflow recession in glaciated watersheds to better inform models of low flow, *Journal of Hydrology*, 434435, 46-54, doi: 10.1016/j.jhydrol.2012.02.034.

Shaw, S. B., T. M. McHardy, S. J. Riha (2013), Evaluating the influence of watershed moisture storage on variations in base flow recession rates during prolonged rain-free periods in medium-sized catchments in New York and Illinois, USA, *Water Resour. Res.*, 49, 60226028, doi:10.1002/wrcr.20507.

Sivapalan, M., M. A. Yaeger, C. J. Harman, X. Xu, P.A. Troch, (2011), Functional model of water balance variability and the catchment scale: 1. Evidence of hydrologic similarity and space-time symmetry, *Water Resour. Res.*, 47, doi:10.1029/2010WR009568.

Smith, P. J., J. Wood, J. Gunn (2003), The influence of habitat structure and flow permanence on invertebrate communities in karst spring systems, *Hydrobiologia*, 510, 5366, doi:10.1023/B:HYDR.0000008501.55798.20.

Stall, J. B., and Y. Fok (1968), Hydraulic geometry of Illinois streams, *Water Res. Center Res. Rep.*, 15, Illinois State Water Survey, Urbana, Illinois

Stanley, E. H., S. G. Fisher, N. B. Grimm (1997), Ecosystem expansion and contraction in streams, *BioScience*, 47, 427435, doi:10.2307/1313058.

Tealdi, S., C. Camporeale, L. Ridolfi (2011), Modeling the impact of river damming on riparian vegetation, *J. Hydro.*, 396(3-4), 302-312, doi:10.1016/j.jhydrol.2010.11.016.

Tealdi, S., C. Camporeale, L. Ridolfi (2013), Inter-species competition-facilitation in stochastic riparian vegetation dynamics, *J. Theor. Biol.*, 318, 13-21, doi: 10.1016/j.jtbi.2012.11.006.

Tetzlaff, D., C. Soulsby, P. J. Bacon, A. F. Youngson, C. Gibbins, I. A. Malcolm (2007), Connectivity between landscapes and riverscapesa unifying theme in integrating hydrology and ecology in catchment science?, *Hydro. Proc.*, 21(10), 13851389. doi:10.1002/hyp.6701

Tetzlaff, D., C. Gibbins, P. J. Bacon, A. F. Youngson, C. Soulsby (2008), Influence of hydrological regimes on the pre-spawning entry of Atlantic salmon (Salmo salar L.) into an upland river, *River Res. Appl.*, 24(5), 528542. doi:10.1002/rra.1144

Thompson, S. E., C. J. Harman, A. G. Konings, M. Sivapalan, A. Neal, P. A. Troch (2011a), Comparative hydrology across AmeriFlux sites: The variable roles of climate, vegetation, and groundwater, *Water Resour. Res.*, 47, W00J07, doi:10.1029/2010WR009797.

Thompson, S. E., C. J. Harman, P. A. Troch, P. D. Brooks, M. Sivapalan (2011b), Spatial scale dependence of ecohydrologically mediated water balance partitioning: A synthesis framework for catchment ecohydrology, *Water Resour. Res.* 47, W00J03, doi:10.1029/2010WR009998.

Thompson, S. E., and G. G. Katul (2012), Hydraulic determinism as a constraint on the evolution of ecosystems and organisms, *J. Hydra. Res.*, 50, 547-557, doi:10.1080/00221686.2012.732969.

Thorntwaite, C. W., (1948), An approach toward a rational classification of climate,*Geogr. Rev.*, 94, 55-94.

Troch, P. A., G. F. Martinez, V. R. N. Pauwels, M. Durcik, M. Sivapalan, C. Harman, P. D. Brooks, H. Gupta, T. Huxman (2009), Climate and vegetation water use efficiency at catchment scales, *Hydrol. Process.*, 23(16), 24092414, doi:10.1002/hyp.7358.

Tockner, K., F. Malard, J. V. Ward (2000), An extension of the flood pulse concept, *Hydrol. Process.*, 14(16-17), 28612883, doi: 10.1002/1099-1085(200011/12)14:16/17¡2861::AID-HYP124¿3.0.CO;2-F.

Voepel, H., B. Ruddell, R. Schumer, P. A. Troch, P. D. Brooks, A. Neal, M. Durcik, M. Sivapalan (2011), Quantifying the role of climate and landscape characteristics on hydrologic partitioning and vegetation response, *Water Resour. Res.*, 47, W00J09, doi:10.1029/2010WR009944.

Vogel, R. M., and N. M. Fennessey (1994), Flow-duration curves .2. New interpretation and confidence-intervals, *J. Water Res. Plan. Manage.*, 120(4), 485-504, doi:10.1061/(ASCE)0733-9496(1994)120:4(485).

Vogel, R. M., and N. M. Fennessey (1995), Flow duration curves II : A review of applications in water resources planning, *J. Am. Water Resour. Assoc.*, 31(6), 10291039, doi:10.1111/j.1752-1688.1995.tb03419.x

Wagener, T., M. Sivapalan, P. Troch, R. Woods (2007), Catchment classification and hydrologic similarity. *Geography Compass*, 1(4), 901931, doi:10.1111/j.1749-8198.2007.00039.x.

Wagener, T., H. S. Wheater, H. V. Gupta (2004), Rainfallrunoff modeling in gauged and ungauged catchments. *Imperial College Press*, London.

Ward, J. V., K. Tockner, U. Uehlinger, F. Malard (2001), Understanding natural patterns and processes in river corridors as the basis for effective river restoration, *Reg. Rivers Res. Manage.*, 17, 311323, doi:10.1002/rrr.646

Weyman, D. R. (1970), Throughflow in hillslopes and its relation to stream hydrograph, *Bul. Int. Ass. Sci. Hydr.*, 15(3), 25-33, doi:10.1080/02626667009493969.

Widder, S., K. Besemer, G. A. Singer, S. Ceola, E. Bertuzzo, C. Quince, W. T. Sloan, A. Rinaldo, T. J. Battin (2014), Fluvial network organization imprints on microbial co-occurrence networks. *Proc. Natl. Acad. Sci.*, 111: 1279912804, doi: 10.1073/pnas.1411723111.

Yokoo, Y., and M. Sivapalan (2011), Towards reconstruction of the flow duration curve: development of a conceptual framework with a physical basis, *Hydr. Earth Sys. Sci.*, 15, 2805-2819, doi:10.5194/hess-15-2805-2011.

Yanosky, T. M. (1982), Effects of flooding upon woody vegetation along parts of the Potomac River flood plain, *USGS Professional Paper*, Report 1206.

Young, H. E., J. H. Ribe, K. Wainwright (1980), Weight tables for tree and shrub species in Maine, *Life Sciences & Agriculture Experiment Station Miscellaneous Report*, Report 230.

Ziv, G., E. Baranb, S. Nam, I. Rodriguez-Iturbe, and A. L. Simon (2012), Trading-off fish biodiversity, food security, and hydropower in the Mekong River Basin, *Proc. Natl. Acad. Sci*, 109(15), 56095614, doi:10.1073/pnas.1201423109.

Zhang, L., N. Potter, K. Hickel, Y. Zhang, Q. Shao (2008), Water balance modeling over variable time scales based on the Budyko frameworkModel development and testing, *J. Hydrol.*, 360(14),117131, doi:10.1016/j.jhydrol.2008.07.021.

Zanardo, S., C. Harman, P. A. Troch, S. C. Rao, M. Sivapalan (2012), Intra-annual rainfall variability controls on inter-annual variability of catchment water balance: A stochastic analysis, *Water Resour. Res.*, 48(16), doi:10.1029/2010WR009869.

Zomer, R. J., D. A. Bossio, A. Trabucco, L. Yuanjie, D. C. Gupta, V. P. Singh (2007), Trees and water: smallholder agroforestry of irrigated lands in northern India, *Colombo, Sri Lanka: International water management institute*, IWMI Research Report 122.